THESIS ON MECHANICAL ENGINEERING E64

Reactivity of Woody and Herbaceous Biomass Chars

SIIM LINK

TUT PRESS

TALLINN UNIVERSITY OF TECHNOLOGY
Faculty of Mechanical Engineering
Department of Thermal Engineering

Dissertation was accepted for the defence of the degree of Doctor of Philosophy in Engineering on November 14, 2011.

Supervisor: Prof. Aadu Paist, Department of Thermal Engineering, Tallinn University of Technology, Estonia.

Co-supervisor: Dr. Chem.-Eng. Stelios Arvelakis, Department of Chemical Engineering, National Technical University of Athens, Greece.

Opponents: Dr. Truls Liliedahl, Senior Researcher, School of Chemical Science and Engineering, KTH Royal Institute of Technology, Sweden.

PhD. Ülo Rudi, Senior Research Scientist, Research Laboratory of Multiphase Media Physics, Tallinn University of Technology, Estonia.

Defence of the thesis: December 20, 2011.

Declaration:
Hereby I declare that this doctoral thesis, my original investigation and achievement, submitted for the doctoral degree at Tallinn University of Technology has not been submitted for any academic degree.

Siim Link

ISSN 1406-4758
ISBN 978-9949-23-224-6 (publication)
ISBN 978-9949-23-225-3 (PDF)

MEHHANOTEHNIKA E64

Puit- ja rohtbiomassi kokside reageerimisvõime

SIIM LINK

TTÜ
KIRJASTUS

CONTENTS

LIST OF PUBLICATIONS

Paper I: Link, S., Arvelakis, S., Spliethoff, H., De Waard, P., Samoson, A. Investigation of biomasses and chars obtained from pyrolysis of different biomasses with solid-state ^{13}C and ^{23}Na nuclear magnetic resonance spectroscopy. *Energy Fuels*, 22, 2008, p. 3523-3530.

Paper II: Link, S., Arvelakis, S., Paist, A., Hupa, M., Yrjas, P., Külaots, I. Effect of leaching pretreatment on the char reactivity of pyrolyzed wheat straw. 17th European Biomass Conference & Exhibition, 29.06-03.07.2009. Hamburg, Germany, p. 1113-1121.

Paper III: Link, S., Arvelakis, S., Hupa, M., Yrjas, P., Külaots, I., Paist, A. Reactivity of the biomass chars originating from reed, Douglas fir and pine. *Energy Fuels*, 24, 2010, p. 6533-6539.

APPROBATION INTERNATIONAL CONFERENCES

1. Külaots, I., Link, S., Arvelakis, S. Adsorption properties of wheat straw, reed and Douglas fir chars. International Carbon 2010 Conference, 11.07-16.07.2010, Clemson, South Carolina, USA. Oral Presentation.
2. Külaots, I., Cooper, N., Link, S., Arvelakis, S., Suuberg, E.M. Characterization of bio-chars obtained from various biomaterials. 241st American Chemical Society National Meeting and Exposition, March 27-31, Anaheim, California, USA. Oral Presentation.

INTRODUCTION

Topicality of the theme

Reed, wheat straw and wood are renewable energy sources, which are considered to be CO_2 neutral. Reed is a widely spread plant among others in the Estonian and southern Finnish coastal areas, both on- and offshore, and its species are well-known all over the world. Reed has gradually encroached upon the coastline, and its expansion has been accelerated by human activities: eutrophication, climate change, and the cessation of coastal meadow management. Being a rotting stationary biomass, reed beds reduce water quality, deplete oxygen supplies in water, and release methane into the atmosphere. The expanse of reed beds also has an adverse effect on landscape and jeopardizes nature's biodiversity. When dry, reed has quite a low weight, and therefore, without preliminary treatment, its transportation costs are high. Reed has been used to provide energy in various parts of Europe, such as Estonia, Finland, the Netherlands, Hungary, and Romania [1]. The annual reed energy production potential is modest (for instance in Estonia 292 GWh/y [1]), and therefore, it could be used by blending with other types of biomasses, such as wood. For 30 years the Douglas fir has been widely planted in Europe, especially in France and Germany, and nowadays, this wood represents an emerging resource for sawing logs, thinning logs, top logs and sawmill chips. It is estimated that the French annual harvest of Douglas fir will be around 6 million m^3 by the year of 2015 [2]. In Europe as well as around the world, the wood pellet production extends to the tens of millions of tons per year [3]. Wheat straw is one of the most promising agricultural residues as a fuel source, suitable for energy production in the Mediterranean region [4] as well as in Europe and worldwide. The wheat production worldwide in 2009 was 685 614 thousand tonnes [5]. For instance, in EU-27 countries the annual production of wheat in 2008/2009 was 138 954 thousand tonnes. France, Germany and Great Britain produce together 56% of wheat of EU-27 countries, but Italy, Greece and Spain together over 9% [6].

In addition, fuel alternative such as biofuel utilization saves otherwise depleting resources of fossil fuels. The usage of residues originating from the reed treatment processes as a roof material, and wheat straw - a residue of harvesting as an energy source, together with the wood residue, serve the goals of European Union policy for wastes and environment.

Power production from biomass, including from different agricultural and forest residues, has been an issue over the last few decades. Generally, power production from biomass in small-scale applications is in most cases under discussion. In principal, the application of the gasification technology together with combined heat and power production gives an opportunity to utilize fuels with higher efficiency. The application of the integrated gasification combined cycle (IGCC) is commonly considered to have higher efficiency compared to the Rankine cycle.

Pyrolysis and gasification are thermochemical conversion routes to recover energy from biomass. Pyrolysis is not only an independent conversion technology but also part of the gasification process, which can be broadly separated into two main stages, solid devolatilization (pyrolysis) and char conversion (gasification). Char reactivity in the second stage is dependent upon the formation conditions (essentially temperature and heating rate) and the amount and composition of the inorganic content. In addition, the type of biomass (chemical composition and physical properties) also largely affects both biomass devolatilization and char conversion [7]. The char conversion stage, following the pyrolysis step in the gasification process, is generally much slower than the pyrolysis itself and is therefore the rate-determining step [8].

Gasification rates are influenced by a number of process variables, such as particle size and size distribution, char porosity and pretreatment, mineral content of char, and temperature and partial pressures of the gasifying agents [9].

Several studies have focused on the influence of wood type in CO_2 gasification process. In general, the mineral matter content, composition and its catalytic properties explain the differences of reactivity among the fuels [10]. The presence of inorganic constituents in chars plays an important role in oxidation kinetics because of their catalytic effects. Sodium, potassium and calcium, which are commonly present in biomass, show a significant activity as gasification catalysts [11,12,13]. It was shown that alkali metals are approximately 10 times more active catalyzing the char gasification than alkali earth metals [14]. According to Kannan et al. [15], the catalytic effect of potassium was reduced by reaction with silica to form silicate during pyrolysis, but catalysis of gasification by Ca does not appear to be significantly reduced by silica. The CO_2 gasification rate depends upon the silicon content in the parent fuel and, when the silicon content is low, also the sum of K and Ca contents. The gasification rate dependency upon parent fuel silicon content was also discussed by Moilanen [16]. Experimental and theoretical studies made by Sørensen et al. [17] have shown that the reactivity of char is dependent upon the silicon as well as the potassium contents and the form of the potassium compound. As can be seen in the literature, the catalytic effect of mineral matter content on biomass char reactivity is mainly related to alkali and alkali earth metals versus silicon content.

Di Blasi et al. [18] have investigated the reactivity of wheat straw, olive husks and grape residue chars in air, and have found that the grape residue char is less reactive than the wheat straw and olive husk chars. The aim of their paper has been the determination of reaction parameters, not explanation of distinctions in the reactivity of the chars.

Zanzi et al. [19] have studied the reactivity of rapid pyrolysis chars of olive waste, wheat straw and birch. They have concluded that due to the higher ash content of agricultural residues, the chars originating from agricultural residues are more reactive compared to wood. Additionally, wood gives more volatiles

and less char than straw and olive waste. The high ash content in agricultural residues favours the charring reactions, increasing the char yield.

Marquez-Montesinos et al. [20] have studied the CO_2 gasification of grapefruit skin char. They have washed the char with H_2SO_4 to decrease the ash content. The results show that the reactivity of washed char is significantly lower compared to original, but the surface area values are comparable.

Risnes et al. [14] have investigated CO_2 reactivity of chars from wheat straw and spruce. The main aim of the study was to determine the kinetic parameters. They have found that the wheat straw and spruce exhibited almost identical reactivity.

Guerrero et al. [21] have investigated the chars of rice husk and eucalyptus, and have concluded that the greater reactivity of rice husk char was imputed to the higher surface area as well as higher O/C and H/C ratio compared to eucalyptus char.

Ikenaga et al. [22] have studied various chars originated from Japanese biomass, such as Japanese cedar wood, fig tree, umemodoki (*Ilex serrata*), Japanese oak, mukuge (*Hibiscus syriacus*), eucalyptus, cherry tree, satsuki (*Rhododendron indicum*), chopstick (*Betula platyphylla*), nandina, pine, bean curd, coffee bean residue, tea leaves and rice straw. According to the study, the gasification rate is affected by the indigenous mineral matter content of calcium and potassium. Though, the discussion about the distinctions in reactivity between various biomass chars was missing.

Zhang et al. [23] have investigated the leaching pretreatment with distilled water, HCl and HF acids on the reactivity of manure chars. The reactivity of the resultant char is affected greatly by the pretreatment processes, except water washing. The oxidation reactivity of the char from the raw manure is much higher than that of the char prepared from de-mineralized manure sample.

According to the literature, the char reactivity depends on a number of variables. The biomass chars investigated by several authors as described above were prepared under different conditions, and the characterization methods of the chars were different as well. Despite of the comprehensive literature related to the gasification reactivity of biomass chars, there is no literature available for instance about the reactivity of the reed char.

Lots of researches have been done on the effect of inorganic matter on the biomass char reactivity and the favourable effect of inorganic matter on char reactivity has been found. However, little work has been done on characterizing the char reactivity with a wide range of methods available for characterizing the properties of chars and using different fuels with the same particle size under the same pyrolysis conditions, while both the particle size and pyrolysis conditions affect the reactivity of chars. Very often the decrease in reactivity by leaching pretreatment or demineralization have been characterized with words “much lower”, “greatly lower”, “significantly lower”, etc. compared to the untreated sample, but no quantity has been given.

Goal of the work

- The goal of the work is the determination of substantial properties and char gasification reactivity of selected materials.
- To compare the outcome of the gasification test, i.e. reactivity of different chars, with the determined properties.
- Estimate the effect of leaching pretreatment method on the gasification reactivity of char.

Activities to be planned

For the purpose of achieving the above posed goal the following activities were carried out:

- preparation of fuels and chars (cutting, milling, pyrolysis, leaching);
- characterization of the materials (proximate analysis, ultimate analysis, gross calorific value, ash chemical analysis, nuclear magnetic resonance spectroscopy, N_2 and CO_2 adsorption techniques, scanning electron microscopy/energy dispersive X-ray spectroscopy);
- reactivity measurements of the chars at different temperatures;
- comparison of the data on material characterization and reactivity measurements, and drawing a conclusion on differences in the reactivity of studied chars.

Methodology of research

In general, the researches on determining the reactivity of chars are based on the mass loss measurements over time in different oxidative environments, but in this work CO_2 is used. Besides the conventional fuel characterization methods such as (proximate analysis, ultimate analysis, gross calorific value, ash chemical analysis etc.), additionally ^{13}C and ^{23}Na nuclear magnetic resonance spectroscopy was applied. The selected method for the characterization have been applied before quite extensively (except ^{23}Na NMR), but not at the same time on the chars prepared under same pyrolysis conditions. A scanning electron microscopy was used for investigating the morphological changes that occur during the pyrolysis and finding the differences between the materials. An energy dispersive X-ray spectroscopy was used for investigating the variations of inorganic chemistry on the surfaces of materials due to pyrolysis and again, the distinctions between the selected materials. Though, when the reactivity is measured in CO_2 environment, for the specific surface area and porosity determination, both gases N_2 and CO_2 are used widely. In this work, the N_2 isotherm is used for determining the total porosity of the char samples, incl. micoporosity, mesoporosity, macroporosity.

Additionally, the properties of the materials were determined and reactivity test results compared with the properties of the chars. Finally, the distinctions in reactivity were explained by different properties of the materials. The properties of the materials vary in a wide range, but in this work we have concentrated on the main issues related to reactivity.

Scientific novelty

- Comprehensive review of different methods characterizing the char properties; all applied to the chars originating from biofuels with a wide range of properties and produced under the same conditions.
- Assessment of the pyrolysis char reactivity with ^{13}C and ^{23}Na solid-state NMR spectroscopy in combination with other conventional methods.
- Impact of the applied leaching pretreatment method on char reactivity.
- Utilization of reed for gasification has not been studied in relation to reactivity before.
- Oxidative reactivity of biomass chars is complicated by a number of different factors, which are explored in this study with the aim to shed light on reactivity of the materials not studied extensively before.
- The chosen materials are different by the properties, which allow to compare and explain the reasons of different char reactivities and draw better conclusions.
- An attempt was made to explain the distinctions in the N_2 BET surface area between the untreated and pre-treated wheat straw char sample.

Practical significance

High char reactivity is needed in order to obtain higher energy outputs from the reactors [24], and the distinctions in reactivity results in different reactor outputs in the case of different fuels. Additionally, the presence of inorganic constituents in biomass fuels is associated with several problems, such as deposition, sintering, agglomeration, corrosion, and/or erosion occurring during the operation of gasification plants [25]. The leaching pretreatment process is an option to eliminate the alkali metals and chlorine from biomass. On the other hand, the lower content of alkali metals may affect the char gasification reactivity.

Acknowledgements

First of all I would like to express my gratitude to my supervisors Dr. Chem.-Eng. Stelios Arvelakis and Prof. Aadu Paist. Prof. Mikko Hupa, D. Sc. Patrik Yrjas, Dr. Indrek Külaots, Prof. Dr.-Ing. Hartmut Spliethoff, PhD. Ago Samoson, PhD. Ivo Heinmaa, Dr. Pieter de Waard, PhD. Jüri Loosaar and Prof. Arvo Ots are acknowledged for the help, co-operation, guidance and valuable comments along the research.

PhD. Tõnu Pihu, Peter Backman, M. Sc. Linus Silvander, Maaris Nuutre, Raaja Aluvee, PhD. Rein Kuusik and PhD. Kaia Tõnsuaadu are acknowledged for their comprehensive assistance on carrying out the tests. Dr. Matthias Thommes, from Quantachrome Inc. is acknowledged for his valuable comments and discussions related to the porosity and specific surface area of the chars.

PhD. Märt Nõges from the Agricultural Research Centre is acknowledged for the help related to the preparation of the sample materials.

I am also deeply thankful to my colleagues from the Department of Thermal Engineering and the co-workers of the institutions where the research work and experiments were performed – Institute of Energy Systems (Technische Universität München), the Wageningen NMR Centre, Process Chemistry Centre (Åbo Akademi), National Institute of Chemical Physics and Biophysics, Agricultural Research Centre, Laboratory of Inorganic Materials (Tallinn University of Technology) and Division of Engineering (Brown University).

As acknowledged in the papers, the research was supported by many of institutions, programmes and projects - Deutsche Bundesstiftung Umwelt, Johan Gadolin Scholarship, the Greek Secretariat for Research and Development through the ENTER research grant (AGRO-GONO) 2006-2008, the European Community activity Large-Scale Facility Wageningen NMR Center [FP6-2004-026164 (2006-2009)], and European Social Fund's Doctoral Studies and Internationalisation Programme DoRa.

I would like to express my gratitude to everyone who has in one way or another contributed to this work.

Finally I would like to thank my family, especially my wife Külli and my son Jako, and my friends, for their encouraging, support and patience when I was preoccupied with experiments and writing and unable to participate in our activities.

ABBREVIATIONS, TERMS AND SYMBOLS

Roman symbols

M_o – the initial mass of the char
M(t) – the mass of the char at time *t*
M_f – the mass of the residue
p_{CO2}^{sat} – saturation pressure of CO_2
p – adsorbate pressure
p_0 – saturation pressure
r – char gasification reaction rate
t – time
X – char conversion

Abbreviations

AAEM	– Alkali and Alkali Earth Metals
ASTM	– American Society for Testing and Materials
BET	– Brunauer-Emmett-Teller
CPMAS	– Cross Polarization Magic-Angle Spinning
DF	– Douglas Fir wood chips
DF800	– Douglas Fir wood chips char pyrolyzed at 800 °C
DFT	– Density Functional Theory
DMT	– Deutsche Montan Technologie
DR	– Dubinin-Radushkevich
EDX	– Energy Dispersive X-Ray
HPTGA	– High-Pressure Thermogravimetric Apparatus
IGCC	– Integrated Gasification Combined Cycle
IUPAC	– International Union of Pure and Applied Chemistry
MAS	– Magic-Angle Spinning
NICPB	– The National Institute of Chemical Physics and Biophysics
NMR	– Nuclear Magnetic Resonance
PSD	– Pore Size Distribution
PP	– Pine Pellets
PP	– Pine Pellets char pyrolyzed at 800 °C
R	– Reed
R800	– Reed char pyrolyzed at 800 °C
SEM	– Scanning Electron Microscopy
TGA	– Thermogravimetric Analyser
WSU	– Untreated Wheat Straw
WSU800	– Untreated Wheat Straw char pyrolyzed at 800 °C
WSL	– Leached Wheat Straw
WSL800	– Leached Wheat Straw char pyrolyzed at 800 °C
daf	– Dry and Ash-Free
n.d.	– Not Determined

1 EXPERIMENTAL

1.1 Materials

The materials for the study were chosen quite different by the properties leading to the distinctions in reactivities. The samples selected for the investigation were the following: pelagian reed (*phragmites australis*) coming from the western coast shorelines and islands of Estonia, wheat straw coming from the area of Thessaly in Greece, and commercial pine pellets and Douglas fir wood chips, both originating from the area of Munich in Germany (see also Figure 1.1).

Reed

Pine pellets

Douglas fir wood chips

Wheat straw [26]

Figure 1.1 Illustrative pictures of the used materials

The reed, untreated and leached wheat straw, Douglas fir wood chips and pine pellets samples, as well as their char samples (hereafter referred as R, WSU, WSL, DF, and PP and char samples R800, WSU800, WSL800, DF800, and PP800) were analysed and characterized regarding their proximate and ultimate composition analyses, gross calorific value, and ash chemical analysis (in all cases, the oxidation for the ash chemical analysis was performed at the temperature of 600 °C) in accordance with the American Society for Testing and Materials (ASTM) methods, such as D 1102-84, D 3175-89a, D 5142-90, D5373-93, D 4208-88, D 2015-95, as shown in Table 2.1 and Table 2.2. Because

of the relatively low char yield of pine pellets in the pyrolysis experiments, the proximate analysis of pine pellet char was performed by a SDT Q600 thermogravimetric analyser (TGA). In these TGA experiments, first the sample was heated 20 °C min^{-1} from ambient temperature to 105 °C in nitrogen gas flow of 90 mL min^{-1} to determine the moisture content. Then the temperature was increased with the heating rate of 50 °C min^{-1} up to 900 °C where it was kept for 7 min to determine the volatile content of the sample. Thereafter the temperature was lowered to 600 °C in 20 minutes followed by supplying air at the flow rate of 100 mL min^{-1} to initiate burning and determine the ash content.

The cellulose, hemicellulose and lignin contents for the wheat straw sample were also determined according to the ASTM standard method D 1106-8 as shown in Table 2.3, and for reed according to the Foss Analytical methods such as ASN 3429, ASN 3431 and ASN 3430. For pine pellets and Douglas fir wood chips, the cellulose, hemicellulose, and lignin contents were evaluated according to the literature [27].

After each direct reactivity measurement of the char sample, the gasification residue remained. Because of the limited amount of the gasification residue (some milligrams), the ash content of this residue was determined applying the Setaram TGA apparatus. The heating rate of 10 °C min^{-1} to 600 °C and the air flow rate of 50 mL min^{-1} were used. The ash content was calculated according to the mass loss data. Because of the insufficient amount of gasification residue of the pine pellet sample, the ash content determination was not performed.

1.2 Leaching

The wheat straw sample was also pre-treated using the leaching pretreatment process. The pretreatment targeted on the elimination of the amounts of alkali metals, chlorine and sulphur in the biomass sample, which are considered to be responsible for the ash-related problems during the combustion and gasification of biomass. The leaching was performed with tap water according to the method developed by Arvelakis et al [25]. The used mass-to-water ratio of leaching was 66.6 g/l.

1.3 Pyrolysis

An atmospheric fixed-bed reactor was used for the preparation of char samples. The pyrolysis set-up shown in Figure 1.2 consists of the gas controlling system, the reactor-heater, and the data acquisition and controlling system. The mass flow of nitrogen was controlled using a calibrated mass flow controller.

A cylindrical electric heater is placed inside the reactor. Inside the heater is placed a quartz pipe that protects the heating wire against corrosive compounds possibly present in the evolved gas mixture. A temperature controller and thermocouple were used to heat the set-up and keep the required temperature.

The sample was loaded into the sample holder made of a stainless steel SS316 bound net with 80μm openings, as shown in Figure 1.3.

The sample holder was filled with biomass. Nitrogen was used as a carrier gas with a flow rate of 1 l/min in the case of all tests.

The applied heating procedure was the following: (i) hold the sample for 45 minutes at 50 ºC, (ii) heat the sample to the end-temperature of 800 ºC using the heating rate of 20 °C/min, (iii) hold the sample 15 minutes at end-temperature, and (iv) cooling down to the room temperature.

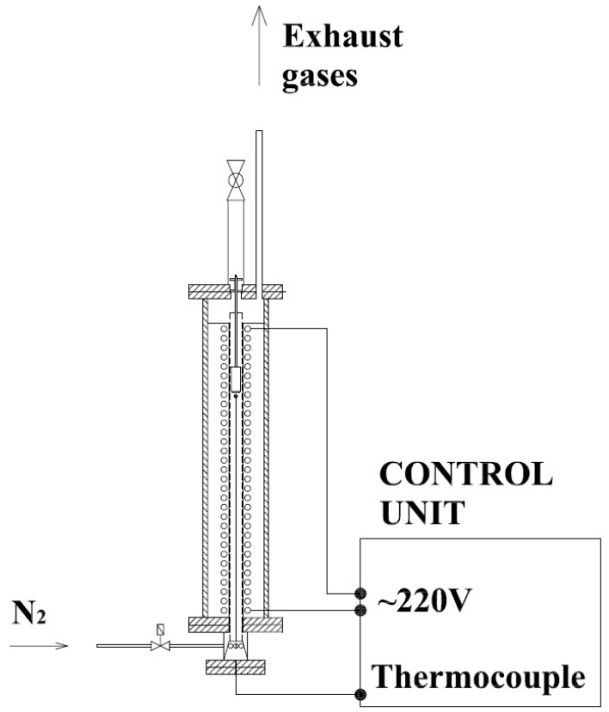

Figure 1.2 Simplified schema of the pyrolysis reactor-heater

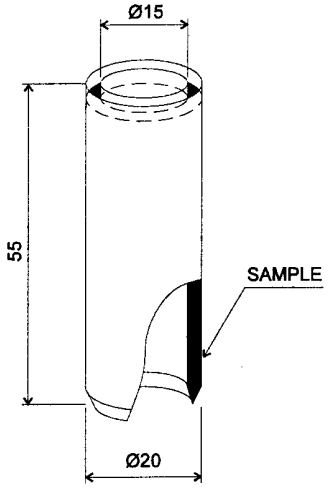

Figure 1.3 Sample holder

1.4 Solid state NMR spectroscopy

For the NMR spectroscopy, a Bruker Avance 300 spectrometer located at the Wageningen NMR Centre, operating at a carbon resonance frequency of 75.5 MHz, or at a sodium frequency of 79.4 MHz, at the temperature of 20 °C, was used. The spinning speed was 5 kHz and 7 mm rotors of ZrO_2 were used. The obtained data were analysed with TOPSPIN software provided by Bruker.

The carbon-13 cross polarization magic-angle spinning (CPMAS) solid-state NMR was used for the characterization of the biomass samples. The cross-polarization contact time was 1 ms; the delay time was 4 s; and the 90 degree pulse for proton was 5 μs.

The carbon-13 single-pulse solid-state MAS NMR was used for the characterization of various biomass char samples. The pulse length was 2 μs and delay time 2 s.

The original biomass samples and char samples were also analysed with the ^{23}Na single-pulse solid-state MAS NMR. The pulse length was 1 μs and delay time 1 s. The chemical shifts were calibrated to separately measured solid NaCl (7.0 ppm).

1.5 Morphology

The morphology of the parent and char material examined by scanning electron microscopy (SEM), and energy dispersive X-ray (EDX) spectroscopy was used for determining the inorganic matter on the surface of the chars. All the SEM/EDX spectroscopy work was performed with a Leo 1530 Gemini at the voltage of 15 kV.

1.6 Surface area and porosity

The nitrogen adsorption isotherms at -196 °C and carbon dioxide isotherms at 0 °C were obtained from all the char samples by a volumetric technique using a Quantachrome Autosorb-1 instrument. Prior to the surface area analysis, all the char samples were outgassed at 280 °C overnight under vacuum to ensure complete removal of surface contaminants. Because of the pressure limitation of the instrument, the maximum relative pressure of 0.03 was obtained when CO_2 isotherms at 0 °C were recorded (p_{CO2}^{sat}= 3484.8 kPa at 0 °C). The adsorption uptake data at partial pressures of N_2 from 10^{-6} up to 1 were requested to obtain the full N_2 isotherms. The specific Brunauer-Emmett-Teller (BET) surface areas from the N_2 isotherms of the char samples were determined over the partial pressure (p/p_0) range where the BET equation had the highest correlation coefficient (at least 0.9999) [28,29]. For most non-microporous samples, the commonly accepted range of p/p_0 for the BET equation is from 0.05 to 0.3 (N_2 isotherms). However, because of the highly microporous nature of the char samples, the relative pressure range of the isotherms for BET area determination requires adjustment. Therefore, the BET areas were, in this work, defined at significantly lower relative pressure p/p_0 values, down to 0.01 to 0.05. The

microporosity specific surface areas were determined from the CO_2 isotherm using the Dubinin-Radushkevich (DR) model [29] as well.

The porosity values presented in this work were calculated using the N_2 adsorption isotherms of the char samples. The microporosity of the char samples was determined using the DR model. The mesoporosity of the char samples was determined by subtracting the DR microporosity value from the total porosity at an isotherm relative pressure of p/p_0=0.95. The macroporosity of the char sample was calculated by subtracting the total porosity at the relative pressure p/p_0 = 0.95 from the porosity value at the relative pressure p/p_0 = 0.99.

The pore size distribution (PSD) of the char samples was determined from the N_2 adsorption isotherms at -196 °C and from the CO_2 adsorption isotherms at 0 °C using the density functional theory (DFT) [30,31]. The PSDs of the char samples were reported according to the classification of International Union of Pure and Applied Chemistry (IUPAC), which defines the micropores as pores less than 20 Å, mesopores as pores in the range of 20-500 Å and macropores as pores above 500 Å.

1.7 Char reactivity measurement

The Deutsche Montan Technologie (DMT) high-pressure thermogravimetric apparatus (HPTGA) operating at the atmospheric pressure was applied in the char reactivity tests as shown in Figure 1.4. The HPTGA has a maximum operating pressure of 100 bar and a maximum temperature of 1100 °C. Up to five gases can be fed into the reactor, and by means of a bypass line around the reactor, the gas composition can be quickly changed. A water-cooled, helium-purged sample lock is located above the reactor and the sample is placed into HPTGA via an opening in the lock. A small, electrically-driven winch lowers and raises the sample into and out of the heated section of the reactor.

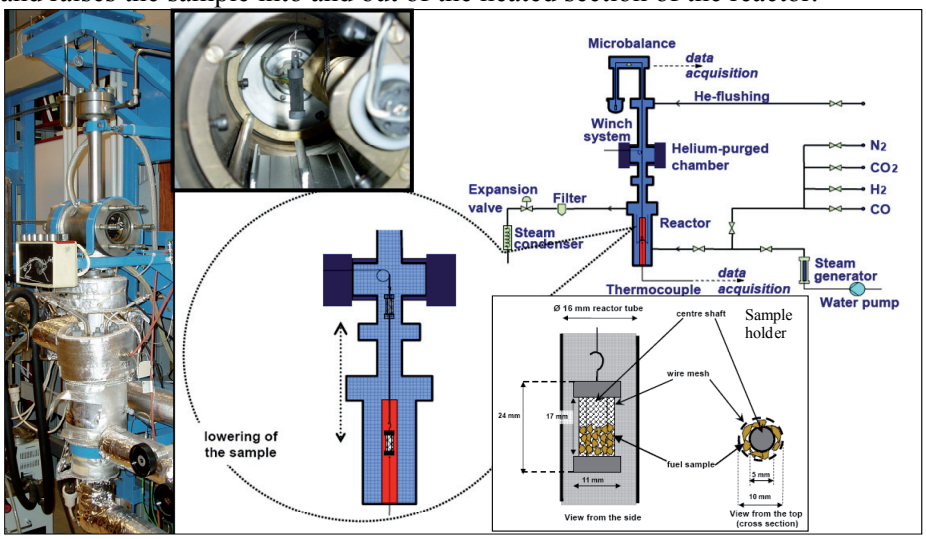

Figure 1.4 High pressure thermogravimetric apparatus

At first, the sample was held in the reactor under the He gas flow. Then the desired reaction temperature was selected, and the reactor was heated to the target temperature (reactivity tests were performed at 750, 800, 850, and 900 °C). After the reactor reached the target temperature, the sample holder was lowered to the preheated reactor. A steady sample mass was achieved in 150-300 s (*Phase I*), after which a gasification agent CO_2 with the flow rate of 1 L min^{-1} was introduced into the reactor (*Phase II*). A schematic diagram together with the detailed description of the system is reported elsewhere [32].

1.8 Reactivity data analysis

A typical HPTGA mass loss curve is shown in Figure 1.5. M_o represents the initial mass of char; M(t) is the mass of char at the time *t*, and M_f is the mass of residue.

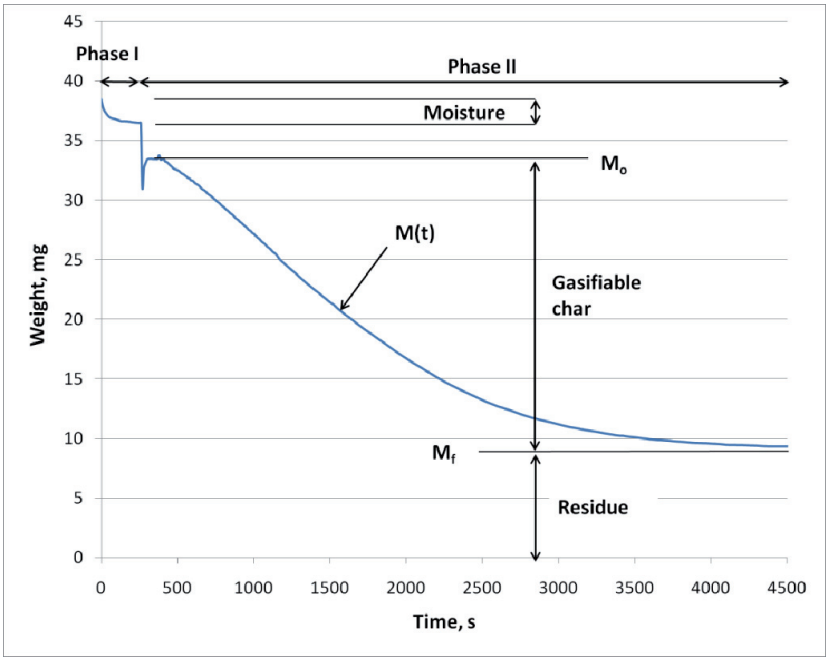

Figure 1.5 A typical HPTGA weight-loss curve

Different definitions are used for the determination of reactivity [10]. In this work, the reactivity results are presented in the figures via the char gasification rate as a function of char conversion. The char gasification rate in units of min^{-1} at any particular conversion value is defined as shown below:

$$r=dX/dt \quad (1)$$

where *r* is the reaction rate,

$$X=(M_o-M(t))/(M_o-M_f). \quad (2)$$

2 RESULTS AND DISCUSSION

2.1 Material Characterization

The PP exhibited relatively low ash content (0.22 wt % on a dry basis, and the ash contained mainly calcium oxide (37.3 wt %), which corresponds to 0.08 wt % in the parent fuel (see also Table 2.1 and Table 2.2). The DF had the ash content of 6.73 wt % (on a dry basis) and contained mainly silica (55.5 wt %). The ash content of reed was 3.21 wt % (on a dry basis), and the ash consisted mainly of silica (73.7 wt %), which corresponds to 2.37 wt % of the parent material, compared to the 3.74 wt % for the DF sample. The potassium oxide content of DF parent fuel was 0.28 wt %, which is comparable with the leached wheat straw sample (0.24 wt %), but higher than the reed sample (0.19 wt %).

In the case of wheat straw, the influence of leaching pretreatment on the properties of parent material could be observed. The removal of the mineral matter by leaching increased the volatile matter content as expected, but decreased the potassium and chlorine content. The increase in volatile matter content by demineralization via leaching or other techniques has also been observed by others [33]. The potassium oxide content of untreated wheat straw was 1.59 wt % calculated from the parent fuel, which is the highest among the studied materials. After leaching the potassium content in the parent fuel lowered approximately 7 times. According to the chemical analysis of ash, the chlorine content in the parent fuel decreased by nine times after leaching in the case of wheat straw.

The reed sample exhibited the highest cellulose and hemicelluloses content (see also Table 2.3). Woody materials have the highest content of lignin.

The O/C and H/C ratios on molar basis of the char samples are shown in Table 2.4. The PP800 and WSU800 have the highest O/C ratio. The ratio of H/C is the highest for WSU800 as well.

2.2 Char Yields

The char yields of the R, DF, PP, WSU, and WSL samples shown in Table 2.5 were calculated on a dry and ash-free (daf) basis. The WSU and DF exhibited the highest char yield on both dry and daf bases. The results of the char yields during pyrolysis calculated on dry and daf bases refer to higher volatile matter content of the R, PP, and WSL in parent materials compared to the DF and WSU samples.

Table 2.1 Analysis and characterization of the biomass samples

	Moisture (wt%)	Proximate analysis, dry basis (wt%)			Ultimate analysis, dry basis (wt%)						Gross calorific value, (MJ/kg)
		Ash	Volatile matter	Fixed carbon	N	C	H	S	Cl	O	
R	5.40	3.21	80.26	16.53	0.44	47.36	5.66	0.19	n.d.	43.14	20.41
DF	7.74	6.73	72.28	20.99	0.63	48.49	4.85	0.05	n.d.	39.25	19.12
PP	5.89	0.22	83.29	16.49	0.32	50.49	5.85	0.15	n.d.	42.97	19.13
WSU	8.10	7.60	76.00	16.40	0.79	43.70	5.08	0.43	0.44	41.96	18.91
WSL	5.75	5.87	80.65	13.48	0.57	46.26	5.31	0.20	0.10	41.68	20.03
R800	6.90	16.01	6.73	77.25	1.72	59.19	1.23	n.d.	n.d.	21.85	n.d.
DF800	6.47	20.80	9.54	69.66	1.45	56.71	0.92	n.d.	n.d.	20.12	n.d.
PP800	8.60	4.08	7.11	88.8	1.03	64.13	1.19	n.d.	n.d.	29.57	n.d.
WSU800	7.96	28.03	10.29	61.68	1.17	46.57	1.13	n.d.	n.d.	23.10	n.d.
WSL800	6.40	36.07	12.26	51.66	1.34	45.48	0.78	n.d.	n.d.	16.33	n.d.

Table 2.2 Chemical analysis of ash in the biomass samples (wt%)

	Reed	Douglas fir wood chips	Pine pellets	WSU	WSL	R800	DF800	WSU800	WSL800
K_2O	5.87	4.13	7.66	20.95	4.01	3.28	4.74	18.13	4.57
Na_2O	8.39	1.48	1.31	0.90	1.88	2.27	1.36	1.58	2.03
CaO	2.90	10.90	37.30	14.40	15.30	4.07	9.64	6.33	18.35
MgO	1.37	4.90	9.08	2.67	2.49	1.46	7.73	0.80	3.59
SiO_2	73.70	55.50	11.20	39.20	49.89	83.42	51.92	51.61	49.54
Al_2O_3	n.d.	11.60	5.00	1.95	1.93	0.86	13.73	1.93	1.22
Fe_2O_3	1.09	7.24	4.83	0.38	0.56	1.44	6.61	0.56	0.45
TiO_2	0.10	0.55	0.30	0.10	0.12	n.d.	n.d.	n.d.	n.d.
SO_3	5.18	0.54	1.33	5.27	3.76	n.d.	n.d.	n.d.	n.d.
P_2O_5	0.97	0.87	2.23	n.d.	n.d.	n.d.	n.d.	n.d.	n.d.
Cl	0.56	0.73	0.99	2.73	1.78	0.19	0.36	0.32	0.26

Table 2.3 Chemical analysis of biomass samples, dry basis (wt%)

	Extractives	Lignin	Cellulose and hemicellulose
Reed	15.5	12.2	72.3
Douglas fir wood chips	6.0	29.0	65.0
Pine pellets	5.0	30.0	65.0
WS	15.5	16.6	60.3

Table 2.4 O/C and H/C ratio on molar basis of char samples

	O/C	H/C
R800	0.28	0.25
DF800	0.27	0.19
PP800	0.35	0.22
WSU800	0.37	0.29
WSL800	0.27	0.21

Table 2.5 Char Yields (wt%)

	R	DF	PP	WSU	WSL
Dry	19.73	29.35	17.27	30.05	27.13
Dry and ash free	15.75	23.02	15.67	21.11	16.64

2.3 Morphology

The scanning electron microscopy (SEM) technique is widely applied on the investigation of biomass char samples [20,24,34,35,36,37,38,39,40,41]. In addition to the SEM technique, an energy dispersive X-ray (EDX) spectroscopy technique has been also applied to obtain better background information about the particles observed by SEM.

The reed parent material shown in Figure 2.1 a and b. Figure 2.1a exhibits an oblong particle with the fibrous structure. The particles with irregular shape representing leafs and flowers of the plant can be seen as well. On the surface slits, holes and white particles containing Si could be observed. Figure 2.1b exhibits oblong particle with strongly bound solid cells representing the stem part of the reed plant. White bubbles containing Si could be observed on the surface. Also some empty holes are visible, i.e. Si bubbles have been removed due to mechanical treatment during the sample preparation. The EDX spectroscopy analysis indicates the inorganic matter on the reed surfaces containing 95-100% of SiO_2.

The pyrolyzed reed sample shown in Figure 2.1 c and d. Figure 2.1c represents irregular char particles with the scabrous surface. In Figure 2.1d the oblong shape of char particles can be seen, indicating that after thermal treatment the reed sample has maintained its shape, but Si bubbles have lost their sharp edges. According to EDX spectroscopy analysis, the mineral matter on the surfaces of oblong char particles contains mainly SiO_2, but on the surfaces the heterogeneous particles, K_2O and CaO could be detected as well. For instance in Figure 2.1 c, 7% and 5% of mineral matter, respectively.

Reed

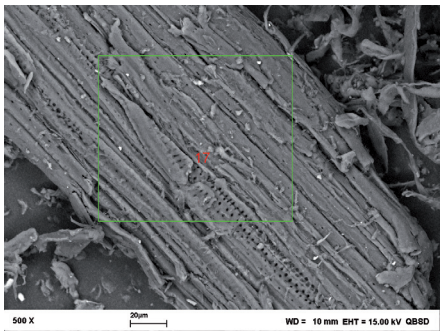

a) Oblong particle having the fibrous structure with slits and holes.

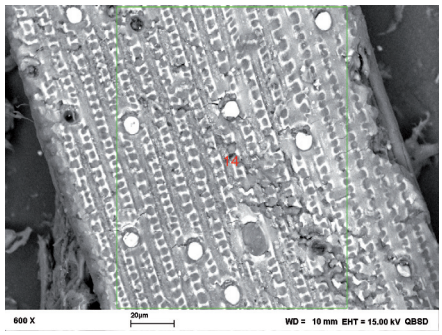

b) Oblong stem particle with strongly bound solid cells. White bubbles representing Si

Reed char

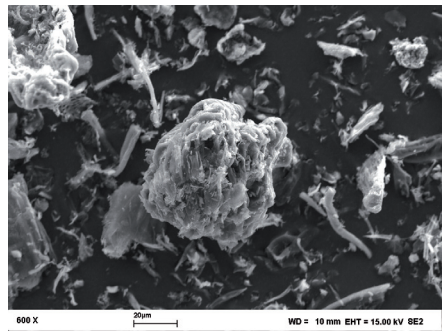

c) Irregular char particle with scabrous surface

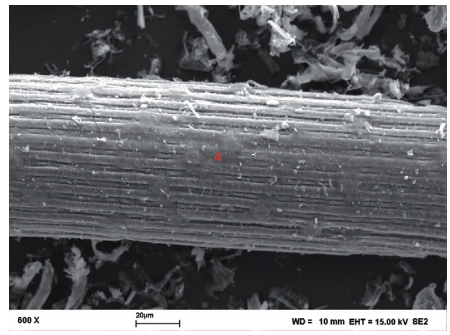

d) Oblong shape of a char particle. Si bubbles have smoothed edges

Figure 2.1 SEM images of reed and reed char (R800)

The sample of Douglas fir parent material is presented in Figure 2.2. In Figure 2.2a oblong and irregular shape of particles with holes, slits and fissures on the surface can be seen. In Figure 2.2b an oblong particle with longitudinal cavities can be observed. In Figure 2.2c the particles with oblong and irregular shape can be detected. In Figure 2.2d the oblong and irregular shape of particles with holes and fissures on the surface can be seen. In all pictures, the inorganic matter on the particles is visible. The main inorganic elements detected on the surfaces of Douglas fir samples are Si, Ca and K.

A pyrolyzed Douglas fir sample is shown in Figure 2.3. Figure 2.3a represents oblong- and irregular-shaped particles. The scabrous edges can be detected as well. In Figure 2.3b a smooth char particle with of irregular shape is presented. In Figure 2.3c a particle with the scabrous surface is shown together with smaller particles of irregular shape. Figure 2.3d shows different size of oblong and irregular particles. The morphology of the surface can be seen changed due to thermal treatment. In all the pictures the mineral matter on the surfaces could be detected. However, after pyrolysis the part of mineral matter contains still mainly Si, Ca and K on the surface.

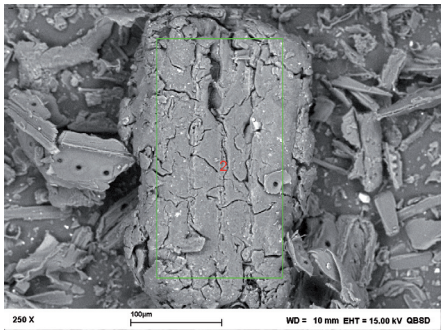

a) Oblong and irregular shape of particles with holes, slits and fissures

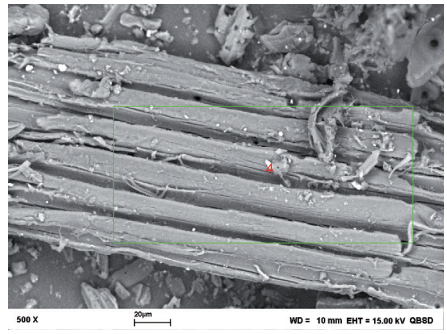

b) Oblong particle with longitudinal cavities

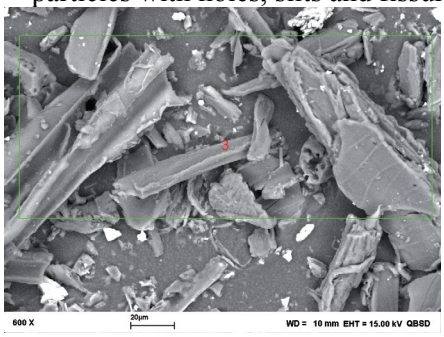

c) Particles with oblong and irregular shape

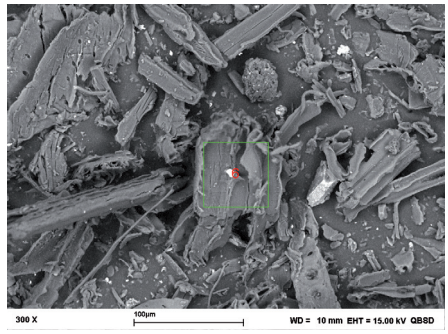

d) Oblong and irregular shape of particles with holes and fissures

Figure 2.2 SEM images of Douglas fir sample (DF).

A parent material of pine pellet sample is shown in Figure 2.4 a and b. Figure 2.4a shows an oblong particle with fissures and cavities on the surface and scabrous edges of the particle together with smaller particles of irregular shape. In Figure 2.4b a particle of irregular shape with fissures and holes on the surface is shown. The holes on the surface constitute the network of cells. Mainly Ca was detected on the surfaces of particles of pine pellet sample.

The pine pellet char sample is shown in Figure 2.4 c and d. In Figure 2.4c, an oblong particle with fissures and cavities could be seen, as well as a thin particle with orders of magnitude larger in length and width than thickness. In Figure 2.4d shows a number of small thin particles with orders of magnitude larger in length and width than thickness having scabrous edges. In general, there could be detected particles which have the length and width many times larger than thickness, representing the so-called irregular thin-plate-shape particles. K and Ca were mainly detected on the particle surfaces. While the parent material of pine pellet sample exhibited almost no K on the surface, it could be assumed that K migrated to the surface during pyrolysis.

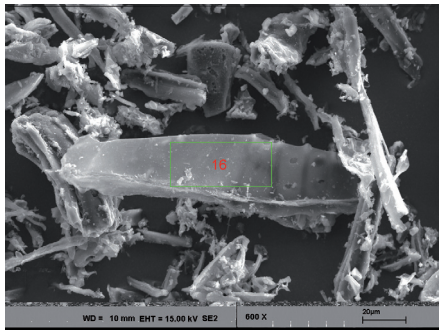

a) Oblong and irregular shape of particles

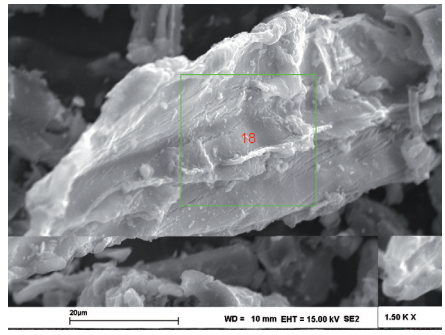

b) Smooth char particle with irregular shape

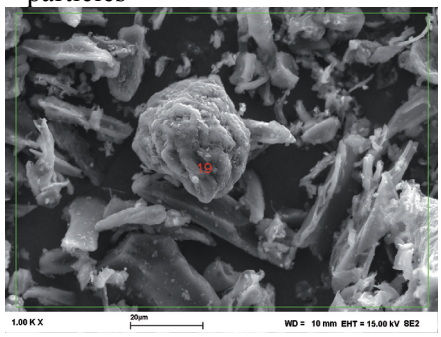

c) Scabrous particles

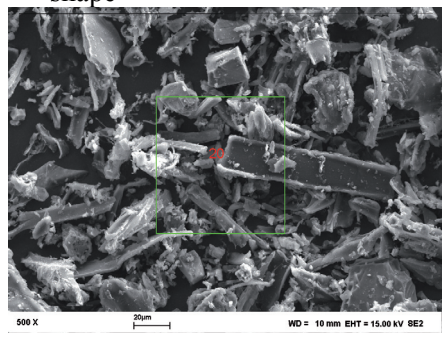

d) Different size of oblong and irregular particles

Figure 2.3 SEM images of Douglas fir char sample (DF800)

The parent material of untreated wheat straw sample is shown in Figure 2.5 a-c. In Figure 2.5a an oblong particle with holes, and similarly to the reed parent material sample, silicon bubbles on the surface are visible as well. In Figure 2.5b an oblong particle with fissures, cavities, holes and scabrous surface can be seen. Figure 2.5c represents the oblong, oval and irregular shape of the particles with longitudinal cavities, holes and fissures on the surface. The EDX spectroscopy analysis indicated a variety of inorganic matter on the surface, however mainly Si, K, Ca, and less Na, Cl and Mg.

The pyrolyzed untreated wheat straw sample is shown in Figure 2.5 d-f where the morphological differences compared to parent material could be observed. In Figure 2.5d an oval char particle can be seen, while the surface could be characterized as a network of cells. In Figure 2.5e an oblong char particle is represented. The circular silicon particles observed on the surface of parent material have lost their initial morphology with the edges smoothed. Inorganic particles could be observed on the surface as well. In Figure 2.5f an oblong char particle with the scabrous surface nature as well as with a network of cells is visible. The migration of inorganic matter on the surface during pyrolysis could be seen. Mainly Si and K were detected on the surface.

Pine pellets

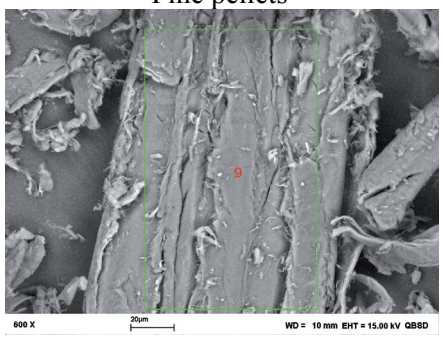

a) Oblong particle with fissures, cavities and scabrous edges

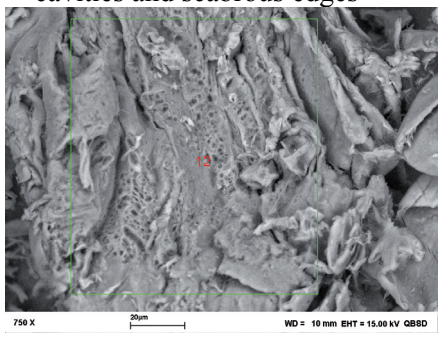

b) Irregular-shaped particle with fissures and holes constituting the network of cells

Pine pellet char

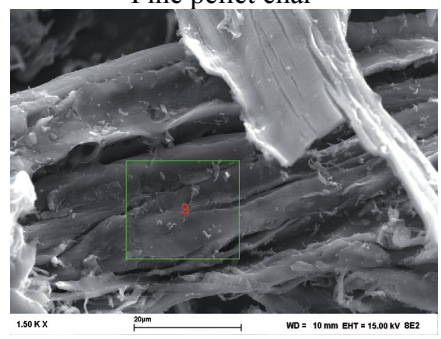

c) Oblong particle with fissures and cavities

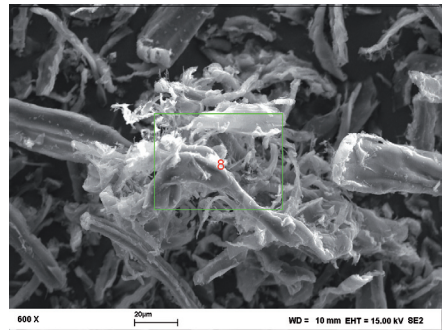

d) Numbers of small thin particles with orders of magnitude larger in length and width than thickness

Figure 2.4 SEM images of pine pellets (PP) and pine pellets char sample (PP800)

The parent material of leached wheat straw sample is shown in Figure 2.6. In Figure 2.6a a fuel particle with silicon bubbles can be seen. In Figure 2.6b the irregular shape of the particle with fissures and holes on the surface is presented. In Figure 2.6c the different shape of particles with longitudinal cavities and network of holes are visible. In Figure 2.6d represents the scabrous surface of the particle with holes. In the WSL case the inorganic matter on the surfaces contains mainly Si and Ca, i.e. K has been removed from the surface via leaching pretreatment.

Untreated wheat straw

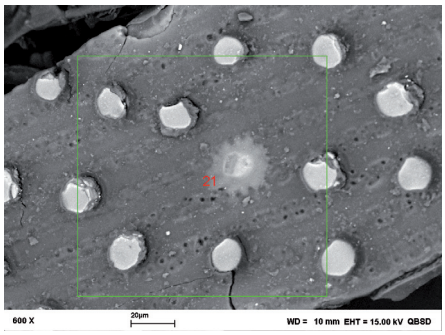

a) Oblong particle with holes and silicon bubbles

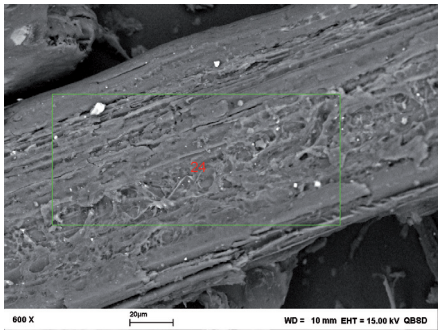

b) Oblong particle with fissures, cavities, holes and scabrous surface

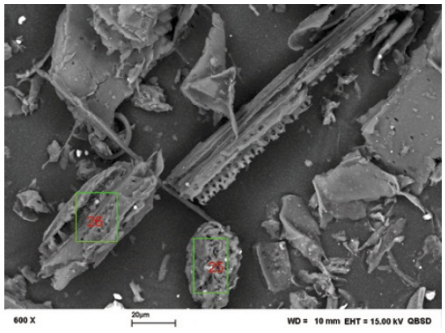

c) Oblong, oval and irregular shape of particles with longitudinal cavities, holes and fissures

Untreated wheat straw char

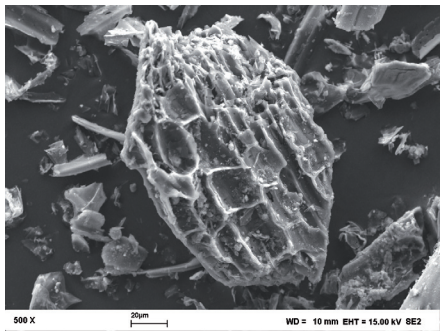

d) Oval particle with a network of cells on the surface

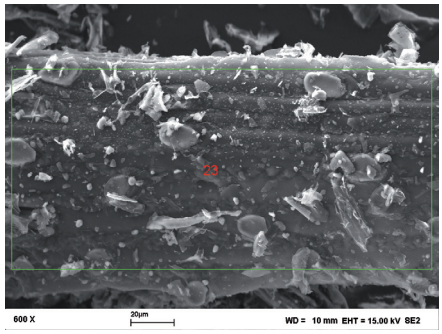

e) Oblong particle with circular silicon particles with smoothed edges and inorganic particles on the surface.

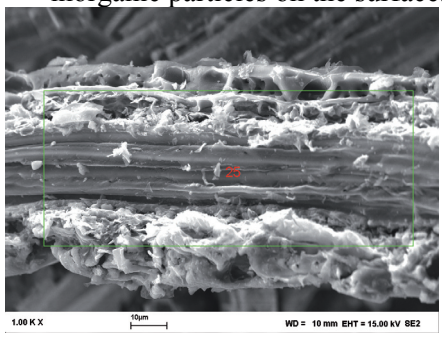

f) Oblong particle with scabrous surface nature as well as with a network of cells

Figure 2.5 SEM images of untreated wheat straw (WSU) and wheat straw char sample (WSU800)

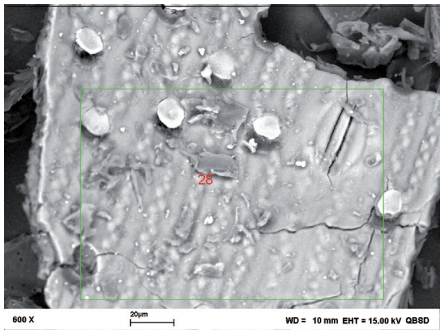

a) Particle with silicon bubbles

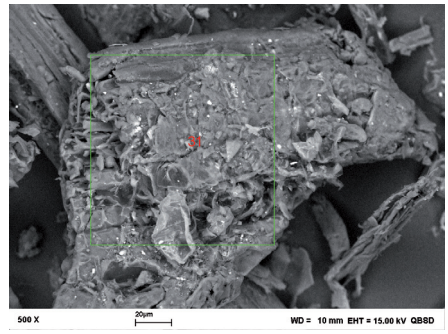

b) Irregular shape of the particle with fissures and holes

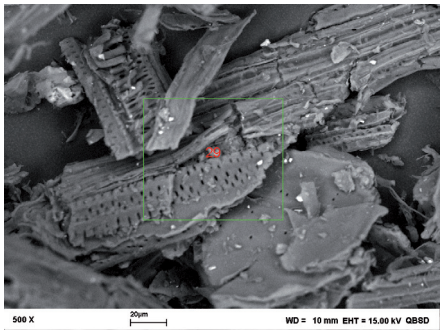

c) Different shape of particles with longitudinal cavities and network of holes

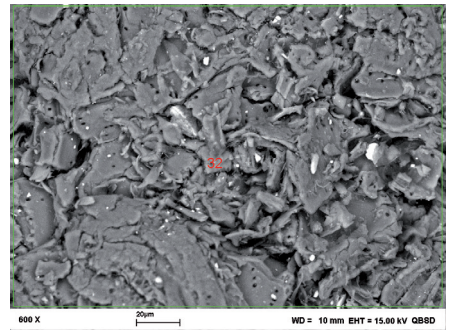

d) Scabrous surface of the particle with holes

Figure 2.6 SEM images of leached wheat straw (WSL)

The pyrolyzed leached wheat straw sample is shown in Figure 2.7. Figure 2.7a represents an oblong particle with the cellular structure inside and softened walls of longitudinal cavities and smoothed edges of silicon bubbles on the surface. In Figure 2.7b a char particle with the smooth surface and holes in the surface of cross-section is presented. The irregular shape of char particle with fissures and scabrous edges can be seen in Figure 2.7c. In Figure 2.7d different size of scabrous particles could be detected. The EDX spectroscopy analysis indicated mainly Si on the surface, but in the moderate amount Ca and K as well. Compared to the parent material, K migrated to the surface during pyrolysis.

Reed had the highest cellulose and hemicellulose content among the studied fuels, and therefore the higher fibrous nature of this material is expected compared to others. While wood and straw samples exhibited higher lignin content, more irregular shapes of those fuel particles can be expected [41].

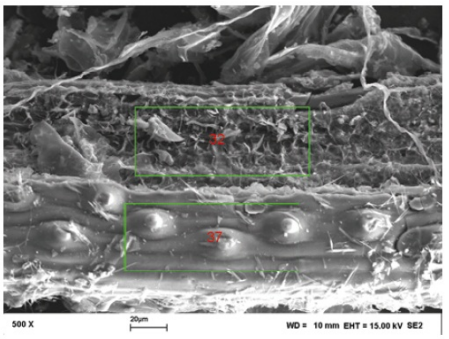

a) Oblong particle with the cellular structure inside and softened walls of longitudinal cavities and smoothed edges of silicon bubbles

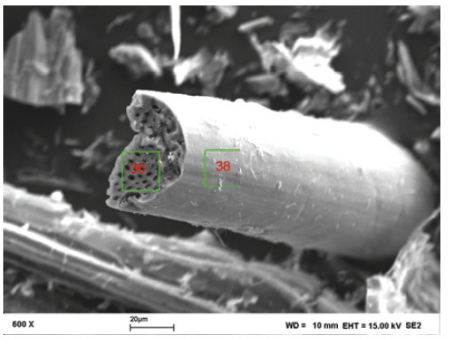

b) Smooth surface and holes in the surface of cross-section

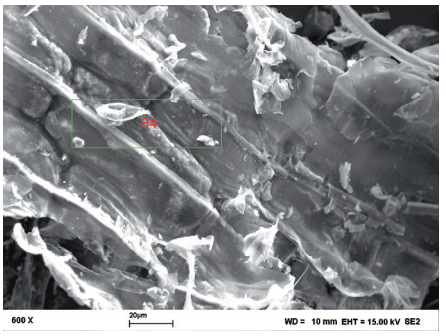

c) Irregular shape of a char particle with fissures and scabrous edges

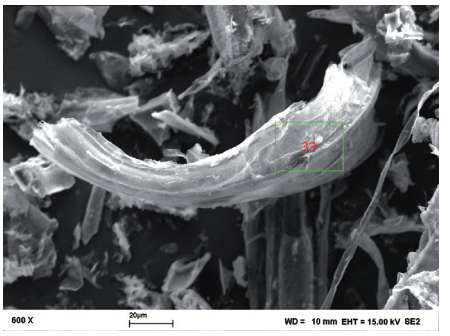

d) Different size of scabrous particles

Figure 2.7 SEM images of leached wheat straw char (WSL800)

Holes, fissures and superficial porosity represent the way for volatile products to escape from the internal zones of fuel particles during pyrolysis and for gaseous reactants to reach the active sites inside the char particle for oxidation or gasification [41].

The images of char samples indicate that the changes during pyrolysis are quite evident resulting from the change of structure and/or mineral matter deposits on the char surface. It could be seen that the carbon morphology was not affected by the leaching process. The migration of inorganic constituents to the surface observed in this study, as a consequence of thermal treatment process, has also taken place with other types of biomass [21,34,42].

2.4 Specific surface area and porosity

The N_2-specific BET (Brunauer-Emmett-Teller) surface area ranges from 25 to 485 $m^2 g^{-1}$ while that of CO_2-specific BET reaches from 348 to 536 $m^2 g^{-1}$, which is slightly lower compared to the values of CO_2 specific DR (Dubinin-Radushkevich) surface area (from 429 to 736 $m^2 g^{-1}$) as shown in Table 2.6. The

N_2-specific BET surface area of the WSU800 exhibits a relatively low value – 25 $m^2 g^{-1}$. It could be presumed that the micropores present on the wheat straw char samples, are not always accessible to N_2, but the leaching pretreatment makes some of the char pores available for the N_2 adsrobate. One reason for this could be blocking of the pores by alkalis on the surface and thus N_2 diffusion through those pores is partially restricted or the pores are fully blocked [43] as visualized in Figure 2.8. The specific BET and DR surface areas are clearly higher for the PP800 sample compared to other studied chars. According to Bar-Ziv et al. [44], the subtraction of volatile matter during pyrolysis is responsible for the formation of new pores. The PP sample exhibits the highest volatile matter content together with the highest specific surface area of char.

Table 2.6 Specific Surface Areas ($m^2 g^{-1}$)

	BET N_2	BET CO_2	DR CO_2
R800	357	435	583
DF800	316	398	545
PP800	485	536	736
WSU800	25	348	429
WSL800	152	354	454

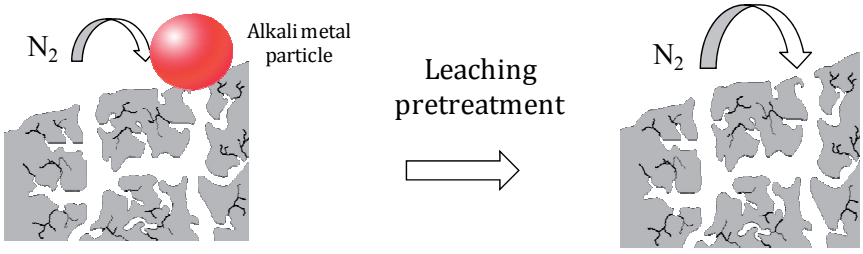

Figure 2.8 Simplified depiction of unblocking the pores after leaching pretreatment

In the literature, Matsumoto et al. [45] report that the cedar char N_2-specific BET surface area is 184 $m^2 g^{-1}$, and Zhou et al. [46] report that the pine tree char N_2-specific BET surface area is 379 $m^2 g^{-1}$. Other studies also suggest that the N_2-specific BET surface areas of other types of wood chars are in the same range of area values when compared to N_2-specific BET surface areas presented in Table 2.6.

The porosity values in Table 2.7 show that the reed and woody fuel chars are mostly microporous, approximately 70-80% of the pores in these chars account for the micropores (pore sizes below 20 Å). In the case of WSU800 the macroporosity is prevailing, and in the case of WSL, the mesoporosity as well.

The results in Table 2.7 also show that the DR CO_2 microporosity is higher than that of DR N_2.

Table 2.7 Porosities obtained from N_2 and CO_2 Isotherms (mL g^{-1})

	DR (CO_2) Microporosity	DR (N_2) Microporosity	(N_2) Mesoporosity	(N_2) Macroporosity	(N_2) Total porosity
R800	0.203	0.137	0.033	0.031	0.200
DF800	0.190	0.121	0.039	0.017	0.176
PP800	0.257	0.184	0.038	0.010	0.231
WSU800	0.150	0.009	0.010	0.015	0.034
WSL800	0.158	0.051	0.082	0.035	0.168

Based on the results, it could be concluded that for some biochars some of the published literature on the values of N_2 adsorption BET area might be slightly underestimated. It seems quite evident that the use of both adsorbates N_2 and CO_2 is needed when the adsorption characteristics of carbonaceous samples with significant microporosity are investigated [31,35] since the micropores contain most of the internal surface area and therefore play the main role in the reactivity of carbons [44].

The results of DFT PSD analysis for R800, DF800, PP800 are shown in Figure 2.9 and Figure 2.10. The results clearly indicate that the PSDs are all quite similar, and therefore completely independent of char origin, whether it is reed or wood.

The WSL800 sample had a network of micropores (Figure 2.11), pores with sizes 8 Å and 16 Å, and a wide network of mesopores 25 Å to 55 Å. The WSU800 exhibits little microporosity (pore sizes around 16 Å), and almost zero mesoporosity compared to the WSL800 sample. Figure 2.12 indicates that all the micropores are accessible for carbon dioxide, and both wheat straw chars have a wide range of supermicropores (pores smaller than 8 Å) as well as reed and woody fuels (not seen with N_2 adsorption DFT analysis).

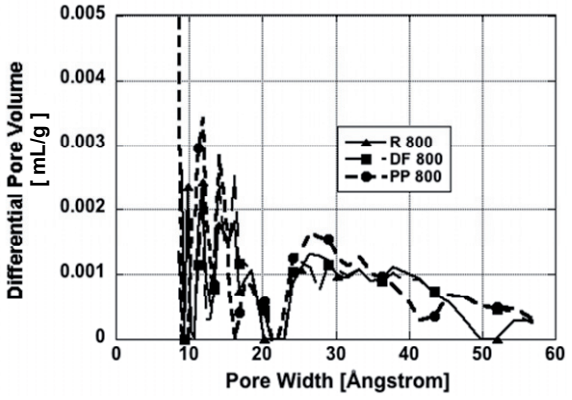

Figure 2.9 DFT/Monte-Carlo differential pore volume distribution of R800, DF800 and PP800. DFT Kernel used: N_2 at –196 °C on carbon

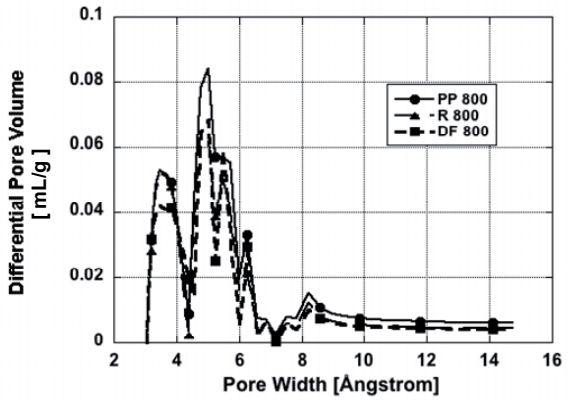

Figure 2.10 DFT/Monte-Carlo differential pore volume distribution of R800, DF800 and PP800. DFT Kernel used: CO_2 at 0 °C on carbon

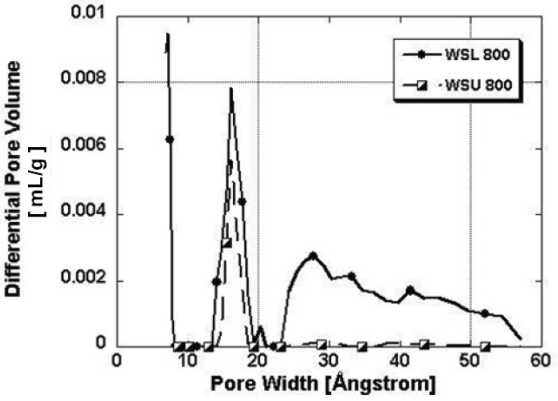

Figure 2.11 DFT/Monte-Carlo differential pore volume distribution of WSU800 and WSL800. DFT Kernel used: N_2 at –196 °C on carbon

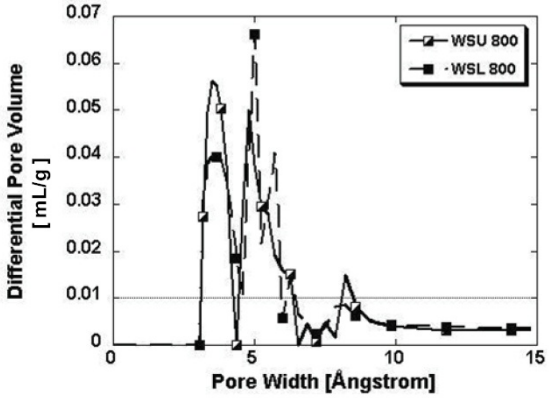

Figure 2.12 DFT/Monte-Carlo differential pore volume distribution of WSU800 and WSL800. DFT Kernel used: CO_2 at 0 °C on carbon

2.5 Carbon-13 NMR spectroscopy

Carbon-13 nuclear magnetic resonance (NMR) spectroscopy was used to identify the various carbon groups in biomass and pyrolysis char samples, to investigate the carbon chemistry of pyrolysis. Also, the change of wheat straw sample after the leaching process was an aim of the investigation.

The ^{13}C CPMAS (Cross Polarization Magic-Angle Spinning) spectra were obtained from the biomass samples within a relatively short time (maximum number of scans was around 200). For the char samples, the needed number of scans was in the range of 4000-6000 due to the fact that chars are less crystalline compared to biomass samples. The single-pulse NMR method results in similar spectra with 3 times shorter period of time. Since the chars are less crystalline and their hydrogen content is lower compared to original fuels, the CPMAS method is relatively inefficient. The same conclusion was also drawn by Freitas et al. [47].

Biomass samples show a variety of carbon resonances, while those of the char samples reveal only a single resonance.

2.5.1 Biomass samples

The results obtained from the NMR spectra of original biomass samples shown in Figure 2.13 and Figure 2.14 show that:

All of the original biomass samples have a peak at 22 ppm assigned to the acetyl methyl groups of hemicelluloses.

At 56 ppm the appeared peak can be assigned to the methoxy groups of lignin.

The peak at 65 ppm is assigned to the aliphatic C6 carbons of crystalline cellulose.

In the region of 72 and 75 ppm, all biomass samples have the highest peak, assigned to the C2, C3, and C5 carbons of cellulose.

All biomass samples have C4 amorphous and crystalline cellulose at 84 and 89 ppm, respectively. Untreated wheat straw has an extra upfield shoulder at 84 ppm that could be attributed to the C_β lignin.

All biomass samples have a sharp peak at 105 ppm assigned to the anomeric carbon of sugars.

The signals in the region of 112 and 115 are assigned to lignin quaiacyl C-2 and C-5, respectively.

Lignin quaiacyl C-6 at 120 ppm is detected only in the case of pine pellets.

Lignin syringyl C-1, syringyl C-5, and quaiacyl C-2 are detected for all biomass samples as a broad line in the region between 134 and 137 ppm.

The signals at 153 ppm are assigned to syringyl C-3 and syringyl C-5. The signals at 148 ppm are assigned to syringyl C-3, syringyl C-5, quaiacyl C-1, and quaiacyl C-4. For the reed the signal at 148 ppm is an upfield shoulder of the signal at 153 ppm. In the case of pine pellets and Douglas fir wood chips, the signal at 153 ppm is a downfield shoulder of the signal at 148 ppm. Wheat straw has a single broad line in this region.

All biomass samples have the acetyl carbonyl groups of hemicelluloses detected at 173 ppm. Although in the case of pine pellets, the signal is very low and scarcely distinguishable from the noise. The carbonyl groups have high reactivity [48].

Ketones in the region of 190-220 ppm are detected only in the case of Douglas fir wood chips. It has to be mentioned that the intensities are very low.

The C_α, C_β, and C_γ carbons of lignin are not detectable because of the high signals of cellulose components in the region of 60-84 ppm. In most cases the peaks of C_α, C_β, and C_γ are much lower, i.e., less intensive, than the peak of Ar-OCH_3 and -OCH_3 functional groups of lignin, and the peaks of cellulose components are more intensive than the peak of Ar-OCH_3 and -OCH_3 [48,49,50].

The broad signals refer to the unordered molecular structure of lignin and hemicelluloses and partly cellulose. Sharp signals at 105, 89, and 65 ppm stand for the ordered cellulose C1, C4, and C6 carbons, respectively [51].

Consequently, it could be said that all of the original biomass samples have basically the same composition with exceptions, only that of Douglas fir wood chips has ketones.

The spectra obtained with the CPMAS method do not allow for any estimation of the contents of lignin, cellulose, or hemicellulose using integrated intensities of the signals because of the interfering peaks of different components. With the spin-locking technique, the spectrum of cellulose can be separated [52,53], but even then, the lignin and hemicellulose spectra remain indistinguishable [54].

When the ^{13}C NMR spectra of the leached wheat straw sample are compared to the original one (Figure 2.14), it is evident that leaching has no effect. The small differences seen in the spectra could be attributed to noise.

2.5.2 Biomass char samples

Different authors have shown that the composition of wood changes during thermal treatment [55].

New carbon groups evolve, but finally at the end temperatures of pyrolysis at 600 °C, there are only aromatic groups left [47,49,56].

Sharma et al. [49] have shown that the amount of aromatic carbons in a lignin char is less than in the original sample material. In their work, the concentration of aromatic lignin was decreased by 10% by weight at a heating temperature of 600 °C compared to the original sample material. Thus, most of the weight loss of the original lignin sample was due to the volatilization of nonaromatic carbons. The aromatic component of lignin is very resistant to thermal degradation, and the resulting char is highly refractory.

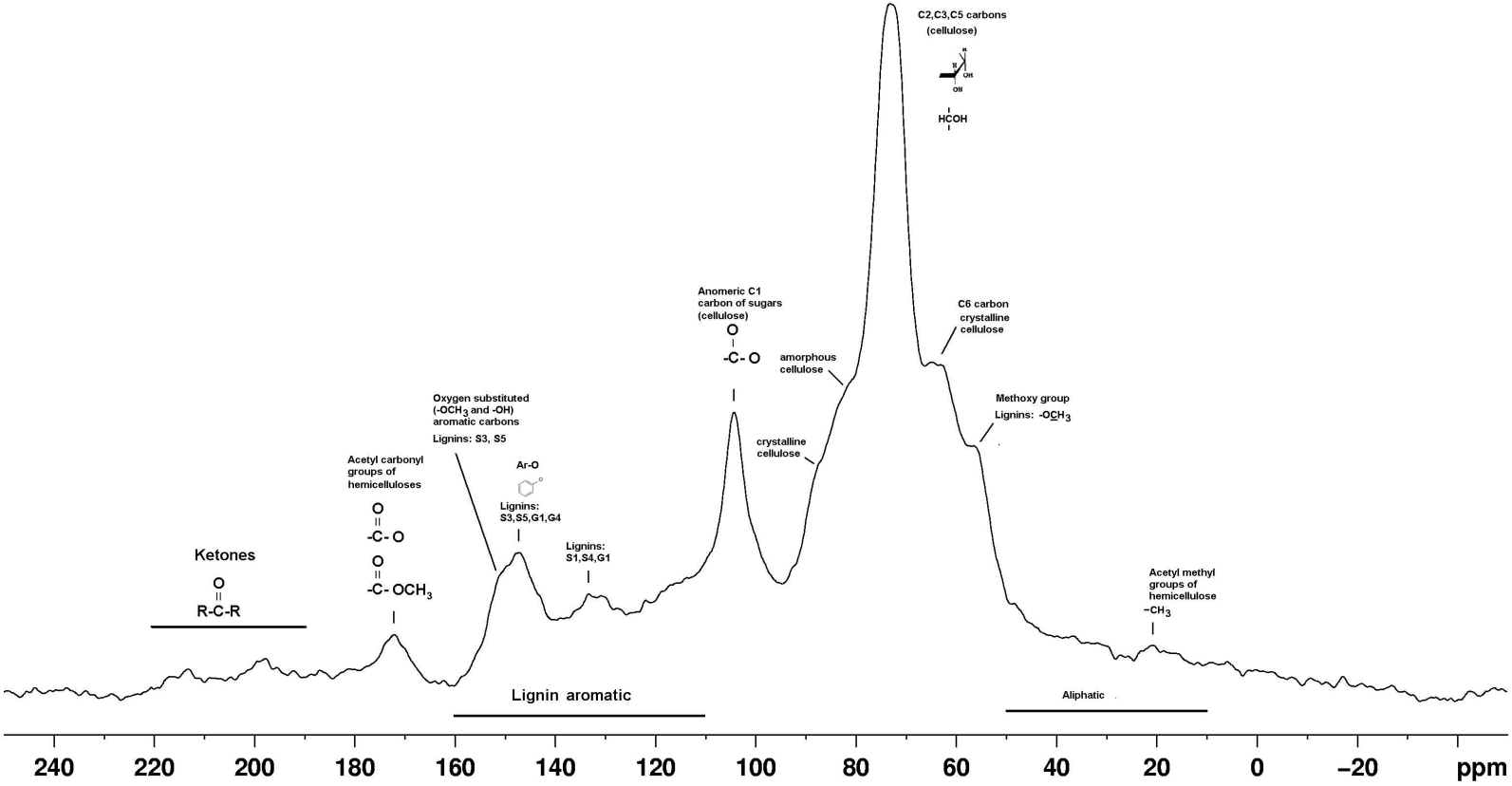

Figure 2.13 Spectrum of ^{13}C CPMAS NMR of the Douglas fir sample

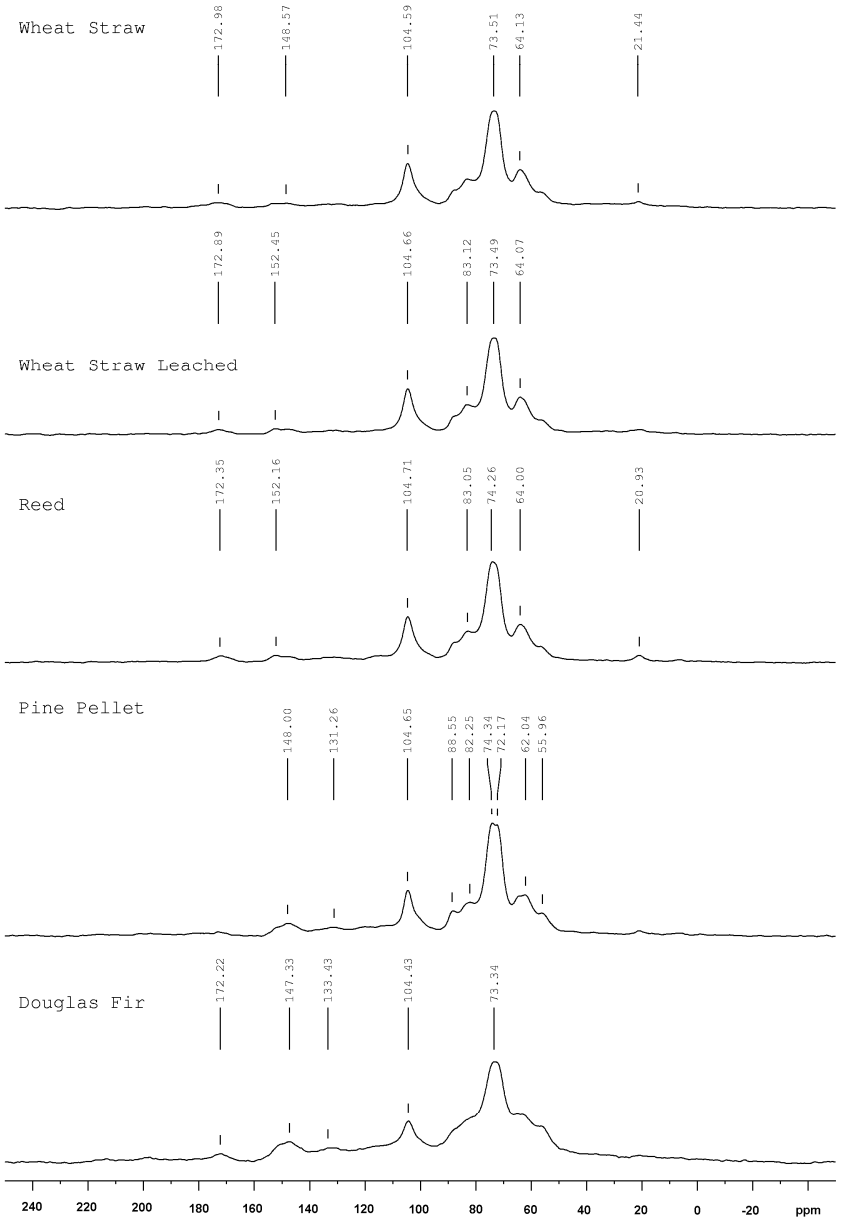

Figure 2.14 Spectra of ^{13}C CPMAS NMR of different biomass samples

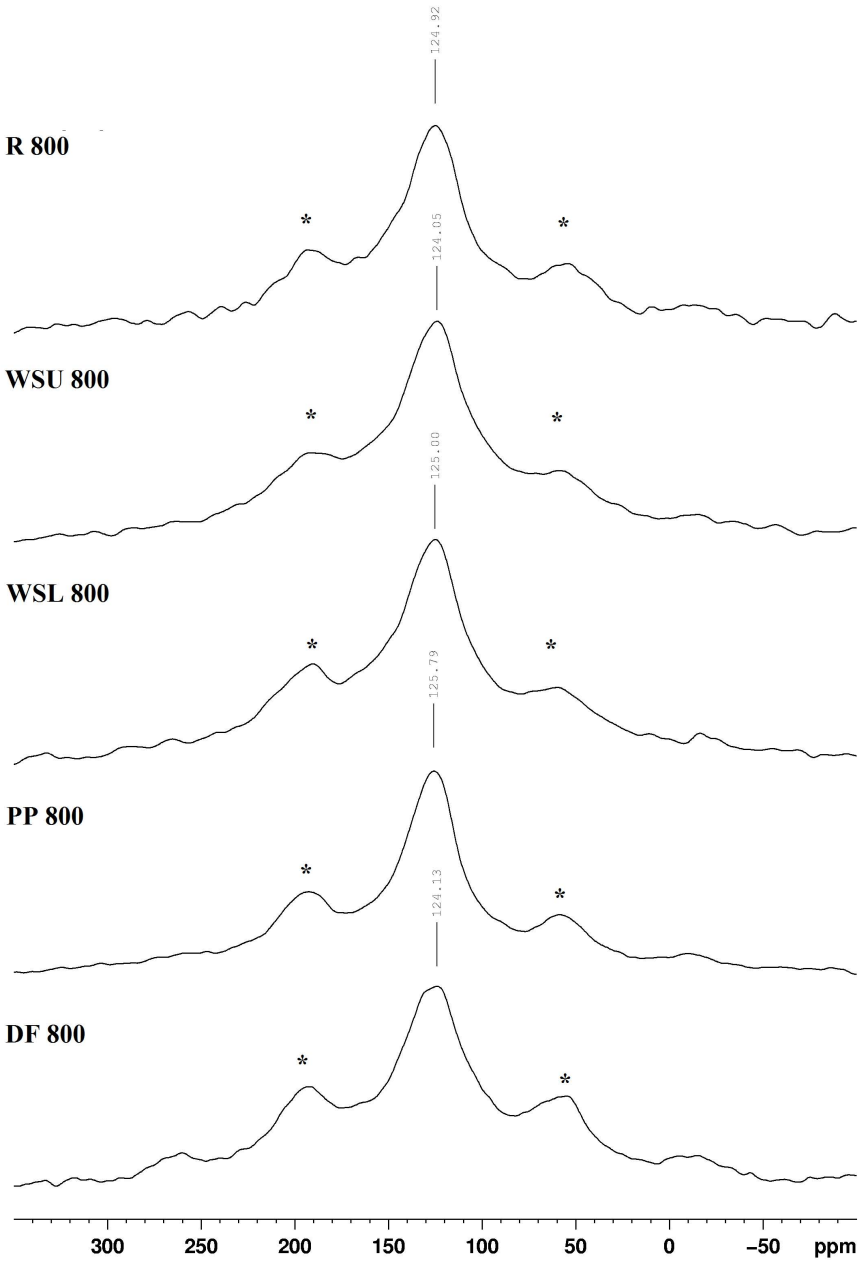

Figure 2.15 Spectra of ^{13}C single-pulse MAS NMR of different biomass char samples (*-spinning sideband)

Bardet et al. [56] have stated that the origin of biomass does not affect the nature of the solid residues formed during the thermal treatment. They all lose their ligno-cellulosic structure and are transformed to polycyclic material with a preponderance of aromatic structures with proton amounts that are decreased drastically as the temperature of treatment increases. It could be said that all cellulose and lingo-cellulosic materials under thermal treatment with the final temperatures between 800 and 1000 °C undergo structural transformation, resulting in a graphitic structure.

All of the pyrolysis char samples (as seen in Figure 2.15) have one peak at 124-126 ppm assigned to aromatic lignin, and no differences were found between various char samples.

2.6 Sodium-23 MAS NMR spectroscopy

Sodium-23 magic-angle spinning nuclear magnetic resonance (MAS NMR) spectra are usually un-informative as to the specific identity of environments surrounding the ^{23}Na nuclei in amorphous systems, mainly because of the broad line shapes encountered. Another difficulty in ^{23}Na NMR is the ability of MAS to completely average away the effects of second-order quadropolar interactions, leading to residual line broadening in ^{23}Na MAS spectra [57]. The sodium content in the sample is extremely low and therefore limited to a very basic single-pulse technique. Considering also relatively modest magnetic field strength available for the study, a certain second-order line shift and broadening can be assumed. Therefore, we can make assumptions based only on peak line shifts, combined of comparable second-order quadrupole and isotropic chemical-shift variations. A true chemical shift can be assumed to range from the peak to the left side foot of the line [58].

The tests with sodium compounds in which the oxygen atoms are bonded to various elements of the third row of the periodic table (Al, Si, P, S, and Cl) carried out by Koller et al. [59] have shown a systematic shift to high field with an increasing atomic number of the third-row elements. As a consequence, they have concluded that the isotropic chemical shift is related to the particular chemical environment of the oxygen atoms coordinated to sodium. The distinct chemical-shift effects observed for ^{23}Na in different compounds have the same origin and the particular bonding situation of the oxygen atoms in the anions. This property can be described by the valence, i.e., the total bond valence of the oxygen atom. Of course, the chemical shift of the solids is further affected by Na-O distances and the coordination number of sodium.

There are few data available about ^{23}Na NMR of fuels and char in the literature. Burchill et al. [60] has investigated sodium with NMR in raw coals. They have shown that the sodium peak appears between 2.3 and -1.7 ppm, i.e., closely comparable to aqueous Na+, but in our case, the peaks are far away from this region. This allows for the assumption that there is no or few aqueous Na+ in the investigated biomass samples.

2.6.1 Biomass samples

The results of the ^{23}Na NMR spectroscopy of biomass samples are shown in Figure 2.16. For all samples, an isotropic peak at -11 ppm is identified in the spectra, except for Douglas fir and leached wheat straw where single resonances are found at -22 and -5 ppm, respectively. Wheat straw has an extra resonance at 7 ppm, which can be attributed to crystalline NaCl. Although high amounts of scans were recorded for pine pellets (Table 2.8), the signal-to-noise ratio is poor, resulting in less reliable results.

Table 2.8 Amounts and Number of Scans of the Biomass Samples, ^{23}Na MAS NMR Spectroscopy

	Reed	Pine pellets	Douglas fir wood chips,	Wheat straw	Wheat straw leached
Sample mass, g	0.2378	0.2416	0.2471	0.2172	0.2236
Number of scans	2 237	63 235	4 400	1 225	1 225

2.6.2 Biomass char samples

The effect of pyrolysis and leaching pretreatment on the sodium environment of biomass samples is shown in Figure 2.17.

The spectra of reed char sample resulted in an isotropic peak at the same region with the reed sample. This allows for the assumption that the sodium environment in the reed sample is resistant to the pyrolysis conditions described above.

The pine pellet char sample displays a broad line in the region of 100 to -100 ppm resembling to the original pine pellets sample.

In comparison to the original Douglas fir wood chips sample, the changes in the line shape of the char samples could be detected. Instead of a relatively symmetrical shape of the peak in the case of original Douglas fir wood chips sample, the char sample of these wood chips exhibited relatively structured lines, which are compatible with a second-order quadrupole line shape, corresponding to a coupling constant of 2.1 MHz and chemical shift of -10 ppm. Equally plausible alternatives to this assumption are two chemical-shift-separated lines with a very low coupling constant at -10 and -25 ppm, respectively.

In comparison to the original wheat straw sample, there is only a one peak in the region from -4 to -7 ppm for the char sample, instead of two peaks at 7 ppm assigned to crystalline NaCl and at -11 ppm for parent fuel.

No difference could be detected between the spectra of wheat straw char samples and leached wheat straw char samples.

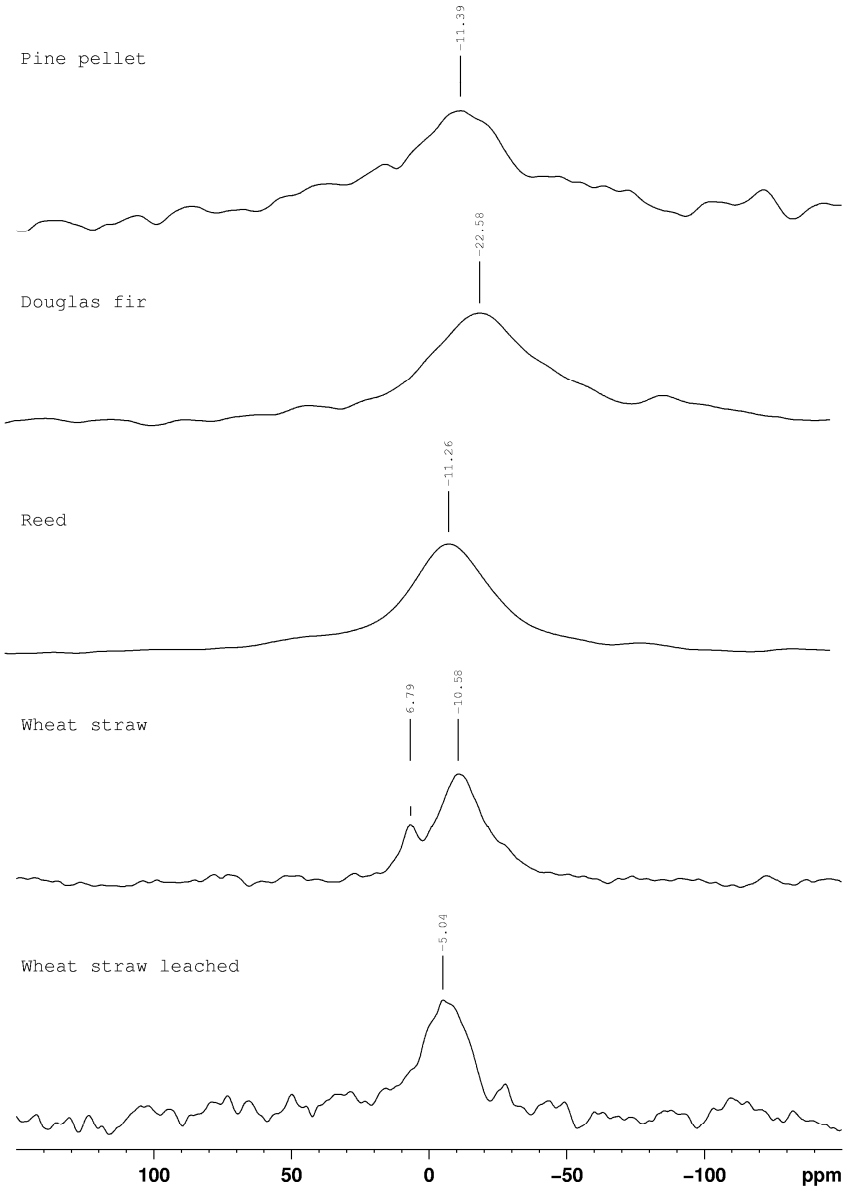

Figure 2.16 Spectra of ^{23}Na single-pulse MAS NMR of different biomass samples

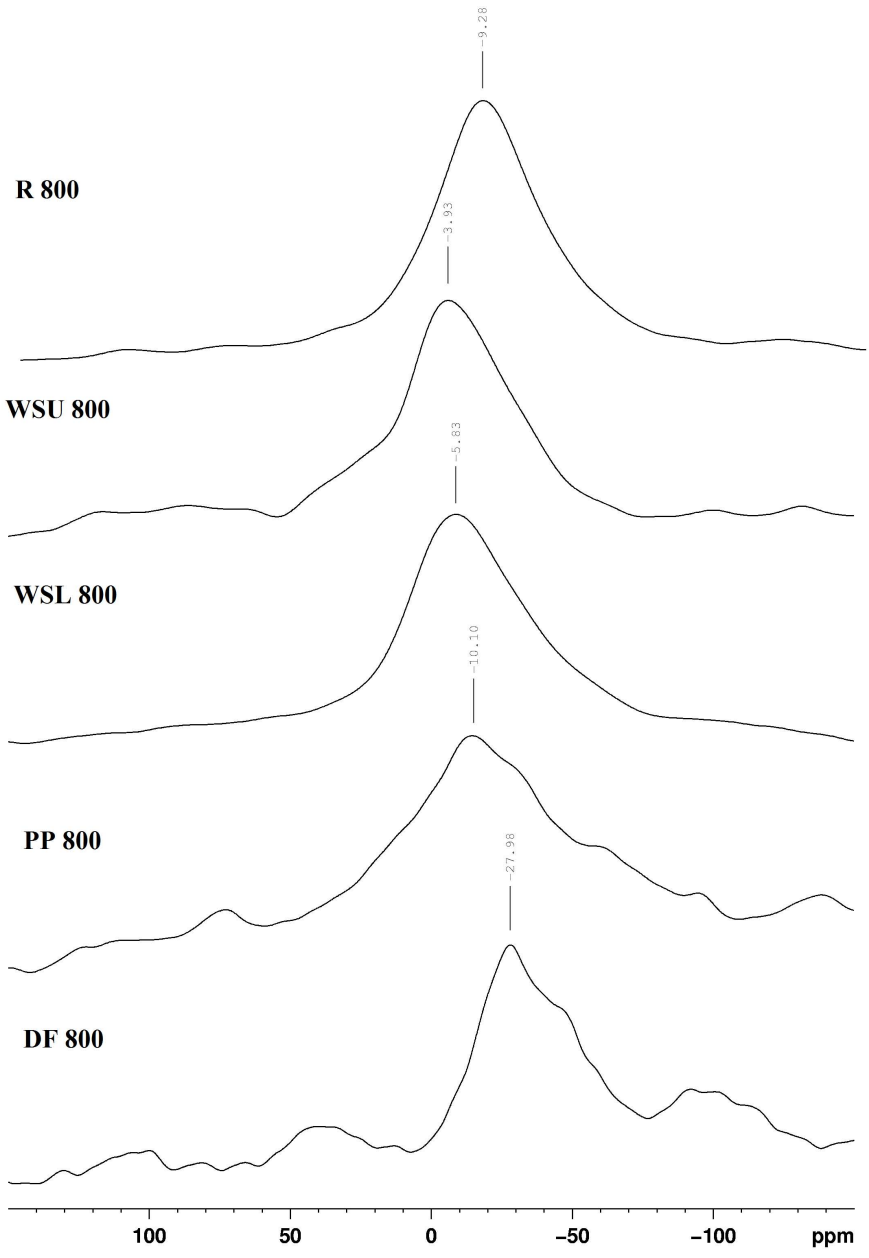

Figure 2.17 Spectra of ^{23}Na single-pulse MAS NMR of different biomass char samples

2.7 Char reactivity

The series of char reactivity measurement tests of the studied chars were performed at 750, 800, 850, and 900 °C. The weight signal curve shifted downward (Phase I; see also Figure 1.5), and increase in the sample weight at the beginning of Phase II was likely due to the buoyancy effect resulting from the change in the reactor feed gas.

The reaction rates versus char conversion of the R800, DF800, PP800, WSU800, and WSL800 samples at different gasification temperatures are shown in Figure 2.18- Figure 2.22. In most cases the initial 10% and 50% of conversion is used for evaluating the kinetic parameters [14]. In this work 50% of conversion was chosen.

The reaction rate of R800 was slightly increased up to the conversion rate of 40% and then declined. The reaction rate of DF800 at the gasification temperatures of 850 and 900 °C decreased until the conversion rate of 40-50%, then remained constant up to the conversion rate of 60-70%, and then declined. The reaction rates of PP800 were constant, with the exception at the beginning in the temperature of 900 °C experiment, up to the conversion rates of 60-70%, and then the reaction rate decreased. Both WSU800 and WSL800 samples exhibited the maximum reaction rate between the char conversion rates of 20 and 40%.

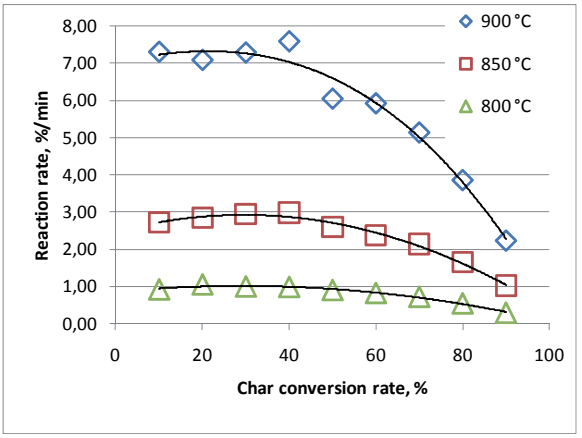

Figure 2.18 Char gasification reactivity of the reed char sample R800

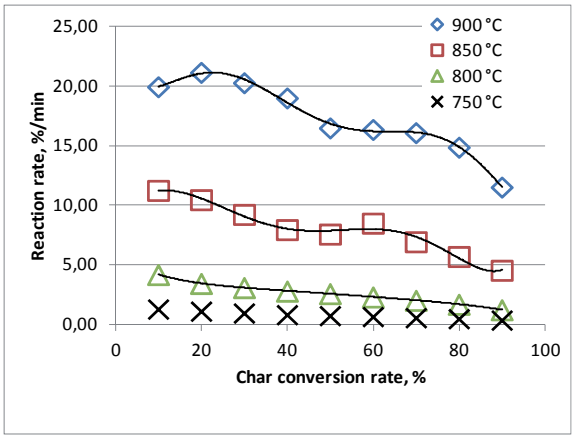

Figure 2.19 Char gasification reactivity of the Douglas fir char sample DF800

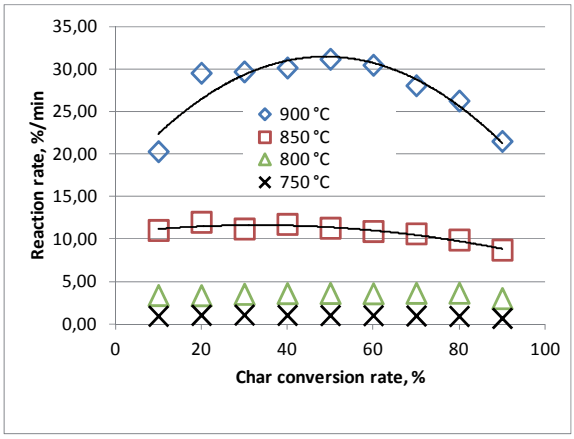

Figure 2.20 Char gasification reactivity of the pine pellets char sample PP800

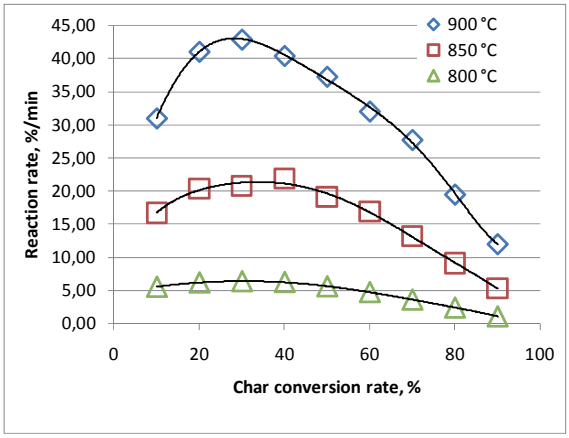

Figure 2.21 Char gasification reactivity of the untreated wheat straw char sample WSU800

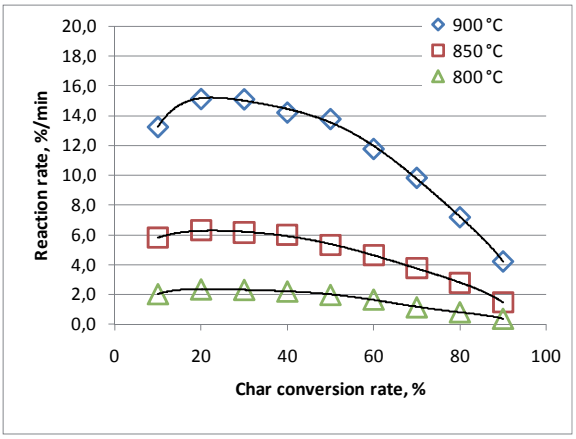

Figure 2.22 Char gasification reactivity of the leached wheat straw char sample WSL800

It could be seen that the untreated wheat straw char exhibited the highest maximum reaction rate among other studied chars. The wood chars had higher reaction rate than the reed and leached wheat straw chars. The reed char exhibited the lowest reaction rate. For instance, the WSU800 reaction rate between the conversion rates of 20 and 40% was ~1.5 times higher compared to PP800 while PP800 reaction rate was approximately 4 times higher between the conversion rates of 20 and 40% compared to that of R800. The DF800 reaction rate was 3 times higher compared to R800. A clear distinction between the DF800 and PP800 reaction rates can be seen at the gasification temperature of 900 °C. Compared to the untreated wheat straw the leached wheat straw chars exhibited from 2 to 4 times lower reaction rates depending on the conversion rate and temperature.

As expected, the char reaction rates increase with the rise of temperature. The reaction rate of the R800 sample was enhanced 3 times between the conversion rates of 20 and 40%, while the temperature was increased by 50 °C. For wood and wheat straw, the rate increased from 2 to 4 times depending upon the fuel and gasification temperature.

The conversion rate versus the time of gasification tests is shown in Figure 2.23-Figure 2.25. PP800 and WSU800 exhibited the shortest gasification time while R800 exhibited the longest gasification time.

According to Figure 2.18-Figure 2.28, the order of reactivity of the studied chars can be seen as following: WSU800≈PP800>DF800>WSL800>R800.

The interaction between the compounds present in the mineral matter could inhibit the catalytic effect of alkali and alkali earth metals (AAEM), which could lead to the compound in which, for instance, potassium is totally inactive [61]. The catalytic deactivation reaction depends only upon time and not so much on temperature and pressure. At high conversion, the catalyst seems to lose its contact with carbon and, consequently, its activity [62]. The deactivation process

of catalysts takes place already in the pyrolysis step, which in this study is so-called slow pyrolysis and continues in the gasification step.

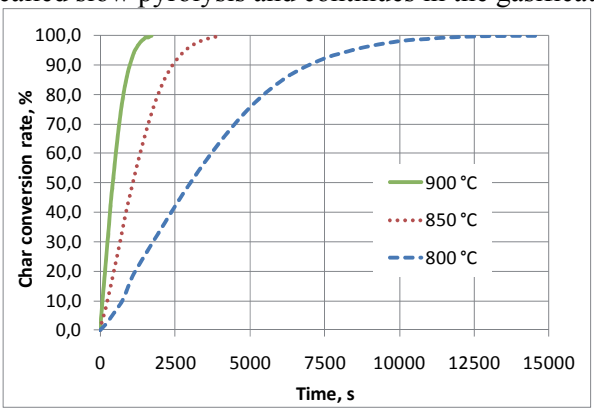

Figure 2.23 Conversion rate versus the time of gasification for the reed char sample

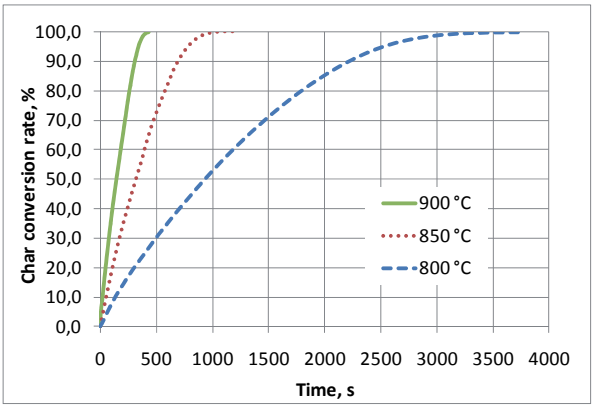

Figure 2.24 Conversion rate versus the time of gasification for the Douglas fir char sample

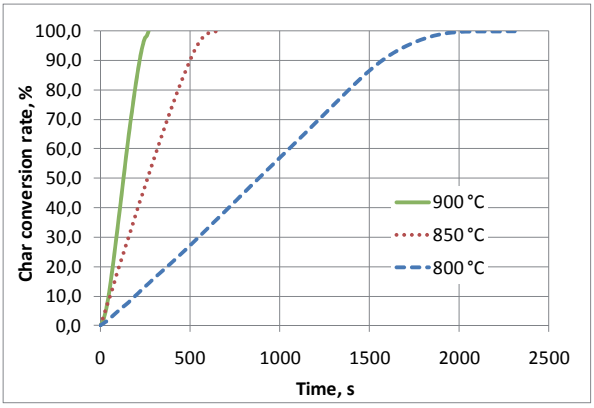

Figure 2.25 Conversion rate versus the time of gasification for the pine pellets char sample

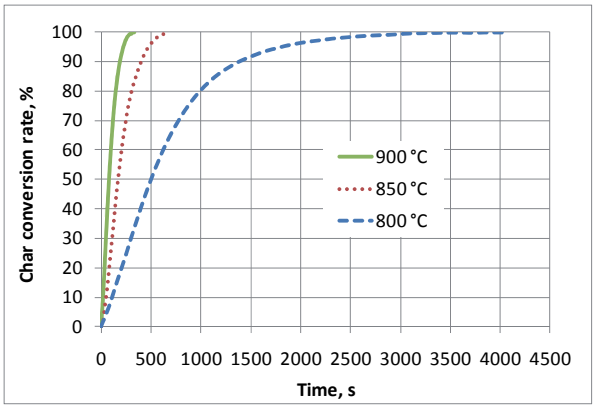

Figure 2.26 Conversion rate versus the time of gasification for the untreated wheat straw char

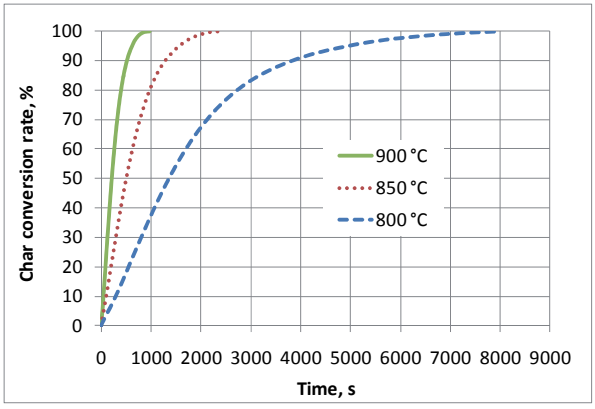

Figure 2.27 Conversion rate versus the time of the gasification for the leached wheat straw char sample

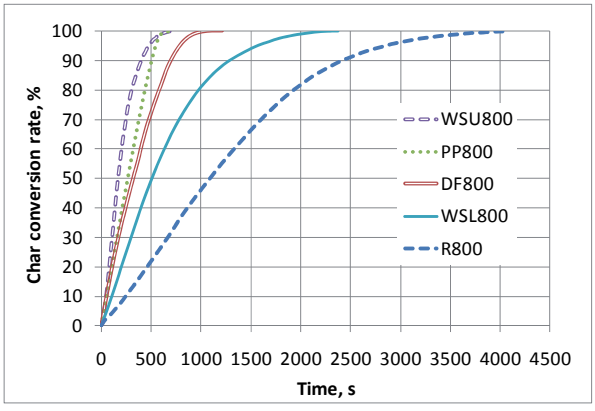

Figure 2.28 Conversion rate versus the time of gasification tests for the studied chars at the gasification temperature of 850 °C

According to Zevenhoven-Onderwater et al. [63], the next processes are expected to take place: (1) formation of calcium, potassium, magnesium, sodium, and aluminium silicates during thermal treatment is expected; (2) high silica content of reed and Douglas fir chars yielded potassium silicates, whereas high silica and high chlorine contents gave potassium silicate formation combined with the release of HCl and the formation of K_2CO_3 did not occur; (3) in the case of a pine pellet, which is low in silica content, K_2CO_3 was formed during the gasification (known as a better catalyst, for instance, compared to sodium and calcium carbonates [64]). The formation of KCl was expected as well.

The formation of silicates reduces the amount of available AAEM taking part in the solid-gas reaction on active sites. According to Radovic et al. [65], the reactivity is rather more dependent upon carbon active sites than the total surface area. Van Heek et al. [61] have concluded that the extension of total surface area could not be alone the dominating factor, which is more likely to be the qualities of the surface, such as activity and accessibility, which give the possibility of blockage areas by minerals. Bar-Ziv et al. [44] concluded that the evolution of reactivity during conversion is influenced by changes in the porous structure, and coalescence of microcrystals can be used to represent the change in the concentration of the reactive sites. Livneh et al. [66] confirmed that the most significant change in reactivity occurs in the range of 0-30% conversion, and the slowdown of reactivity at the conversion rate above 55% can be explained by the consumption of small microcrystals, which are generally more reactive than large ones.

The initial increase in the reaction rate in the case of R800 and wheat straw chars could be associated with the increase of the surface area as well as active sites in the early phase of gasification. The maximum in the reaction rate, considering porosity, is thought to arise from two opposing effects, namely, increase in the reaction surface area as micropores grow and their decline as pores collapse progressively at their intersection (coalescence) [67]. The decrease in the reaction rate is affected by the deactivation of catalysts, and therefore, less active sites are available along the process as well.

The oxidation reactivity of chars is affected by the mineral matter content and composition, and according to the tests, we can order the char samples by different items as following:

- Ash content:

WSL800(36%)>WSU800(28%)>DF800(21%)>R800(16%)>PP800(4%).

- Si content:

WSL800(8.33%)>WSU(6,74%)>R800(6.15%)>DF800(5.03%).

- K content:

WSU800(4.22%)>WSL(1.37%)>DF800(0.82%)>R800(0.44%).

- Ca content:

WSL800(4.73%)>DF800(1.43%)>WSU800(1.27%)>R800(0.47%).

- AAEM content:

WSL800(7.42%)>WSU800(5.95%)>DF800(3.42%)>R800(1.31%).

- O/C ratio:

WSU800(0.37)≈PP800(0.35)>DF800(0.27)≈WSL800(0.27)≈R800(0.28).

- H/C ratio:

WSU800(0.29)> R800(0.25)>PP800(0.22)>WSL800(0.21)>DF800(0.19).

The WSL800 sample exhibited the highest Si content in the chars as well as the highest AAEM content. The high AAEM content results from the highest ash content in the char where the main AAEM element is Ca. But for instance, the K content in the WSL800 sample is 3 times lower compared to WSU800. K is considered to be the most active catalyzing element for the char gasification [64,68,69].

The O/C and H/C ratio was the highest for WSU800. For WSU 800 and PP800 the O/C ratio was quite similar, but higher compared to the values for DF800, PP800 and R800. Last three samples had the similar O/C ratio values as well.

The results in this work indicate that PP800 is more reactive compared to R800 and DF800, despite the fact that the pine pellet contains over 5 and 15 times less elements acting as catalysts (K, Na, Ca, Mg, and Fe) compared to reed and Douglas fir wood chips, respectively. The ash content of pine pellet char is 4%, and according to the parent material ash chemical analysis, it contains mainly Ca and K as well and is not rich in silicon. Therefore, according to the results, the high porosity of PP800, together with the structure of pores, nature of mineral matter and relatively high O/C ratio can be seen to be the reason, considering the total gasification time, for the high reactivity comparable with WSU800 and higher compared to the others. K and Ca did not form silicates, but rather compounds bound to the carbon matrix acting as an active site. Heteroatoms such as hydrogen and oxygen may act as adsorption sites and thus could be related to the availability of active sites in char and therefore influence its reactivity with different gases present in the combustion systems [70,71]. The SEM images have shown that the pine pellet char particles have the so-called thin plate shape, i.e. the length and width of the particle is an order of magnitude larger compared to thickness and the surface of particles is porous as well. One could consider that these plates are placed one by one and the space between the plates could be considered pores as presented in Figure 2.29 while these pores are also opened at both ends (through pore), as shown in Figure 2.30 [72]. The steady reaction rate of PP800 along the gasification process can be attributed to the nature of char particles, i.e., the gasification agent reacts with the char material on the so called plate wall and consumes the material, but the total and active surface areas together did not change along the process significantly. However, the evolution of the total surface area of studied chars along the gasification process needs further investigations.

The leaching pretreatment of parent fuel affects the char gasification reactivity. The char of leached wheat straw sample contains more AAEM and it is due to the higher ash content of the char sample, but higher Si content as well compared to the untreated wheat straw char. As mentioned above, K is the main catalyzing element, and the K content of leached wheat straw char is three times lower than the untreated one. The lowered amount of K and relatively high Si content in the leached wheat straw char reduces the catalytic effect of K. The O/C and H/C ratio of leached wheat straw char is lower than that of untreated wheat straw and this is also the reason for lower reactivity.

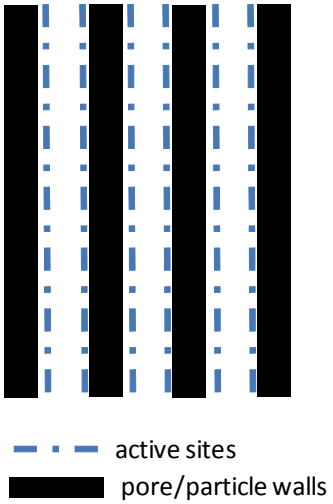

Figure 2.29 Visualisation of pore walls of PP800

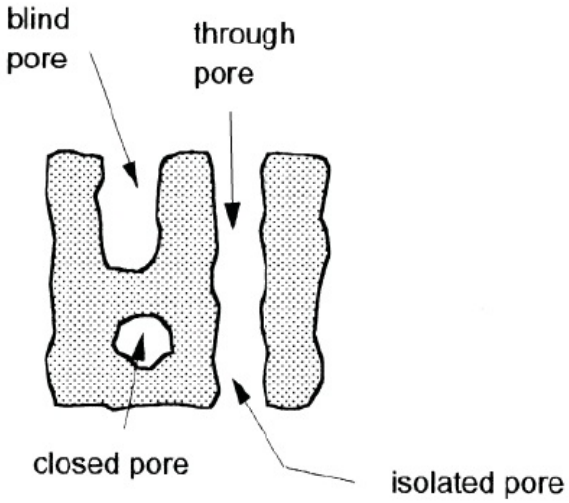

Figure 2.30 Types of pores [72]

The results of the residue yields, i.e. ash and unconverted carbon, in the char gasification tests at the temperature of 850 °C and the total residue yields calculated from the initial parent material mass after the conversion because of pyrolysis and gasification are shown in Table 2.9 and Table 2.10. PP800 exhibited the lowest residue yield after char gasification on a dry basis (see also Table 2.9). The residue yield from the gasification of DF800 was higher by 4.6% compared to that of R800, but when calculated on a dry and ash-free (daf) basis, R800 exhibited a 9 times higher residue yield compared to DF800. Accordingly, it can be seen that DF800 reached a higher carbon conversion during gasification than R800.

Table 2.9 Residue yield of char gasification at 850 °C (%)

	Dry basis	Daf basis
R800	15.62	0.80
DF800	20.26	0.09
PP800	1.96	n.d.
WSU800	23.72	6.47
WSL800	38.60	6.11

Table 2.10 Total residue yield after pyrolysis and char gasification with the gasification temperature of 850 °C (%)

	Dry basis	Daf basis
R800	3.08	0.17
DF800	5.94	0.02
PP800	0.34	n.d.
WSU800	7.13	1.35
WSL800	10.47	1.02

The total residue yield shown in Table 2.10 has been calculated over the pyrolysis and gasification steps. A lower total residue yield of DF800 on a daf basis indicates better carbon conversion to a gaseous substance along the pyrolysis and gasification steps compared to R800. It could be considered that there is almost no carbon left in the gasification residue for PP800 (see also Figure 2.31), and therefore, the total residue yield on a daf basis is principally almost zero.

The wheat straw samples exhibited the highest residue yield (daf basis), and compared to other studied chars the remained residue, i.e., the ash of wheat straw contains more carbon.

For the activation energy determination in the gasification reaction, it is necessary to know when the process is in a kinetically controlled regime (see also Figure 2.32). The activation energies (were in the range of 199-229 kJ/mol) and the pre-exponential factors of the chars tested are shown in Table 8. According to Barrio et al. [73], most values of the activation energy for different biomasses, gathered from various studies for the CO_2 gasification remain in the range of 196-250 kJ/mol, which is in good agreement with results of this work.

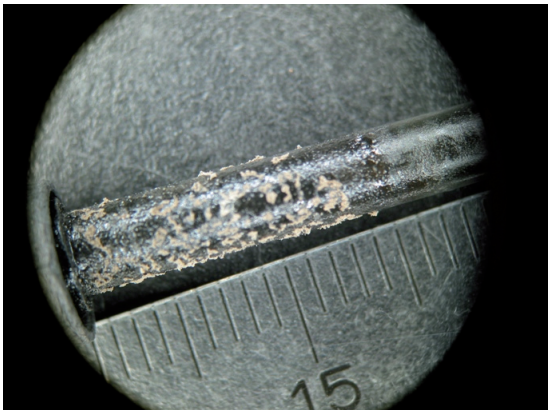

Figure 2.31. Sample of the light brown coloured gasification residue of pine pellet char sample PP800

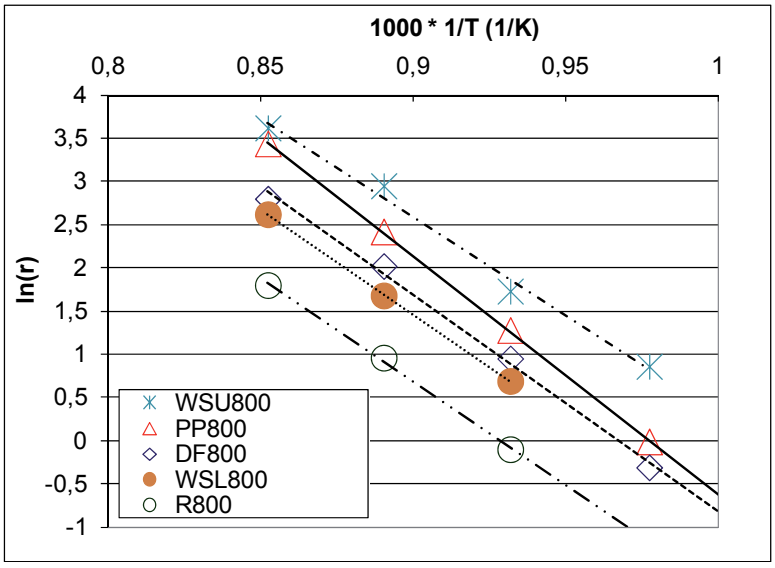

Figure 2.32. Arrhenius plots when gasifying the chars in CO_2 (rates taken at 50% of conversion)

Table 2.11 Gasification activation energies and pre-exponential factor at 50% of conversion

	Activation energy kJ/mol	Pre-exponential factor 1/s
R800	199	$1{,}30 \times 10^6$
DF800	208	$9{,}95 \times 10^6$
PP800	229	$1{,}40 \times 10^8$
WSU800	190	$3{,}66 \times 10^6$
WSL800	202	$3{,}69 \times 10^6$

3 CONCLUSION

- All the studied chars showed different reactivity under the CO_2 gasification conditions. In general, based on this study, the order of the reactivity of chars can be seen as following: WSU800≈PP800>DF800>WSL800>R800.
- The gasification time for reaching the conversion rate of 100% was the longest for the reed char and shortest for the pine pellet and untreated wheat straw chars.
- The leaching pretreatment of parent fuel affects the char gasification reactivity. The gasification time for reaching the conversion rate of 100% was 3.5 times higher for the leached wheat straw char sample than for the untreated one.
- According to the ^{23}Na NMR spectroscopy, sodium chlorine present in the untreated wheat straw was removed via leaching.
- According to the ^{13}C nuclear magnetic resonance (NMR) spectroscopy, there is no difference between the chars, though the distinctions in the parent fuel are quite clear. All the chars contain aromatic lignin.
- According to the ^{23}Na NMR spectroscopy, there is no difference between the sodium environment of untreated and leached wheat straw chars. Though, in the future, using more sophisticated NMR methods, the distinctions could be visible.
- Scanning electron microscopy (SEM) tests showed changes in the surface morphology and migration of inorganic matter onto the surface of char particle as a result of pyrolysis.
- The specific BET (Brunauer-Emmett-Teller) and DR (Dubinin-Radushkevich) surface areas are clearly higher for the PP800 sample than for other studied chars.
- According to the SEM images, the pine pellet char (PP800) has plate like particles and when arranged tightly close to each other the spaces between them could also be considered pores.
- The reaction rate of PP800 was quite stable along the gasification process behaving differently for other studied chars. This so-called stable reactivity has been explained in such a way that although the mass of char material declines during the reaction, the surface area or active surface where the gas reacts with char remains almost constant during the process. With the reaction on the plate like particle surface the plate thickness will be reduced when its length and width do not change significantly. To the end the material mass will be totally exhausted during the reaction process and with the loss of mass there will be no surface left for the reaction, thus the reactivity will drop to zero.
- The short gasification time of PP800 is due to the nature of char particle, the high surface area, i.e., the active sites, high O/C ratio and low Si content in ash. The example of PP800 showed that the amount of inorganic matter

acting as catalyst in the material is not always the dominant factor towards higher reactivity.

- The impact of alkali and alkali earth metals (AAEM) on the gasification catalysis was inhibited by high Si content in the case of Douglas fir wood chip, leached wheat straw and reed chars.
- Relatively high Si content and lower AAEM content in the reed char are expected to be the main reason for the lowest gasification reactivity among the studied chars.
- The high reactivity of untreated wheat straw char (WSU800) could be imputed to the higher O/C and H/C ratio compared to other chars as well as to the highest potassium content in the char, though the Si content is relatively high as well.
- The lower reactivity of a leached wheat straw char sample could be attributed mainly to the lower K content together with the relatively high Si content and lower O/C ratio compared to untreated wheat straw char.
- In practice, one must optimize or find a balance between the leaching costs, capacity loss of the reactor due to a less reactive fuel, and maintenance costs due to corrosion etc.
- The N_2-specific BET surface area of WSU800 exhibits a relatively low value – 25 m^2 g^{-1}, i.e., approximately eight times lower compared to WSL800. One reason for this could be blocking of pores by alkalis on the surface while the N_2 diffusion is partially restricted through those pores or the pores are fully blocked.
- On the basis of the results, pine pellets would be preferred as a fuel source compared to other studied materials. The pine pellets char showed high reactivity, which means a smaller size of the reactor requirement at the same output, and lower ash amount removal from the reactor to save on otherwise high ash landfilling costs. Lower alkali metal content leads to higher ash melting temperatures and less corrosive environment. The higher is the ash melting point, the higher temperature can be used in the reactor and the higher is the temperature in reactor, the better is the thermal cracking of tars evolved during gasification process. Additionally, according to the Arrhenius law the higher the temperature, the higher is reactivity as well.
- The reed sample exhibited a relatively low gasification reactivity and therefore using reed as a fuel, the decrease in the reactor output could be associated, for instance, with other studied materials.
- The evolvement of surface area on the studied char material during gasification process and its behaviour in the commercial gasifier needs further investigation.

REFERENCES

1. Ikonen, I., Hagelberg, E. Read Up on Reed! Southwest Finland Regional Environment Centre, Finland, 2007.
2. Chantre, G., Rozenberg, P., Baonza, V., Macchioni, N., Le Turcq, A., Rueff M., Petit-Conil M., Heois, B. Genetic selection within Douglas fir (Pseudotsuga menziesii) in Europe for papermaking issues. *Ann. For. Sci*., 59, 2002, p. 583–593.
3. The World of Pellets. *Bioenergy International*, No41, 6-2009, p. 9.
4. Arvelakis, S., Vourliotis, P., Kakaras, E., Koukis, E.G. Effect of leaching on the ash behavior of wheat straw and olive residue during fluidized bed combustion. *Biomass and Bioenergy*, 20, 2001, p. 459–470.
5. FAOSTAT. http://faostat.fao.org/, 2011.
6. Eurostat. http://epp.eurostat.ec.europa.eu/portal/page/portal/eurostat/home, 2011.
7. Di Blasi, C., Signorelli, G., Di Russo, C., Rea, G. Product distribution from pyrolysis of wood and agricultural residues. *Ind. Eng. Chem. Res.*, 38, 1999, p. 2216–2224.
8. Cetin, A., Gupta, R., Moghtaderi, B. Effect of pyrolysis pressure and heating rate on radiata Pine char structure and apparent gasification reactivity. *Fuel*, 84, 2005, p. 1328–1334.
9. Liliedahl, T., Sjöström K. Modelling of char-gas reaction kinetics. *Fuel*, 76, 1997, p. 29–37.
10. Barrio, M., Gøbel, B., Risnes, H, Henriksen, U., Hustad, J. E., Sørensen, L. H. Steam gasification of wood char and the effect of the hydrogen inhibition on the chemical kinetics. Progress In Thermochemical Biomass Conversion, Vol. 1, IEA Bioenergy (Edit. A.V. Bridgwater), 2001, p. 32–46.
11. Figueiredo, J.L., Moulijn, J.A. Carbon and Coal Gasification: Science and Technology. Springer, New York, 1986.
12. Jüntgen, H. Application of catalysts to coal gasification processes. Incentives and perspectives. *Fuel*, 62, 1983, p. 234–238.
13. Wood, B.J., Sancier, K.M. The mechanism of the catalytic gasification of coal char: A critical review. *Catal. Rev.-Sci. Eng.*, 26, 1984, p. 233–279.
14. Risnes, H., Sørensen, L.H., Hustad, J.E. CO_2 reactivity of chars from wheat, spruce and coal. Progress In Thermochemical Biomass Conversion, Vol.1, IEA Bioenergy (Edit. A.V. Bridgwater), 2001, p. 61–72.
15. Kannan, M.P., Richards, G.N. Gasification of biomass chars in carbon dioxide: dependence of gasification rate on the indigenous metal content. *Fuel*, 69, 1990, p. 747–753.
16. Moilanen, A. Thermogravimetric Characterisations of Biomass and Waste for Gasification Processes. PhD thesis, VTT Publications 607, 2006.
17. Sørensen, L. H., Fjellerup, J., Henriksen, U., Moilanen, A., Kurkela, E., Winther, E. An Evaluation of Char Reactivity and Ash Properties in

Biomass Gasification. Fundamental Processes in Biomass Gasification. ReaTech, Roskilde, Denmark, 2000.
18. Di Blasi, C., Buonanno, F., Branca, C. Reactivities of some biomass chars in air. *Carbon*, 37, 1999, p. 1227–1238.
19. Zanzi R., Sjöström K., Björnbom E. Rapid pyrolysis of agrucultural residues at high temperature. *Biomass and Bioenergy*, 23, 2002, p. 357–366.
20. Marquez-Montesinos, F., Cordero, T., Rodríguez-Mirasol, J., Rodríguez, J.J. CO_2 and steam gasification of a grapefruit skin char. *Fuel*, 81, 2002, p. 423–429.
21. Guerrero, M., Ruiz, M.P., Millera, Á., Alzueta, M.U., Bilbao, R. Characterization of biomass chars formed under different devolatilization conditions: differences between rice husk and eucalyptus. *Energy Fuels*, 22, 2008, p. 1275–1284.
22. Ikenaga, N., Nakajima, H., Oda, H., Suzuki. T. CO_2 gasification behavior of various biomass chars. Effect of mineral mattes in biomass chars. *Science and Technology Reports of Kansai University*, 51, 2009, p. 61–74.
23. Zhang, S.-Y., Cao, J.-P., Takarada, T. Effect of pretreatment with different washing methods on the reactivity of manure char. *Bioresource Technology*, 101, 2010, p. 6130–6135.
24. Zanzi, R., Sjöström, K., Björnbom, E. Rapid high-temperature pyrolysis of biomass in a free-fall reactor. *Fuel*, 75, 1996, p. 545–550.
25. Arvelakis, S., Koukios, E.G. Physicochemical upgrading of agroresidues as feedstocks for energy production via thermochemical conversion methods. *Biomass Bioenergy*, 22, 2002, p. 331–348.
26. Hamilton, T. SunOpta emerging as silent leader in cellulose ethanol race, http://tyler.blogware.com/2006/7/27/, 2011.
27. Grønli, M.G., Várhegyi, G., Di Blasi, C. Thermogravimetric analysis and devolatilization kinetics of wood. *Ind. Eng. Chem. Res.*, 41, 2002, p. 4201–4208.
28. Brunauer, S., Emmett, P.H., Teller, E. Adsorption of gases in multimolecular layers. *J. Amer. Chem. Soc.*, 60, 1938, p. 309–319.
29. Gregg, S.J., Sing, K.S.W., Adsorption, Surface Area and Porosity**.** Academic Press, 1982.
30. Lastoskie, C., Gubbins, K.E., Quirke, N. Pore-size distribution analysis of microporous carbons - a density-functional theory approach. *J. Phys. Chem.*, 97, 1993, p. 4786–4796.
31. Lozano-Castello, D., Cazorla-Amoros, D., Linares-Solano, A. Usefulness of CO_2 adsorption at 273 K for the characterization of porous carbons. *Carbon*, 42, 2004, p. 1233–1242.
32. Whitty, K., Backman, R., Hupa, M. Influence of char formation conditions on pressurized black liquor gasification rates. *Carbon*, 36, 1998, p. 1683–1692.

33. Raveendran, K., Ganesh, A., Khilart, K C. Influence of mineral matter on biomass pyrolysis characteristics. *Fuel*, 74, 1995, p. 1812–1822.
34. Wornat, M.J., Hurt, R.H., Yang, N.Y.C., Headley, T.J. Structural and compositional transformations of biomass chars during combustion. *Combustion and Flame*, 100, 1995, p. 131–145.
35. Della Rocca, P.A., Cerrella, E.G., Bonelli, P.R., Cukierman, A.L. Pyrolysis of hardwoods residues: on kinetics and char characterization. *Biomass and Bioenergy*, 16, 1999, p. 79–88.
36. Bonelli, P.R., Della Rocca, P.A., Cerrella, E.G., Cukierman, A.L. Effect of pyrolysis temperature on composition, surface properties and thermal degradation rates of Brazil nut shells. *Bioresource Technology*, 76, 2001, p. 15–22.
37. Fushimi, C., Araki, K., Yamaguchi, Y., Tsutsumi, A. Effect of heating rate on steam gasification of biomass. 1. Reactivity of char. *Ind. Eng. Chem. Res.*, 42, 2003, p. 3922–3928.
38. Cetin, E., Moghtaderi, B., Gupta, R., Wall, T.F. Influence of pyrolysis conditions on the structure and gasification reactivity of biomass chars. *Fuel*, 83, 2004, p. 2139–2150.
39. Guerrero, M., Ruiz, M.P., Alzueta, M.U., Bilbao, R., Millera, Á. Pyrolysis of eucalyptus at different heating rates: studies of char characterization and oxidative reactivity. *J. Anal. Appl. Pyrolysis*, 74, 2005, p. 307–314.
40. Boateng, A.A., Cooke, P.H., Hicks, K.B. Microstructure development of chars derived from high-temperature pyrolysis of barley (*Hordeum vulgare* L.) hulls. *Fuel*, 86, 2007, p. 735–742.
41. Biagini, E., Narducci, P., Tognotti, L. Size and structural characterization of lignin-cellulosic fuels after the rapid devolatilization. *Fuel*, 87, 2008, p. 177–186.
42. Della Rocca, P.A. Study on Biomass Thermal Conversion Processes. Facultad de Ciencias Exactas y Naturales. Universidad de Buenos Aires. PhD thesis, 1998.
43. Külatots, I., Link, S., Arvelakis, S. Adsorption properties of wheat straw, reed, pine and Douglas fir chars. International Carbon 2010 conference, July 11th to 16th, Clemson, SC, USA.
44. Bar-Ziv, E., Kantorovich, I.I. Mutual effects of porosity and reactivity in char oxidation. *Progress in Energy and Combustion Science*, 21, 2001, p. 667–697.
45. Matsumoto, K., Takeno, K., Ichinose, T., Ogi, T., Nakanishi, M. Gasification reaction kinetics on biomass char obtained as a by-product of gasification in an entrained-flow gasifier with steam and oxygen at 900–1000 °C. *Fuel,* 88, 2009, p. 519–527.
46. Zhou, Z., Shi, D., Qiu, Y., Sheng, G.D. Sorptive domains of pine chars as probed by benzene and nitrobenzene. *Environ. Pollut.*, 158, 2010, p. 201–206.

47. Freitas, J.C.C., Emmerich, F.G., Bonagamba, T.J. High-resolution solid-state NMR study of the occurrence and thermal transformations of silicon containing species in biomass materials. *Chem. Mater*., 12, 2000, p. 711–718.
48. Scholze, B., Hanser, C., Meier, D. Characterization of the water-insoluble fraction from fast pyrolysis liquids (pyrolytic lignin) Part II. GPC, carbonyl groups, and ^{13}C-NMR. *J. Anal. Appl. Pyrolysis*, 58-59, 2001, p. 387–400.
49. Sharma, R.K., Booten, J.B., Baliga, V.L., Lin, X., Chan, W.G., Hajaligol, M.R. Characterization of chars from pyrolysis of lignin. *Fuel*, 83, 2004, p. 1469–1482.
50. Kolodzlejski, W., Frye, J.S., Maclel, G.E. Carbon-13 nuclear magnetic resonance spectrometry with cross polarization and magic-angle spinning for analysis of lodgepole pine wood. *Anal. Chem.*, 54, 1982, p. 1419–1424.
51. Maunu, S.L. NMR studies of wood and wood products. *Prog. NMR Spectrosc.*, 40, 2002, p. 151–174.
52. Newman, R.H., Hemmingson, J.A. Determination of the degree of cellulose crystallinity in wood by carbon-13 nuclear magnetic resonance spectroscopy. *Holzforschung*, 44, 1990, p. 351–355.
53. Newman, R.H., Hemmingson, J.A. Carbon-13 NMR distinction between categories of molecular order and disorder in cellulose. *Cellulose*, 2, 1995, p. 95–110.
54. Wikberg, H. Advanced Solid State NMR Spectroscopy Techniques in the Study of Thermally Modified Wood. Doctoral Thesis, University of Helsinki, Helsinki, Finland, 2004.
55. Inari, G.N., Mounguengui, S., Dumarçay, S., Pétrissans, M., Gérardin, P. Evidence of char formation during wood heat treatment by mild pyrolysis. *Polym. Degrad. Stab.*, 92, 2007, p. 997–1002.
56. Bardet, M., Hediger, S., Gerbaud, G., Gambarelli, S., Jacquot, J.F., Foray, M.F., Gadelle, A. Investigation with ^{13}C NMR, EPR and magnetic susceptibility measurements of char residues obtained by pyrolysis of biomass. *Fuel*, 86, 2007, p. 1966–1976.
57. Egan, J.M., Müller, K.T. Detection and identification of corrosion products of sodium aluminoborosilicate glasses by ^{23}Na MQNMR and ^{1}H→^{23}Na CPMAS NMR. *J. Phys. Chem. B*, 104, 2000, p. 9580–9586.
58. Kundla, E., Samoson, A., Lippmaa, E. High-resolution NMR of quadropolar nuclei in rotating solids. *Chem. Phys. Lett.*, 83, 1981, p. 229–232.
59. Koller, H., Engelhardt, G., Kentgens, A.P.M., Sauer, J. ^{23}Na NMR spectroscopy of solids: Interpretation of quadrupole interaction parameters and chemical shifts. *J. Phys. Chem.*, 98, 1994, p. 1544–1551.
60. Burchill, P., Howarth, O.W., Sword, B.J. MAS NMR studies of inorganic elements in coals and combustion residues. *Fuel*, 70, 1991, p. 361–366.
61. Van Heek, K.H.; Mühlen, H.-J. Aspects of coal properties and constitution important for gasification. *Fuel*, 64, 1985, p. 1405–1414.

62. Moilanen, A., Mühlen, H.-J. Characterization of gasification reactivity of peat char in pressurized conditions: Effect of product gas inhibition and inorganic material. *Fuel*, 75, 1996, p. 1279–1285.
63. Zevenhoven-Onderwater, M., Backman, R., Skrifvars, B.-J., Hupa, M. The ash chemistry in fluidised bed gasification of biomass fuels. Part I: predicting the chemistry of melting ashes and ash–bed material interaction. *Fuel*, 80, 2001, p. 1489–1502.
64. Sutton, D., Kelleher, B., Ross, J.R.H. Review of literature on catalysts for biomass gasification. *Fuel Process. Technol.*, 73, 2001, p. 155–173.
65. Radović, L.R., Walker, P.L.Jr., Jenkins, R.G. Importance of carbon active sites in the gasification of coal chars. *Fuel*, 62, 1983, p. 849–856.
66. Livneh, T., Bar-Ziv, E., Salatino, P., Senneca, O. Evolution of Reactivity of Highly Porous Chars from Raman Microscopy. *Combustion Science and Technology*, 153, 2000, p. 65–82.
67. Struis, R.P.W.J., Von Scala, C., Stucki, S., Prins, R. Gasification reactivity of charcoal with CO_2. Part I: Conversion and structural phenomena. *Chem. Eng. Sci.*, 57, 2002, p. 3581–3592.
68. Hippo, E.J., Jenkins, R.G., Walker, P.L.Jr. Enhancement of lignite char reactivity to steam by cation addition. *Fuel*, 58, 1979, p. 338–244.
69. Yip, K., Tian, F., Hayashi, J., Wu, H. Effect of alkali and alkali earth metallic species on biochar reactivity and syngas composition during steam gasification. *Energy Fuels*, 24, 2010, p. 173–181.
70. Chan, M.-L., Jones, J.M., Pourkashanian, M., Williams, A. The oxidative reactivity of coal chars in relation to their structure. *Fuel*, 78, 1999, p. 1539–1552.
71. Arenillas, A., Pevida, C., Rubiera, F., Palacios, J.M., Navarette, R., Denoyel, R., Rouquerol, J., Pis, J.J. Surface characterisation of synthetic coal chars made from model compounds. *Carbon*, 42, 2004, p. 1345–1350.
72. Leofanti, G., Padovan, M., Tozzola, G., Venturelli, B. Surface area and pore texture of catalysts. *Catal. Today*, 41, 1998, p. 207–219.
73. Barrio, M., Hustad, J.E. CO_2 gasification of birch char and the effect of CO inhibition on the calculation of chemical kinetics. Progress In Thermochemical Biomass Conversion, Vol. 1, IEA Bioenergy (Edit. A.V. Bridgwater), 2001, p. 47–60.

KOKKUVÕTE

Pilliroogu, nisupõhku ja puitu loetakse taastuvaks energiaallikaks ja nö CO_2 vabadeks kütusteks. Pilliroogu on kasutatud energeetilistel eesmärkidel erinevates Euroopa riikides nagu Eesti, Soome, Holland, Ungari ja Rumeenia [1]. Ebatsuugat on Euroopas kasvatatud laialdaselt kolmkümmend aastat, eriti just Prantsusmaal ja Saksamaal [2]. Nii Euroopas kui maailmas on puidupelleti toodang kasvanud kuni kümnete miljonite tonnideni aastas [3]. Nisupõhk on üks paljulubavaid põllumajanduslikke jääke ja seda on võimalik kasutada kütusena energia tootmiseks võttes arvesse nisu toodangut nii Vahemeremaades [4] kui ka Euroopas ja maailmas [5,6].

Pürolüüs ja gaasistamine on termokeemilise muundamise viisid kasutamaks biomassi energeetilistel eesmärkidel. Pürolüüs ei ole ainult eraldiseisev muundamise tehnoloogia, vaid ka üks gaasistamisprotsessi osa. Viimast võib laias laastus jagada kaheks etapiks: lendosade eraldumine (pürolüüs) ja koksi lagunemine (gaasistamine). Koksi reageerimisvõime, koksi muundamise faasis, mis järgneb gaasistusprotsessi pürolüüsifaasile, on üldjuhul kordades aeglasem kui pürolüüs ise ja seetõttu määrav kogu gaasistusprotsessi kiirusele [8].

Käesolev doktoritöö eesmärgiks on uurida pilliroo, nisupõhu ja kahe puitpõhise kütuse (ebatsuugahake ja männipellet) kokside reageerimisvõimet ning leostamise mõju koksi reageerimisvõimele. Selleks kasutatakse nö erinevaid kaudseid meetmeid, mille abil määratakse materjalide erinevad omadused ning neid tulemusi võrreldakse CO_2 keskkonnas kokside gaasistamisel saadud reageerimisvõimetega.

Kütuste ja kokside omaduste iseloomustamiseks kasutati järgnevaid meetodeid:

- kütuse ja koksi materjali standard- ja keemiline analüüs,
- kütuse ja koksi tuha keemiline analüüs,
- tuuma magnetilise resonantsi spektroskoopia meetod (^{13}C ja ^{23}Na),
- N_2 and CO_2 adsorptsiooni kaudu koksi poorsuse ja eripinna määramine,
- Skaneeriva elektronmikroskoobiga kütuste ja kokside pindade morfoloogia uurimine ning täiendavalt energiadispersiivse röntgenkiire (EDX) spektroskoopia kasutamine koksi pinnal oleva anorgaanika määramiseks.

Kokside reageerimisvõime määramaised viidi läbi kõrgrõhu termogravimeetrilises seadmes, mis võimaldab rakendada rõhkusid kuni 100 bar. Siiski, reageerimisvõime määramised teostati antud uurimuses atmosfäärirõhul. Esmalt hoiti proovi heeliumi keskkonnas nö eelkambris. Kui reaktori temperatuur oli saavutanud soovitud temperatuuri juhiti proov reaktorisse. Pärast 150-300 sekundit oli proov kuivanud ning saavutanud stabiilse massi, misjärel vahetati gaas reaktoris CO_2 vastu. Tulemuseks saadi massikaokõver, mille põhjal arvutati reageerimisvõime.

Töö teadusliku uudsuse koha pealt võib välja tuua järgmist:

- laialdane ülevaade erinevatest meetoditest iseloomustamaks kokside omadusi, mis on samaaegselt rakendatud koksidele, mis pärinevad suhteliselt erinevate omadustega biokütustest, aga samas on koksid valmistatud samade pürolüüsitingimuste juures;
- süsinik-13 ja naatrium-23 tuuma magnetilise resonantsi spektroskoopia kasutamine koos teiste üldkasutatavate meetoditega;
- leostamise mõju uurimine koksi reageerimisvõimele;
- pilliroo kui kütuse kasutamist gaasistamisel ei ole varem uuritud;
- valitud materjalid on väga erinevate omadustega ning nende reageerimisvõime uurimine samadel tingimustel heidab uut valgust teguritele, mis mõjutavad kokside reageerimisvõimet;
- lisaks eelnevale, esitatakse nägemus, miks erineb töötlemata nisupõhu koksi lämmastiku BET eripind hinnanguliselt kuni kaheksa korda võrreldes leostatud nisupõhu eripinnaga.

Praktilisest seisukohast on reageerimisvõime oluline reaktori toodangu suhtes, st mida suurem on reageerimisvõime, seda rohkem toodangut (nt gaasi) ajaühikus tekib. Energeetiliselt võib seda piltlikult vaadelda kui, et mida suurem on reageerimisvõime, seda suurem on reaktori energeetiline võimsus. On teada, et leelismetallid mõjuvad seadme metallile korrodeeruvalt ning samuti alandavad tuha sulamistemperatuure. Samas on leelismetallid koksi ja gaasi vahelise reaktsiooni katalüsaatoriteks. Seega, leostamisega ühelt poolt vähendatakse mõju katla metallile ja tõuseb tuha sulamistemperatuur, kuid teiselt poolt kaotame kogu protsessi kulgemise kiiruses.

Nisupõhu leostamiseks on kasutatud lihtsat ja suhteliselt odavat meetodit, kus leostamine toimub kraaniveega läbipesemise kaudu ning hilisem kuivatamine toimub päikese käes.

Kütuste omadustest võib näha, et pilliroo tuhk sisaldab suhteliselt palju räni, kuid siiski on ebatsuugahakkes räni sisaldus suurem vaatamata madalamale räni sisaldusele tuhas, kuna ebatsuuga tuhasus on hinnanguliselt kaks korda suurem võrreldes pilliroo omaga. Männipelleti tuhasus on kõige madalam ning põhiliselt sisaldab tuhk kaltsiumi. Tuha keemiline analüüs ilmestab, et tänu leostamisele on nisupõhu kaaliumi sisaldus kütuses langenud hinnanguliselt 7 korda.

SEM/EDX spektroskoopia meetodiga tehtud analüüside põhjal täheldati, nii pilliroo kui nisupõhu osakestel ringikujulisi räniosakesi, mille servad pärast pürolüüsi olid muutunud ümaramaks. Pärast pürolüüsi võis täheldada anorgaanika kontsentratsiooni suurenemist koksi pinnal võrreldes lähtematerjaliga. Männipelleti koksi osakeste korral võis täheldada iseloomulikku nö plaadikujulist kuju, kus osakese paksus on kordades väiksem võrreldes pikkuse ja laiusega.

Eripinna määramised näitasid, et N_2 BET eripind on väiksem võrreldes CO_2 BET eripinnaga, mistõttu lämmastik ei iseloomusta poorsust ja eripinda täielikult. Nisupõhu korral oli töötlemata nisupõhu koksi N_2 BET eripind

kaheksa korda madalam leostatud nisupõhu koksi omast, mida võib seletada sellega, et leostamise tõttu ei blokeeri enam leelismetallide osakesed kütuse pooride avausi ning lämmastik on võimeline tungima pooridesse. CO_2 BET korral seda probleemi ei esinenud, kuna CO_2 on võimeline tungima väiksematesse pooridesse (st läbima kitsamaid avausi) võrreldes lämmastikuga antud meetodeid kasutades. CO_2 tehtud katsed näitasid, et koksid on mikropoorsed. Märgatavalt kõrgemat CO_2 eripinda näitas männipelletikoks, st viimast võib lugeda uuritud koksidest kõige suurema eripinnaga koksiks.

Tuuma magnetilise resonantsi (TMR) spektroskoopia analüüside põhjal võib öelda, et sõltumata lähtekütustest on koksi süsiniku struktuur sama. Naatrium-23 TMR spektroskoopia näitas selgesti, et töötlemata nisupõhk sisaldab NaCl, mis eemaldatakse leostamise käigus.

Kõik vaadeldud koksid näitasid CO_2 keskkonnas gaasistamisel erinevaid reageerimisvõimeid. Üldiselt, reageerimisvõime alusel võib koksid seada pingeritta järgmiselt: 1) töötlemata nisupõhk≈männipellet; 2) ebatsuugahake; 2) leostatud nisupõhk; 4) pilliroog.

Üldiselt saab reageerimisvõimet seletada mineraalosa sisalduse ja koostisega, eripinnaga, aktiivpinnaga ja poorse struktuuri iseloomuga. Pilliroo, ebatsuuga ja lesotatud nispõhu korral kõrge räni sisaldus pärsib leelismetallide toimimist katalüsaatorina koksi reageerimisel gaasiga, rohkem kui töötlemata nisupõhu korral. Gaasistamise algfaasis suurenev reageerimisvõime pilliroo ja nisupõhu kokside korral on seletatav protsessi käigus suureneva eripinnaga, mis toob kaasa suurema aktiivpinna ning protsessi kulgemisel see väheneb põhjustades koos katalüsaatorite deaktiveerumisega reageerimisvõime languse.

Kuigi leostamine vähendab leelismetallide sisaldust kütuses, on pärast pürolüüsi leostatud nisupõhu koksi leelismetallide ja räni sisaldus suurim vaadeldud kütuse koksidest, tänu suurimale tuha sisaldusele. Põhiliseks leelismetalliks on kaltsium ja kaaliumi sisaldus on leostatud koksis kolm korda madalam võrreldes töötlemata nisupõhu koskiga. Kuna leelismetalle hinnatakse kümme korda aktiivsemateks katalüsaatoriteks võrreldes muldleelismetallidega [14], siis sellest tulenevalt mõjutab see ka reageerimisvõimet. Kütuse leostamine alandab koksi reageerimisvõimet ning leostatud nisupõhu koksi reageerimisvõime on võrreldes leostamata nisupõhu koksiga, arvestades reageerimisele kulunud aega, kuni 4 korda madalam. Siiski on leostatud nisupõhu koksi reageerimisvõime näiteks suurem pilliroo koksi omast.

Kuigi männipelletikoks sisaldab võrreldes teiste kütustega vähem leelismetalle, annab tulemuste põhjal parema reageerimisvõime madalam räni sisaldus, suhteliselt suur O/C suhe ning suurem aktiivpind, mis püsib tänu osakeste plaadikujulisele iseloomule kogu protsessi jooksul suhteliselt ühtlasena, mille tulemusena on männipelleti koksi kogu reageerimisaeg võrdeline töötlemata nisupõhu omaga.

Tulemsute põhjal võib hinnata, et männipelleteid on soovitav eelistada kütusena võrreldes teiste vaadeldud materjalidega. Männipelletikoks omab kõrget reageerimisvõimet, mis tähendab konkreetse väljundvõimsuse juures

väiksemat reaktorit. Väikse tuhasuse tõttu on eemaldatav ja ladestatav tuha kogus, sh kulutused selleks, võrreldes teiste kütustega, madalamad. Madalama leelismetallide sisalduse tõttu on eeldada, et tuha sulamistemperatuur on kõrgem ja korrosioonioht seadme metallile väiksem. Mida kõrgem on tuha sulamistemperatuur, seda kõrgemat temperatuuri on võimalik reaktoris rakendada ning seda parem on gaasistamisel tekkivate tõrvaühendite termiline lagunemine.

Pilliroo kasutamisel, tuleb arvestada suhteliselt madala koksi reageerimisvõimega, mis oli töös vaadeldud kütustest kõige madalam, ning seega ka madalama reaktori toodanguga/väljundvõimsusega.

ABSTRACT

Reed, wheat straw and wood are renewable energy sources that are considered to be CO_2 neutral. Reed has been used to provide energy in various parts of Europe [1]. The Douglas fir has been widely planted in Europe for 30 years, especially in France and Germany [2]. In Europe as well as around the world, the wood pellet production extends to tens of millions of tons per year [3]. Wheat straw is one of the most promising agricultural residues suitable for energy production in the Mediterranean region [4] as well as elsewhere in Europe [5,6].

Gasification is a thermochemical process, which can be broadly split into two main stages: solid devolatilization (pyrolysis) and char conversion (gasification). Char reactivity in the char conversion stage, following the pyrolysis step, is generally much slower than the pyrolysis itself and is therefore the rate-determining step [8].

The goal of the work is the determination of substantial properties and gasification reactivity of selected materials, compare the outcome of the gasification test, i.e. reactivity of different materials, with the determined properties and estimate the effect of leaching pretreatment method on the gasification reactivity of char.

The distinctions in reactivity can be explained by the differences in the mineral matter content, internal surface area, active sites, and nature of porous structure.

According to the results of the ^{13}C NMR spectroscopy, it can be anticipated that the carbon structure does not affect the reactivity of char. The ^{23}Na NMR spectroscopy proves that leaching affects the fuel properties, i.e., sodium chemistry in a biomass sample. But, no difference could be detected between the spectra of ^{23}Na NMR spectroscopy of the untreated and leached wheat straw char samples.

The pine pellets char exhibited almost steady reaction rate along the gasification process and relatively high reactivity that could be imputed to the nature of material, i.e., high porosity, shape of char particle, high O/C ratio, high Ca and low Si content of ash.

The leaching pretreatment of parent fuel affects the char gasification reactivity. The char of leached wheat straw sample exhibited lower reactivity and it could be attributed mainly to the lower K content together with relatively high Si content and lower O/C ratio compared to the untreated char.

All the chars studied showed different reactivity under CO_2 gasification conditions. In general, the order of reactivity of the studied chars can be observed as following: 1) untreated wheat straw≈pine pellets; 2) Douglas fir wood chips; 3) leached wheat straw; 4) reed.

APPENDIX 1

ELULOOKIRJELDUS

Eesnimi Siim
Perekonnanimi Link
Sünniaeg ja –koht 04.12.1979, Tallinn
Kodakondsus Eesti
Kontaktandmed Kopli 116, 11712 Tallinn, Eesti
Telefon: +372 620 39 00
E-mail: E-mail: siim.link@ttu.ee
Töökoht Tallinna Tehnikaülikool, soojustehnika instituut
Ametikoht Insener

Hariduskäik

Õppeasutus	Lõpetamise aeg	Haridus
Tallinna Tehnikaülikool	2004	tehnikateaduste magister
Tallinna Tehnikaülikool	2002	tehnikateaduste bakalaureus
Gustav Adolfi Gümnaasium	1997	keskharidus

Teenistuskäik

Töötamise aeg	Organisatsiooni nimetus	Ametikoht
2007-käesoleva ajani	Tallinna Tehnikaülikool, soojustehnika instituut	insener
2001-2006	ÅF-Estivo AS	projektijuht

Keelteoskus

Keel	Tase
Inglise keel	hea
Saksa keel	rahuldav
Eesti keel	emakeel

Täiendõpe

Õppimise aeg	Täiendusõppe läbiviija nimetus
2008	Uurimistöö Åbo Akademi's.
2007	Uurimistöö Rootsi Kuninglikus Tehnikaülikoolis (KTH).
2007	Uurimistöö Wageningeni TMR Keskuses.
2006	Uurimistöö Müncheni Tehnikaülikoolis.
2000 – 2001	Fachhochschule Stralsund. Taastuvad energiaallikad ja vesinikutehnoloogia,

Teadustöö põhisuunad biokütuste kasutamise võimalused soojuse ja elektri (koos)tootmiseks, energiamajandus, taastuvate energiaallikate kasutamine, energiasääst.

APPENDIX 2

CURRICULUM VITAE

First name Siim
Last name Link
Date and place of birth 04.12.1979, Tallinn
Citizenship Estonian
Contact Kopli 116, 11712 Tallinn, Estonia
Telephone: +372 620 39 00
E-mail: siim.link@ttu.ee
Organization Tallinn University of Technology,
Department of Thermal Engineering
Current position Engineer

Education

Educational institution	Year of graduation	Education
Tallinn University of Technology	2004	Master degree
Tallinn University of Technology	2002	Barchelor degree
Gustav Adolf Grammar School	1997	Secondary education

Professional Employment

Period	Organisation	Position
2007-present	Tallinn University of Technology, Department of Thermal Engineering	Engineer
2001-2006	ÅF-Estivo AS	Project manager

Language skills

Language	Level
English	good
German	sufficient
Estonian	mother tongue

Training courses

Period	Educational organization
2008	Research work at Åbo Akademi.
2007	Research work at KTH Royal Institute of Technology.
2007	Research work at Wageningen NMR Centre.
2006	Research work at Technical University of Munich.
2000-2001	Fachhochschule Stralsund. Renewable Energy and Hydrogen Technology.

Research Interest possibilities of utilization of biomass for production of heat and power, incl. combined production; energy management, utilization of renewable energy resources, energy savings.

PAPER I

Link, S., Arvelakis, S., Spliethoff, H., De Waard, P., Samoson, A. Investigation of biomasses and chars obtained from pyrolysis of different biomasses with solid-state ^{13}C and ^{23}Na nuclear magnetic resonance spectroscopy. *Energy Fuels*, 22, 2008, p. 3523-3530.

Investigation of Biomasses and Chars Obtained from Pyrolysis of Different Biomasses with Solid-State ^{13}C and ^{23}Na Nuclear Magnetic Resonance Spectroscopy

Siim Link,*,† Stelios Arvelakis,‡ Hartmut Spliethoff,‡ Pieter De Waard,§ and Ago Samoson||

Thermal Engineering Department, Tallinn University of Technology, Kopli 116, 11712, Tallinn, Estonia, Department of Mechanical Engineering, Institute for Energy Systems, Munich University of Technology, Boltzmannstrasse 15, 85747, Garching, Germany, Laboratory of Biophysics, Wageningen NMR Centre, 6700 ET Wageningen, The Netherlands, and National Institute of Chemical Physics and Biophysics, Akadeemia tee 23, 12618 Tallinn, Estonia

Received May 5, 2008. Revised Manuscript Received June 25, 2008

A number of biomass samples (reed, pine pellets, Douglas fir wood chips, wheat straw, peach stones, and olive residue), pretreated biomass samples (leached wheat straw, leached peach stones, and leached olive residue), as well as their chars obtained by pyrolysis using different heating rates (5, 10, and 20 °C/min) at the end temperature of 800 °C were characterized with ^{13}C and ^{23}Na nuclear magnetic resonance (NMR) spectroscopy. In the case of the biomass samples, ^{13}C solid-state cross-polarization magic-angle spinning (CPMAS) NMR was used, resulting in spectra indicating the various groups of carbons present in the biomass samples. No evidence was found that the leaching process could affect the carbon composition of the biomass samples. In the char samples, only aromatic groups of carbon were left, shown by ^{13}C solid-state single-pulse MAS NMR. According to the results, the origin of biomass, the leaching procedure, and the different heating rates do not affect the char carbon composition. Therefore, it could be assumed that the carbon structure does not affect the reactivity of the char. ^{23}Na single-pulse solid-state MAS NMR was applied to investigate the sodium environment in the biomass and char samples. Despite experimental difficulties, we were able to observe definite differences in line width and shifts of the studied compounds. This proves that leaching affects the fuel properties, i.e., sodium chemistry in a biomass sample, and therefore, it could be assumed that the char reactivity is affected. Higher magnetic fields and more sophisticated techniques of resolution enhancement multiple-quantum magic-angle spinning (MQ-MAS) or double rotation (DOR) may provide more detailed local information regarding the sodium environment in biomasses and their char samples.

1. Introduction

Power production from biomass, including from different agricultural and forest residues, has been an issue over the last few decades. Generally, power production from biomass in small-scale applications is in most cases under discussion. In principal, the application of the integrated gasification combined cycle (IGCC) in the case of the gasification technology is considered to have higher efficiency compared to the Rankine cycle. In addition, biomass is considered to be CO_2-neutral, and using biomass for energy purposes is an option to decrease CO_2 emissions.

Pyrolysis and gasification are thermochemical conversion routes to recover energy from biomass. Pyrolysis is not only an independent conversion technology but also part of the gasification process, which can be broadly separated into two main stages, solid devolatilization (pyrolysis) and char conversion (gasification). Char reactivity in the second stage is dependent upon the formation conditions (essentially temperature and heating rate) and the amount and composition of the inorganic content. In addition, the type of biomass (chemical composition and physical properties) also largely affects both biomass devolatilization and char conversion.[1] The char conversion following the pyrolysis step in the gasification process is generally much slower than the pyrolysis itself and is therefore the rate-determining step.[2] High char reactivity is important for the capacity of the reactors.[3]

Marquez-Montesinos et al.[4] pointed out based on the cited literature that the presence of some inorganic constituents plays in many cases a very important role because of catalytic effects. Sodium, potassium, and calcium, which are commonly present in biomass, show a significant activity as gasification catalysts.

The presence of inorganic constituents in biomass fuels is associated with problems such as deposition, sintering, agglomeration, corrosion, and/or erosion caused during the opera-

* To whom correspondence should be addressed. Telephone: +372-6203903. Fax: +372-6203901. E-mail: siim.link@ttu.ee.
† Tallinn University of Technology.
‡ Munich University of Technology.
§ Wageningen NMR Centre.
|| National Institute of Chemical Physics and Biophysics.

(1) Di Blasi, C.; Signorelli, G.; Di Russo, C.; Rea, G. Product distribution from pyrolysis of wood and agricultural residues. *Ind. Eng. Chem. Res.* **1999**, *38*, 2216–2224.
(2) Cetin, A.; Gupta, R.; Moghtaderi, B. Effect of pyrolysis pressure and heating rate on radiata pine char structure and apparent gasification reactivity. *Fuel* **2005**, *84*, 1328–1334.
(3) Zanzi, R.; Sjöström, K.; Björnbom, E. Rapid high-temperature pyrolysis of biomass in a free-fall reactor. *Fuel* **1996**, *75*, 545–550.
(4) Marques-Montesinos, F.; Cordero, T.; Rodrígues-Mirasol, J.; Rodrígues, J. J. CO_2 and steam gasification of a grapefruit skin char. *Fuel* **2002**, *81*, 423–429.

10.1021/ef800305g CCC: $40.75
Published on Web 08/16/2008

tion of gasification plants.[5] The leaching pretreatment process is an option to eliminate alkali metals and chlorine in biomass. On the other hand, the lower content of alkali metals may affect the char gasification reactivity.

The present work focuses on studying the effect of the properties of the different biomass samples, the leaching pretreatment process, and the pyrolysis heating rate on the composition of chars obtained during pyrolysis. An attempt was undertaken to investigate the changes in carbon structure and sodium environment because of pyrolysis with nuclear magnetic resonance (NMR) spectroscopy.

2. Experimental Section

2.1. Materials. The different biomass samples selected for investigation are the following: Reed coming from West Estonia and from the islands of Estonia, being pelagian from nature; commercial pine pellets and Douglas fir wood chips both coming from the area of Munich in Germany; wheat straw, peach stones, and olive residue coming from the area of Thessaly, Macedonia, and Crete in Greece.

The biomass samples are prepared and characterized regarding their proximate and ultimate analysis, calorific value, and ash analysis in accordance with American Society for Testing and Materials (ASTM) methods. For the Greek biomass samples, the cellulose, hemicellulose, and lignin contents were also determined according to the ASTM standard method D 1106-84.

2.2. Leaching. The wheat straw, peach stones, and olive residue samples were also pretreated using the leaching pretreatment process. The pretreatment targeted on the elimination of the amounts of alkali metals, chlorine, and sulfur in these biomass samples, which are considered to be responsible for the ash-related problems during the combustion and gasification of biomass. The leaching was performed using tap water according to the method developed by Arvelakis et al.[5] The used mass/water ratios are 66.6 g/L for wheat straw and 88.8 g/L for peach stones and olive residue.

2.3. Pyrolysis. A fixed-bed pyrolyzer under atmospheric pressure was used for the preparation of the char samples used in the NMR study. The pyrolysis setup shown in Figure 1 consists of the gas-controlling system, the reactor heater, and the data acquisition and controlling system. The mass flow of nitrogen was controlled using a calibrated mass flow controller.

A cylindrical electric heater is placed inside the reactor. Inside the heater is placed a quartz pipe that protects the heating wire against corrosive compounds possibly present in the evolved gas mixture. The temperature controller and thermocouple were used to heat the setup and keep the required temperature.

The sample is loaded into the sample holder that is made of a stainless-steel SS316 bound net with 80 μm openings, as is shown in Figure 2.

The sample holder was filled with biomass, as it is shown in Table 3. Three different heating rates were used: 5, 10, and 20 °C/min. Nitrogen was used as a carrier gas in the case of all tests, with a flow rate of 1 L/min.

The applied heating procedure was the following: (i) hold the sample 45 min at 50 °C, (ii) heat the sample to the end temperature of 800 °C using the relevant heating rate (5, 10, and 20 °C/min), (iii) hold the sample 15 min at end temperature, and (iv) cooling down.

2.4. Solid-State NMR. For the NMR spectroscopy, a Bruker Avance 300 spectrometer located at the Wageningen NMR Centre, operating at a carbon resonance frequency of 75.5 MHz or at a sodium frequency of 79.4 MHz, at a temperature of 20 °C, was used. The spinning speed was 5 kHz, and 7 mm rotors of ZrO_2 were used. The obtained data were analyzed with TOPSPIN provided by Bruker.

(5) Arvelakis, S.; Koukios, E. G. Physicochemical upgrading of agroresidues as feedstocks for energy production via thermochemical conversion methods. *Biomass Bioenergy* **2002**, *22*, 331–348.

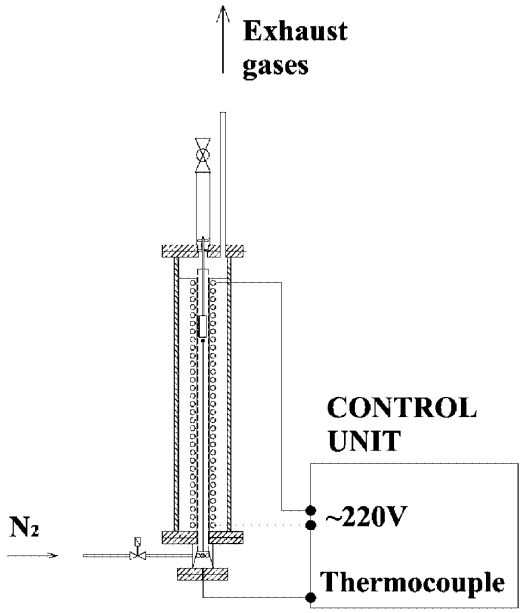

Figure 1. Simplified schema of the pyrolysis reactor heater.

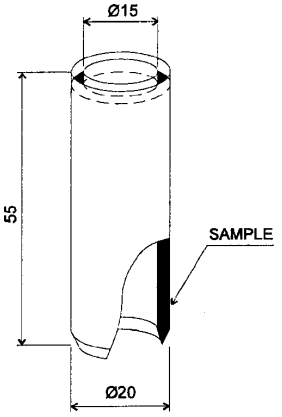

Figure 2. Sample holder.

^{13}C cross-polarization magic-angle spinning (CPMAS) solid-state NMR was used for the characterization of the biomass samples. The cross-polarization contact time was 1 ms; the delay time was 4 s; and the 90° pulse for proton was 5 μs.

^{13}C single-pulse solid-state MAS NMR was used for the characterization of the various biomass char samples. The pulse length was 2 μs, and the delay time was 2 s.

The original biomass samples and char samples were also analyzed with ^{23}Na single-pulse solid-state MAS NMR. The pulse length was 1 μs, and the delay time was 1 s. The chemical shifts were calibrated to separately measure solid NaCl (7.0 ppm).

3. Results and Discussion

3.1. ^{13}C NMR Spectroscopy. ^{13}C NMR spectroscopy was used to identify the various carbon groups in biomass and pyrolysis char samples, to investigate the influence of various heating rates during pyrolysis on the obtained char samples, and to compare the carbon groups left after pyrolysis in various char samples compared to the biomass samples. Also, the

Table 1. Analysis and Characterization of Biomass Samples

	proximate analysis, dry basis (wt %)				ultimate analysis, dry basis (wt %)						chemical analysis, dry basis (wt %)				
	moisture	ash	volatile matter	fixed carbon	N	C	H	S	Cl	O	extractives	lignin	cellulose and hemmicellulose	moisture	calorific value (MJ/kg)
reed	5.40	3.21	80.26	16.53	0.44	47.36	5.66	0.19	nd[a]	43.14	nd	nd	nd	nd	20.41
pine pellets	5.89	0.22	83.29	16.49	0.32	50.49	5.85	0.15	nd	42.97	nd	nd	nd	nd	19.13
Douglas fir wood chips	7.74	6.73	72.28	20.99	0.63	48.49	4.85	0.05	nd	42.97	nd	nd	nd	nd	19.12
wheat straw	8.10	7.60	76.00	16.40	0.79	43.70	5.08	0.43	0.44	41.96	15.5	16.6	60.3	5.7	18.91
wheat straw leached	5.75	5.87	80.65	13.48	0.57	46.26	5.31	0.20	0.10	41.68	nd	nd	nd	nd	20.03
peach stones	8.53	0.65	81.30	18.10	0.796	51.95	5.76	<0.01	0.14	40.70	8.9	42.4	48.0	11.7	21.55
peach stones leached	11.98	0.43	81.61	17.96	0.95	53.45	6.23			38.94	nd	nd	nd	nd	22.80
olive residue	9.50	4.6	76.00	19.40	1.36	50.70	5.89	0.30	0.18	36.97	24.9	32.6	37.9	11.4	21.21
olive residue leached	11.13	2.73	78.70	18.57	1.64	51.10	5.58	0.302	0.10	38.60	nd	nd	nd	nd	21.28

[a] nd = not determined.

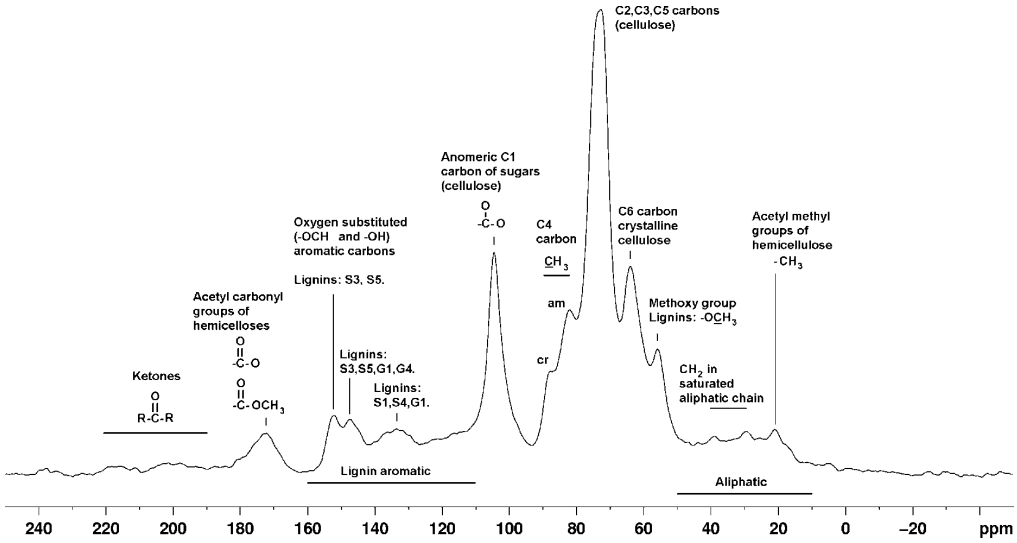

Figure 3. Spectrum of ^{13}C CPMAS NMR of the olive residue sample (cr, crystalline; am, amorphous).

changes of the biomass samples after the leaching process was an aim of the investigation.

The ^{13}C CPMAS spectra were obtained from the biomass samples within relatively a short time (maximum number of scans was 208). For the char samples, the needed number of scans was in the range of 4000−6000, because of the fact that chars are less crystalline compared to biomass samples. The single-pulse NMR method results in similar spectra, with 3 times shorter scanning time. Because chars are less crystalline and their hydrogen content is lower compared to the original fuels, the CPMAS method is relatively inefficient. The same conclusion is also drawn by Freitas et al.[6]

Biomass samples show a variety of carbon resonances, while those of the char samples reveal only a single resonance.

3.1.1. Biomass Samples. The results obtained from the NMR spectra of the original biomass samples shown in Figures 3 and 4 show that:

All of the original biomass samples have a peak at 22 ppm assigned to the acetyl methyl groups of hemicelluloses.

The olive residue also has in addition to the peak at 22 ppm two extra peaks in the aliphatic region that could be assigned to aliphatic CH_2[7] of lignin[8] and to the residual lipids still present in the olive residue after treatment.

At 56 ppm, most of original biomass samples have a peak assigned to the methoxy groups of lignin.

The peak at 65 ppm is assigned to the aliphatic C6 carbons of crystalline cellulose.

In the region of 72 and 75 ppm, all biomass samples have the highest peak, assigned to the C2, C3, and C5 carbons of cellulose.

All biomass samples have C4 amorphous and crystalline cellulose at 84 and 89 ppm, respectively. Wheat straw has an extra upfield shoulder at 84 ppm that could be attributed to the C_β lignin.

All biomass samples have a sharp peak at 105 ppm assigned to the anomeric carbon of sugars.

(6) Freitas, J. C. C.; Emmerich, F. G.; Bonagamba, T. J. High-resolution solid-state NMR study of the occurence and thermal transformations of silicon containing species in biomass materials. *Chem. Mater.* **2000**, *12*, 711–718.

(7) Sharma, R. K.; Hajaligol, M. R.; Smith, P. A. M.; Wooten, J. B.; Baliga, V. Characterization of char from pyrolysis of chlorogenic acid. *Energy Fuels* **2000**, *14*, 1083–1093.

(8) Xia, Z.; Akim, L. G.; Argyropoulos, D. S. Quantitative ^{13}C NMR analysis of lignins with internal standards. *J. Agric. Food Chem.* **2001**, *49*, 3573–3578.

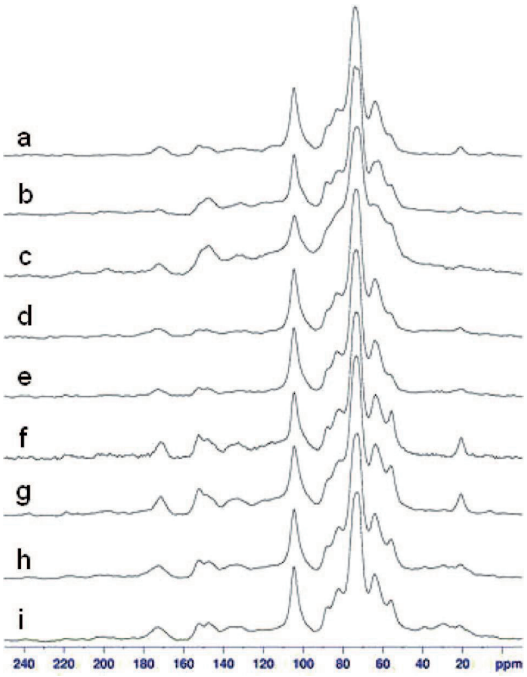

Figure 4. Spectra of ^{13}C CPMAS NMR of the different biomass samples (a, reed; b, pine pellets; c, Douglas fir wood chips; d, wheat straw; e, wheat straw leached; f, peach stones; g, peach stones leached; h, olive residue; i, olive residue leached).

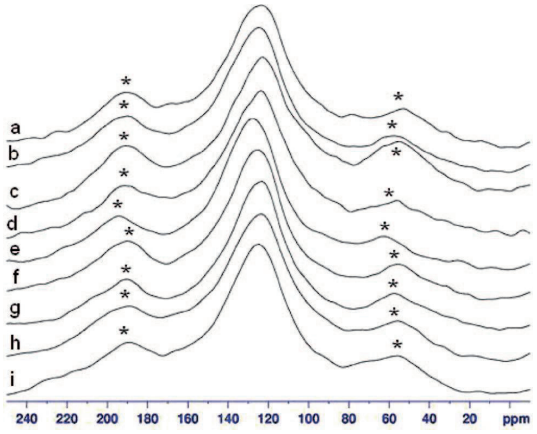

Figure 5. Spectra of ^{13}C single-pulse MAS NMR of the different biomass char samples, with a heating rate of 5 °C/min (∗, spinning sideband; a, reed char; b, pine pellets char; c, Douglas fir wood chips char; d, wheat straw char; e, wheat straw leached char; f, peach stones char; g, peach stones leached char; h, olive residue char; i, olive residue leached char).

The signals in the region of 112 and 115 ppm are assigned to lignin quaiacyl C-2 and C-5, respectively.

Lignin quaiacyl C-6 at 120 ppm is detected only in the case of pine pellets, peach stones, and olive residue.

Lignin syringyl C-1, syringyl C-5, and quaiacyl C-2 are detected for all biomass samples as a broad line in the region between 134 and 137 ppm.

The signals at 153 ppm are assigned to syringyl C-3 and syringyl C-5. The signals at 148 ppm are assigned to syringyl C-3, syringyl C-5, quaiacyl C-1, and quaiacyl C-4. For the reed,

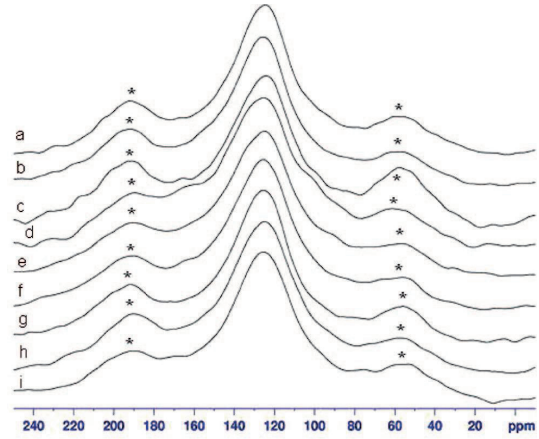

Figure 6. Spectra of ^{13}C single-pulse MAS NMR of the different biomass char samples, with a heating rate of 10 °C/min (∗, spinning sideband; a, reed char; b, pine pellets char; c, Douglas fir wood chips char; d, wheat straw char; e, wheat straw leached char; f, peach stones char; g, peach stones leached char; h, olive residue char; i, olive residue leached char).

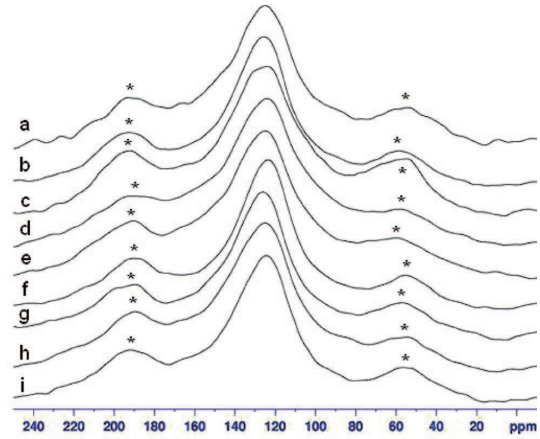

Figure 7. Spectra of ^{13}C single-pulse MAS NMR of the different biomass char samples, with a heating rate of 20 °C/min (∗, spinning sideband; a, reed char; b, pine pellets char; c, Douglas fir wood chips char; d, wheat straw char; e, wheat straw leached char; f, peach stones char; g, peach stones leached char; h, olive residue char; i, olive residue leached char).

the signal at 148 ppm is an upfield shoulder of the signal at 153 ppm. In the case of pine pellets and Douglas fir wood chips, the signal at 153 ppm is a downfield shoulder of the signal at 148 ppm. Wheat straw has a single broad line in this region. Peach stones and olive residue have two neighboring peaks.

All biomass samples have the acetyl carbonyl groups of hemicelluloses detected at 173 ppm. Although in the case of pine pellets, the signal is very low and scarcely distinguishable from noise. The carbonyl groups have a high reactivity.[9]

Ketones in the region of 190−220 ppm are detected in the case of Douglas fir wood chips, peach stones, and olive residue. It has to be mentioned that the intensities are very low.

(9) Scholze, B.; Hanser, C.; Meier, D. Characterization of the water-insoluble fraction from fast pyrolysis liquids (pyrolytic lignin) Part II. GPC, carbonyl groups, and ^{13}C-NMR. *J. Anal. Appl. Pyrolysis* **2001**, *58*−*59*, 387–400.

Table 2. Ash Chemical Analysis of the Biomass Samples (wt %)

	wheat straw	wheat straw leached	olive residue	olive residue leached	peach stones	peach stones leached	reed	Douglas fir wood chips	pine pellets
K_2O	15.86	10.94	27.23	10.033	38.45	21.24	5.87	4.13	7.66
Na_2O	4.3	0.48	4.17	0.05	0.07	0.02	8.39	1.48	1.31
CaO	14.4	15.3	10.22	23.94	7.14	19.32	2.9	10.9	37.3
MgO	2.67	2.49	3.79	0.92	2.73	2.53	1.37	4.9	9.08
SiO_2	39.2	49.89	32.6	39.32	5.97	10.47	73.7	55.5	11.2
Al_2O_3	1.95	1.93	2.96	0.93	0.47	0.02		11.6	5.0
Fe_2O_3	0.38	0.56	1.9	2.82	0.52	0.086	1.09	7.24	4.83
TiO_2	0.1	0.12	0.1	0.16	0.15	0.04	0.1	0.55	0.3
SO_3	5.27	3.76	4.97	5.85	5.24	3.16	5.18	0.54	1.33
P_2O_5							0.97	0.87	2.23
Cl	2.73	1.78	1.43	0.03	0.06	0.02	nd[a]	nd	nd

[a] nd = not determined.

Table 3. Pyrolysed Biomass Samples and Their Initial Amounts (g)

heating rate (°C/min)	wheat straw	wheat straw leached	olive residue	olive residue leached	peach stones	peach stones leached	reed	Douglas fir wood chips	pine pellets
5	2.4978	1.5376	4.7964	4.9685	5.0467	5.4364	1.6297	3.2032	2.4430
10	1.3986	1.5496	4.9347	4.8974	4.4554	5.4982	2.4469	3.4573	2.3707
20	1.5751	1.5350	5.0961	5.2441	5.1563	4.7607	2.2897	2.9861	2.2255

Table 4. Amounts and Number of Scans of the Biomass Samples, ^{23}MAS NMR Spectroscopy

	wheat straw	wheat straw leached	olive residue	olive residue leached	peach stones	peach stones leached	reed	Douglas fir wood chips	pine pellets
sample mass (g)	0.2172	0.2236	0.3752	0.3493	0.3119	0.324	0.2378	0.2471	0.2416
number of scans	1225	1225	2105	6160	221999	12300	2237	4400	63235

The C_α, C_β, and C_γ carbons of lignin are not detectable because of the high signals of the cellulose components in the region of 60−84 ppm. In most cases, the peaks of C_α, C_β, and C_γ are much lower, i.e., less intensive, than the peak of $Ar-OCH_3$ and $-OCH_3$ functional groups of lignin, and the peaks of cellulose components are more intensive than the peak of $Ar-OCH_3$ and $-OCH_3$.[9−11]

The broad signals refer to the unordered molecular structure of lignin and hemicelluloses and partly cellulose. Sharp signals at 105, 89, and 65 ppm stand for the ordered cellulose C1, C4, and C6 carbons, respectively.[12]

Consequently, it could be said that all of the original biomass samples have basically the same composition with some exceptions: only the Douglas fir wood chips, olive residue, and peach stones have ketones, and the olive residue sample also has an aliphatic CH_2 of lignin and lipids.

The spectra obtained with the CPMAS method do not allow for any estimation of the contents of lignin, cellulose, or hemicellulose using integrated intensities of the signals because of the interfering peaks of the different components. With the spin-locking technique, the spectrum of cellulose can be separated[13,14] but even then, the lignin and hemicellulose spectra remain indistinguishable.[15]

When the ^{13}C NMR spectra of the leached samples are compared to those of the original ones (Figure 4), it is evident that leaching has no effect. The small differences seen in the spectra could be attributed to noise.

3.1.2. Biomass Char Samples. Different authors have shown that the composition of wood changes during thermal treatment.[16] New carbon groups evolve, but finally at the end temperatures of pyrolysis at 600 °C, there are only aromatic groups left.[6,7,17]

Sharma et al.[10] have shown that the amount of aromatic carbons in a lignin char is less than in the original sample material. In their work, the concentration of aromatic lignin was decreased by 10% by weight at a heating temperature of 600 °C compared to the original sample material. Thus, most of the weight loss of the original lignin sample was due to the volatilization of the nonaromatic carbons. The aromatic component of lignin is very resistant to thermal degradation, and the resulting char is highly refractory.

Bardet et al.[17] have stated that the origin of biomass does not affect the nature of the solid residues formed during the thermal treatment. They all loose their ligno-cellulosic structure and are transformed to polycyclic material with a preponderance of aromatic structures with proton amounts that are decreased drastically as the temperature of treatment increases. It could be said that all cellulose and lingo-cellulosic materials under thermal treatment with final temperatures between 800 and 1000 °C undergo structural transformation, resulting in a graphitic structure.

In this study, we tested the effect of different heating rates and also the leaching pretreatment on the composition of the chars derived from the pyrolysis of the biomass samples at the

(10) Sharma, R. K.; Booten, J. B.; Baliga, V. L.; Lin, X.; Chan, W. G.; Hajaligol, M. R. Characterization of chars from pyrolysis of lignin. *Fuel* **2004**, *83*, 1469–1482.

(11) Kolodzlejski, W.; Frye, J. S.; Maclel, G. E. Carbon-13 nuclear magnetic resonance spectrometry with cross polarization and magic-angle spinning for analysis of lodgepole pine wood. *Anal. Chem.* **1982**, *54*, 1419–1424.

(12) Maunu, S. L. NMR studies of wood and wood products. *Prog. NMR Spectrosc.* **2002**, *40*, 151–174.

(13) Newman, R. H.; Hemmingson, J. A. Determination of the degree of cellulose crystallinity in wood by carbon-13 nuclear magnetic resonance spectroscopy. *Holzforschung* **1990**, *44*, 351–355.

(14) Newman, R. H.; Hemmingson, J. A. Carbon-13 NMR distinction between categories of molecular order and disorder in cellulose. *Cellulose* **1995**, *2*, 95–110.

(15) Advanced solid state NMR spectroscopy techniques in the study of thermally modified wood. Doctoral Thesis, University of Helsinki, Helsinki, Finland, 2004.

(16) Inari, G. N.; Mounguengui, S.; Dumarçay, S.; Pétrissans, M.; Gérardin, P. Evidence of char formation during wood heat treatment by mild pyrolysis. *Polym. Degrad. Stab.* **2007**, *92*, 997–1002.

(17) Bardet, M.; Hediger, S.; Gerbaud, G.; Gambarelli, S.; Jacquot, J. F.; Foray, M. F.; Gadelle, A. Investigation with ^{13}C NMR, EPR and magnetic susceptibility measurements of char residues obtained by pyrolysis of biomass. *Fuel* **2007**, *86*, 1966–1976.

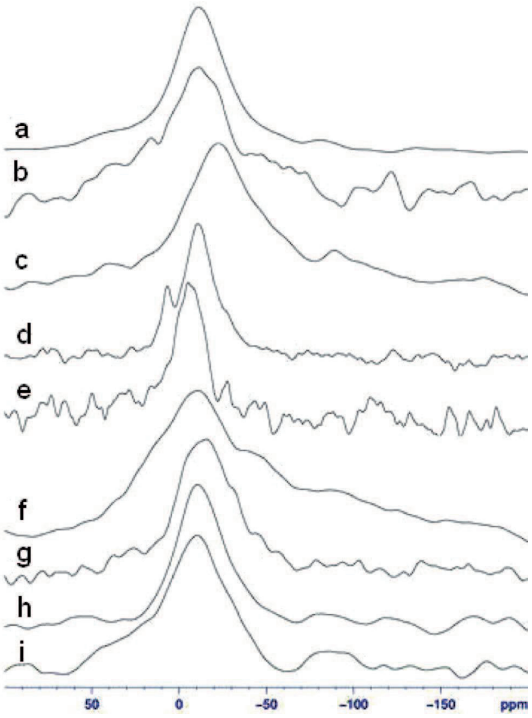

Figure 8. Spectra of ^{23}Na single-pulse MAS NMR of the different biomass samples (a, reed; b, pine pellets; c, Douglas fir wood chips; d, wheat straw; e, wheat straw leached; f, peach stones; g, peach stones leached; h, olive residue; i, olive residue leached).

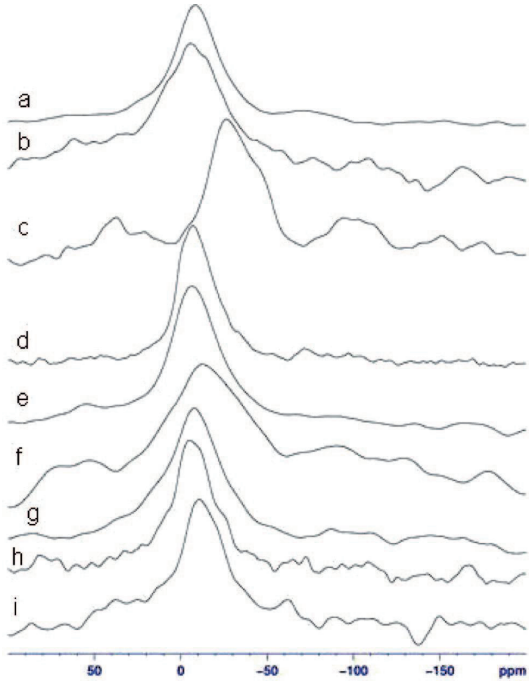

Figure 9. Spectra of ^{23}Na single-pulse MAS NMR of the different biomass char samples, with a heating rate of 5 °C/min (∗, spinning sideband; a, reed char; b, pine pellets char; c, Douglas fir wood chips char; d, wheat straw char; e, wheat straw leached char; f, peach stones char; g, peach stones leached char; h, olive residue char; i, olive residue leached char).

end temperature of 800 °C, and the results about carbon structure are shown in Figures 5−7.

All of the pyrolysis char samples prepared with different heating rates have one peak at 124−126 ppm assigned to aromatic lignin, and no differences were found between various char samples.

3.2. ^{23}Na MAS NMR Spectroscopy. ^{23}Na MAS NMR spectra are usually un-informative as to the specific identity of environments surrounding the ^{23}Na nuclei in amorphous systems, mainly because of the broad line shapes encountered. Another difficulty in ^{23}Na NMR is the ability of MAS to completely average away the effects of second-order quadropolar interactions, leading to residual line broadening in ^{23}Na MAS spectra.[18] Because the sodium content in the sample is extremely low, we were limited to a very basic single-pulse technique. Considering also relatively modest magnetic field strength available for the study, a certain second-order line shift and broadening can be assumed. Therefore, we can make assumptions based only on peak line shifts, combined of comparable second-order quadrupole and isotropic chemical-shift variations. A true chemical shift can be assumed to range from the peak to the left side foot of the line.[19]

The tests with sodium compounds in which the oxygen atoms are bonded to various elements of the third row of the periodic table (Al, Si, P, S, and Cl) carried out by Koller et al.[20] have shown a systematic shift to high field with an increasing atomic number of the third-row elements. As a consequence, they have concluded that the isotropic chemical shift is related to the particular chemical environment of the oxygen atoms coordinated to sodium. The distinct chemical-shift effects observed for ^{23}Na in different compounds have the same origin and the particular bonding situation of the oxygen atoms in the anions. This property can be described by the valence, i.e., the total bond valence of the oxygen atom. Of course, the chemical shift of the solids is further affected by Na−O distances and the coordination number of sodium.

There are few data available about ^{23}Na NMR of fuels and char in the literature. Burchill et al.[21] has investigated sodium with NMR in raw coals. They have shown that the sodium peak appears between 2.3 and −1.7 ppm, i.e., closely comparable to aqueous Na^+, but in our case, the peaks are far away from this region. This allows for the assumption that there is no or few aqueous Na^+ in the investigated biomass samples. Another trend common for the coals was that the higher the coal rank (i.e., carbon content), the lower the observed shift. The results of biomass samples support this finding, while the shifts are much lower than the ones in the case of coals. The carbon content of biomass samples is in the range of 46−52 wt % (see also Table 1) and for coals 67−85 wt %.

3.2.1. Biomass Samples. Table 4 presents a review regarding the used amounts of the samples and number of scans. The data such as the number of scans, sample mass, and chemical composition (see also Table 2) allow for an estimation of the ability to record the spectra.

The results of the ^{23}Na NMR spectroscopy of biomass samples are shown in Figure 8. For all samples, an isotropic peak at −11 ppm is identified in the spectra, except for Douglas fir and leached wheat straw, where single resonances are found at −22 and −5 ppm, respectively. Wheat straw has an extra

(18) Egan, J. M.; Müller, K. T. Detection and identification of corrosion products of sodium aluminoborosilicate glasses by ^{23}Na MQNMR and ^{1}H → ^{23}Na CPMAS NMR. *J. Phys. Chem. B* **2000**, *104*, 9580–9586.

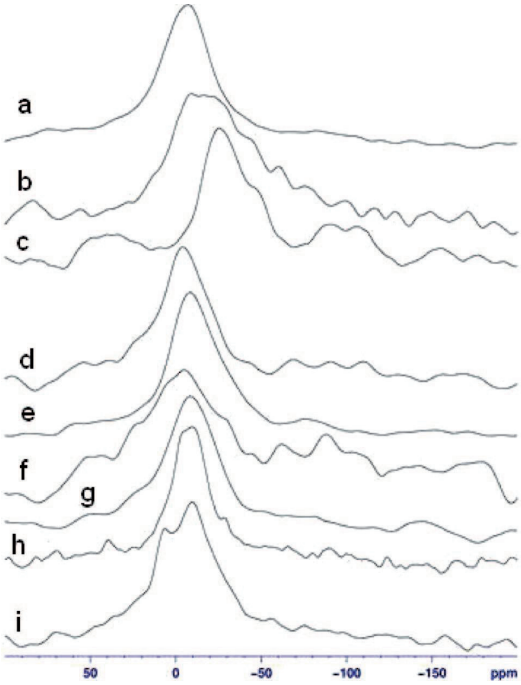

Figure 10. Spectra of ^{23}Na single-pulse MAS NMR of the different biomass char samples, with a heating rate of 10 °C/min (∗, spinning sideband; a, reed char; b, pine pellets char; c, Douglas fir wood chips char; d, wheat straw char; e, wheat straw leached char; f, peach stones char; g, peach stones leached char; h, olive residue char; i, olive residue leached char).

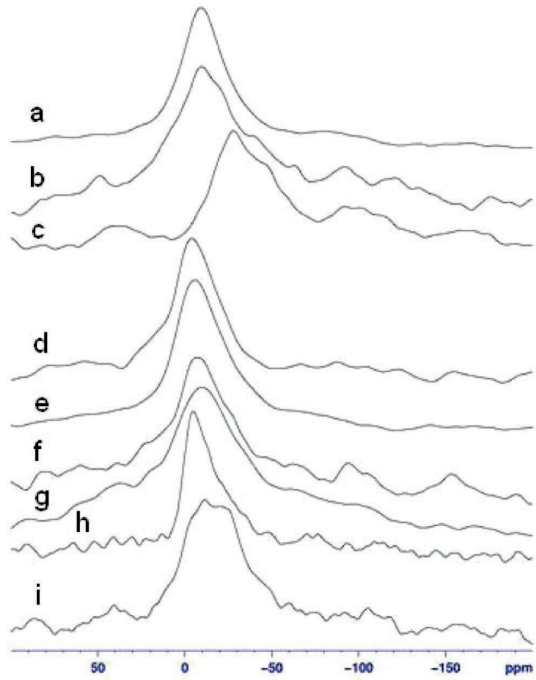

Figure 11. Spectra of ^{23}Na single-pulse MAS NMR of the different biomass char samples, with a heating rate of 20 °C/min (∗, spinning sideband; a, reed char; b, pine pellets char; c, Douglas fir wood chips char; d, wheat straw char; e, wheat straw leached char; f, peach stones char; g, peach stones leached char; h, olive residue char; i, olive residue leached char).

resonance at 7 ppm, which can be attributed to crystalline NaCl. Although high amounts of scans were recorded for pine pellets and peach stones (Table 4), the signal-to-noise ratio is poor, resulting in less reliable results.

3.2.2. Biomass Char Samples. The effect of the different heating rates and the leaching pretreatment on the sodium environment of the chars derived from the pyrolysis of the biomass samples at the end temperature of 800 °C are shown in Figures 9−11.

The spectra of all three different reed char samples resulted in an isotropic peak at the same region with the reed sample. This allows for the assumption that the sodium environment in the reed sample is resistant to the pyrolysis conditions described above.

The pine pellets char samples display broad line in the region of 100 to −100 ppm resembling to the original pine pellets sample.

In comparison to the original Douglas fir wood chips sample, the changes in line shape of the char samples could be detected. Instead of a relatively symmetrical shape of the peak of the original Douglas fir wood chips sample, the Douglas fir wood chips char samples exhibit relatively structured lines, which are compatible with a second-order quadrupole line shape, corresponding to a coupling constant of 2.1 MHz and chemical shift of −10 ppm. Equally plausible alternatives to this assumption are two chemical-shift-separated lines with a very low coupling constant at −10 and −25 ppm, respectively.

In comparison to the original wheat straw sample, there is only a one peak in the region from −4 to −7 ppm, instead of two peaks at 7 ppm assigned to crystalline NaCl and at −11 ppm.

The peach stone char samples have a peak in the region from −5 to −13 ppm. Similar to the original peach stones sample, also the chars do not have enough good properties for ^{23}Na MAS NMR spectroscopy measurements.

The olive residue char samples have a peak in the region from −5 to −10 ppm. In comparison to the original sample, the char samples do not have a symmetrical peak.

The leached wheat straw char samples have better properties for ^{23}MAS NMR spectroscopy measurements than the original sample, comparing the relevent spectra (Figures 8−11) and taking into account the number of scans of the chars that was 2 times lower from the original sample. Nevertheless, the shape and the region of the peak remain unchanged. No difference could be detected between the spectra of the wheat straw char samples and leached wheat straw char samples.

The spectra of the leached peach stone char samples have a narrower peak than the original leached peach stones sample. However, the region of the peak remains unchanged.

In the case of the leached olive residue char samples, the line shapes of the different pyrolysis char samples prepared with different heating rates could be distinguished. Further investigations with sophisticated methods are needed to elucidate wheth-

(19) Kundla, E.; Samoson, A.; Lippmaa, E. High-resolution NMR of quadropolar nuclei in rotating solids. *Chem. Phys. Lett.* **1981**, *83*, 229–232.

(20) Koller, H.; Engelhardt, G.; Kentgens, A. P. M.; Sauer, J. ^{23}Na NMR spectroscopy of solids: Interpretation of quadrupole interaction parameters and chemical shifts. *J. Phys. Chem.* **1994**, *98*, 1544–1551.

(21) Burchill, P.; Howarth, O. W.; Sword, B. J. MAS NMR studies of inorganic elements in coals and combustion residues. *Fuel* **1991**, *70*, 361–366.

er the differences are caused by noise or changes in the sodium environment.

4. Conclusions

The solid-state ^{13}C CPMAS spectra of a variety of biomasses consist of mainly acetylated carbonyl groups of hemicelluloses, lignin S1, S3, S4, S5, G1, and G4, anomeric C1 of cellulose, crystalline and amorphous C4 of cellulose, C2, C3, and C5 of cellulose, C6 of crystalline cellulose, methoxy groups of lignin, and acetylated methyl groups of hemicellulose could be identified. It was also detected that the leaching process does not affect the carbon composition of the biomass samples.

The single-pulse solid-state ^{13}C MAS analysis has proven that the origin of biomass, the leaching procedure, and the different heating rate do not affect the carbon composition of chars.

The final result of the char carbon structure in the present study confirms that it is not dependent upon fuel and heating rate and, moreover, also not affected by leaching. In every case, the ^{13}C NMR spectra show the aromatic structure of the char at the end temperature of 800 °C. Therefore, it can be anticipated that the carbon structure does not affect the reactivity of char.

The wheat straw sample, olive residue sample, the reed sample, and also the pine pellets sample have all of the peaks at −11 ppm, which would indicate that they all contain the same kind of Na compound.

^{23}Na NMR spectroscopy proves that the leaching affects the fuel properties, i.e., sodium chemistry in a biomass sample, and therefore, it could be assumed that the char reactivity is affected. Unfortunately, the single-pulse MAS at 79 MHz is not the best tool for ^{23}Na NMR spectroscopy because of broad spectra.

The NMR spectroscopy tests with the peach stone original and leached samples indicate that the abundance of sodium in the fuel is not the only issue in obtaining the NMR spectra; also the other properties of the fuels, such as the chemical composition, surrounding environment of Na^+ and/or magnetic susceptibility, and/or the relaxation behavior play an important role.

The effect of the heating rate on the sodium environment in chars prepared with different heating rates needs further investigation with sophisticated NMR methods.

Despite experimental difficulties, we were able to observe definite differences in line width and shifts of studied compounds. It is then quite possible that higher magnetic fields and more sophisticated techniques of resolution enhancement, multiple-quantum magic-angle spinning (MQ-MAS),[22] and double rotation (DOR)[23] may provide more detailed local information about the sodium environment in biomass and their char samples. Because this field of study is in a very exploratory stage, also comprehensive investigation of sodium model compounds is needed to identify the different compounds.

Acknowledgment. This research was supported by the European Community activity Large-Scale Facility Wageningen NMR Center [FP6-2004-026164 (2006−2009)].

EF800305G

(22) Medek, A.; Frydman, L. Quadrupolar and chemical shift tensor characterized by 2D multiple-quantum NMR spectroscopy. *J. Magn. Reson.* **1999**, *138*, 298–307.

(23) Wu, Y.; Sun, B. Q.; Pines, A.; Samoson, A.; Lippmaa, E. NMR experiments with a new double rotor. *J. Magn. Reson.* **1990**, *89*, 297–309.

PAPER II

Link, S., Arvelakis, S., Paist, A., Hupa, M., Yrjas, P., Külaots, I. Effect of leaching pretreatment on the char reactivity of pyrolyzed wheat straw. 17th European Biomass Conference & Exhibition, 29.06-03.07.2009. Hamburg, Germany, p. 1113-1121.

EFFECT OF LEACHING PRE-TREATMENT ON THE CHAR REACTIVITY OF PYROLYZED WHEAT STRAW

Link S.
Thermal Engineering Department, Tallinn University of Technology
Kopli 116, 11712, Tallinn, Estonia
Tel: +372 620 3900 Fax: +372 620 3901
e-mail: siim.link@ttu.ee
Arvelakis S.
Department of Chemical Engineering, National Technical University of Athens
Zografou Campus, GR-15700, Athens, Greece
Tel: +302 1 077 23163 Fax: +302 1 077 23288
e-mail: sarvel_1999@yahoo.com
Paist A.
Thermal Engineering Department, Tallinn University of Technology
Kopli 116, 11712, Tallinn, Estonia
Tel: +372 620 3902 Fax: +372 620 3901
e-mail: apaist@sti.ttu.ee
Hupa M., Yrjas P.
Åbo Akademi Process Chemistry Centre, c/o Combustion and Materials Chemistry
Biskopsgatan 8, FI-20500, Åbo, Finland
Tel: +358 2 215 4722 Fax: +358 2 215 4962
e-mail: mikko.hupa@abo.fi, patrik.yrjas@abo.fi
Külaots I.
Division of Engineering, Brown University
Box D, RI 02912, Providence, USA
Tel: +1 401 863 3977, Fax: +1 401 863 9120
e-mail: indrek_kulaots@brown.edu

ABSTRACT: In this study the oxidation reactivity of chars derived from the pyrolysis of untreated and pre-treated wheat straw samples is investigated. The direct reactivity measurements are compared with the results from indirect methods used to characterize the physical and chemical properties of materials such as proximate and ultimate analysis, ash chemical analysis, scanning electron microscopy (SEM), and specific surface area measurements. The direct reactivity measurements prove the effect of leaching pre-treatment on the lower reactivity during the gasification of the wheat straw pyrolysis char. The results from the gasification tests with steam indicate that the reaction rate is not affected by the evolution of porosity and internal surface area, and it is rather dependent on the alkali content behaving as catalyst in the sample material. The differences in reaction rates between the untreated and leached wheat straw pyrolysis char samples are smaller in the case of steam gasification compared to CO_2 gasification. The total conversion is seen to be higher in the case of leached material.
Keywords: wheat straw, pretreatment, pyrolysis, char, reactivity

1 INTRODUCTION

Power generation from biomass, such as agricultural residues, has been investigated by the research community over the last decades. More specifically, the power generation from biomass in small scale units is under investigation. In addition, the thermochemical conversion of biomass is considered to be CO_2 neutral and utilizing biomass for energy generation is the alternative to decrease CO_2 emissions from the fossil fuel power stations. Wheat straw is one of the most promising agricultural residues as a fuel source, suitable for energy production in the Mediterranean region [1] as well as in Europe and worldwide.

Pyrolysis and gasification are thermochemical conversion processes to recover energy from biomass. Pyrolysis is not only an independent conversion process but also part of the gasification process, which can be broadly separated into two main stages, solid devolatilization (pyrolysis) and char conversion (gasification). Char reactivity in the second stage is dependent upon the formation conditions (essentially temperature and heating rate) and the amount and composition of the inorganic content. In addition, the type of biomass (chemical composition and physical properties) also largely affects both biomass devolatilization and char conversion [2]. The kinetics of char oxidation is generally much slower than the pyrolysis itself and is therefore the rate determining [3]. High char reactivity is important for the energy output capacity of the reactors [4].

Marquez-Montesinos *et al* [5] shows that the presence of inorganic constituents in chars play important role to oxidation kinetics due to catalytic effects. Sodium, potassium and calcium, which are commonly present in biomass, show a significant activity as gasification catalysts.

The inorganic constituents such as K, Na, Cl in biomass fuels elevate the problems associated with mineral deposition, sintering, agglomeration, corrosion and/or erosion in combustion and gasification plants [6]. The leaching pre-treatment process is considered to be a low cost treatment technique for the elimination of alkali metals and chlorine from the biomass. On the other hand, after complete or partial removal, the lower content of alkali metals could affect the char gasification reactivity.

The oxidation reactivity of biomass chars is affected by several chemical and physical properties of the

material such as char morphology, chemical composition, porosity and the specific surface area. On top of the conventional proximate, ultimate, and ash chemical analysis there are several analytical techniques available to determine the different physical properties of a material such as the Scanning Electron Microscopy to study the morphology of the surface and the surface area and porosity using N_2 and CO_2 adsorption techniques.

The SEM technique is widely applied on the investigation of biomass char samples [4,5,7-14]. In addition to the SEM technique, we have also applied an energy dispersive X-ray spectroscopy technique to obtain better background information of the particles observed by SEM.

Today, physical adsorption volumetric techniques of N_2 (77 K) and CO_2 (273 K) are recommended for use by several studies, gathering information regarding the porosity of carbonized solids, i.e. chars, activated carbons [8,15,]. This is because the N_2 and CO_2 adsorbates do not measure the same range of microporosity [16]. That is explained as the diffusional limitation, of the nitrogen molecules at 77 K into super micropores with dimensions similar to those of the nitrogen molecule at the low temperature used for adsorption [15,17] and this was seen more than 20 years ago [18].

The present work focuses on studying the effect of leaching as a pre-treatment process to the properties and reactivity of wheat straw pyrolysis char.

2 EXPERIMENTAL SECTION

2.1 Materials and procedures

The wheat straw sample was obtained from the area of Thessaly in Greece. The raw wheat straw sample was pre-treated using the leaching pre-treatment process. The leaching was performed with tap water according to the method developed by Arvelakis *et al* [6]. The used mass-to-water ratio of leaching is 66.6 g/l.

The untreated and leached wheat straw samples (hereafter used as WSU and WSL respectively, and for char samples WSU800 and WSL800) are prepared and characterized regarding their proximate and ultimate analysis, calorific value and ash content (in all cases the oxidation is performed at the temperature of 600 °C) in accordance with ASTM methods (Table I-IV).

An atmospheric pressure fixed-bed reactor was used for the preparation of the char samples. The pre-treated and untreated wheat straw samples were heated up with heating rate of 20 °C/min up to 800°C and held isothermal for 15 minutes before cooling down. The schematic diagram and detailed description of the system along with the procedure have been reported elsewhere [19]. Nitrogen was used as a carrier gas with a flow rate of 1 L/min in all pyrolysis experiments.

Similarly with the wheat straw analysis, the wheat straw char product samples were characterized regarding their proximate and ultimate analysis and ash content in accordance with ASTM methods (Table I-IV).

The ash content of gasification residue for the calculation of the total residue yield (Table VIII-IX) dry and ash free (daf) basis was determined with a Setaram thermogravimetric analysis (TGA) set-up. The heating rate of 10K/min up to 600°C was applied. The ash content was calculated according to mass loss data after burning process indicated by DTA (differential thermal analysis) as exothermal peak, in the temperature range of 350-500 °C. The air flow rate of 50 mL/min was used.

2.2 Morphology

The morphology of the parent and char material is examined by SEM. All the SEM work was performed with a Leo 1530 Gemini with operating voltage at 15 kV.

2.3 Surface area and porosity

Nitrogen adsorption isotherms at 77K and carbon dioxide isotherms at 273 K were obtained on the char samples using a Quantachrome Autosorb-1 instrument. Prior to the surface area analysis, all the char samples were out-gassed at 300°C overnight under vacuum to ensure complete removal of surface contaminants. 84-point nitrogen and carbon dioxide isotherms were obtained to calculate the Brunauer, Emmett and Teller (BET) surface areas and porosities of the samples [20,21]. The BET surface area of the char samples was determined over the partial pressure (P/Po) range where the BET equation had the highest correlation coefficient (at least 0.9999). For most non-microporous samples, the commonly accepted range of P/Po for BET equation is from 0.05 to 0.3 (nitrogen isotherms). However, due to the highly microporous nature of the char samples, the isotherms' relative pressure range for BET area determination requires adjustment. Therefore, the BET areas were defined at significantly lower relative pressure P/Po values, down to P/Po 0.01 to 0.05.

The porosity values presented in this work were calculated using the nitrogen adsorption isotherms of the char samples. The microporosity of the char samples was determined using the Dubinin-Radushkevitch (DR) model [21]. The mesoporosity of the char samples was determined by subtracting from the total porosity at an isotherm relative pressure of P/Po=0.95 the DR microporosity value. The macroporosity of the char sample was calculated by subtracting the total porosity at relative pressure P/Po = 0.95 from the porosity value at relative pressure P/Po = 0.99.

The pore-size distribution of the char samples was determined from the nitrogen adsorption isotherms at 77 K and carbon dioxide adsorption isotherms at 273 K using density functional theory (DFT). The pore size distributions of the wheat straw chars are reported according to classification of International Union of Pure and Applied Chemistry (IUPAC), which defines micropores as pores less than 20Å, pores in the range of 20Å to 500Å as mesopores, and pores above 500Å as macropores.

2.4 Char reactivity measurement

The reactivity of the char samples was determined by recording the weight change of the sample as a function of time using a Deutche Montan Technologie (DMT) high pressure thermogravimetric apparatus (TGA) operating at atmospheric pressure. At first, the sample is held in the reactor under helium-purged environment. Then the desired reaction temperature was selected and the reactor heated up to target temperature (reactivity tests are performed at 750, 800, 850, and 900 °C). After the reactor has reached to the isothermal set temperature, the sample holder was lowered down to the reaction tube with an electrically driven winch system. The stable sample mass is achieved after 150-300 s counting from the registered first data point by the measurement device having time delay of some seconds after lowering the sample. When the stable mass is reached the gasification

agent is introduced into the reactor. CO_2 with a flow rate of 1 L/min and steam/nitrogen mixture with a total flow rate of 2 L/min are used as gasification agents. Different steam to nitrogen ratios were utilized with a steam content of 10%, 20% and 100%. The schematic diagram and detailed description of the system have been reported elsewhere [22].

2.5 Reactivity data analysis

In this work the results are presented as plots of the char gasification rate as a function of conversion for conversions between 10 and 90%. The gasification rate at any particular conversion is defined as the slope of the weight-loss curve at that point divided by the total mass of char gasified and is expressed in units of % min^{-1}.

$$r=dX/dt$$

where *r* is the reaction rate,

$$X=(M_o-M(t))/(M_o-M_f)$$

where M_0 - is the initial mass of the char, M(t) is the mass of char at time *t*, and M_f is the mass of the residue.

3 RESULTS AND DISCUSSION

3.1 Material characterization

The influence of leaching pre-treatment on the properties of the parent material could be observed (Tables I-IV). The removal of mineral matter by leaching increases the volatile matter content and as expected, decreases the potassium and chlorine contents. The increase in volatile matter content by demineralization via leaching or other technique has also been observed by others [23].

Table I: Proximate analysis of the materials, dry basis (wt%)

Material	Moisture	Ash	Volatile matter	Fixed carbon
WSU	8.10	7.60	76.00	16.40
WSL	5.75	5.87	80.65	13.48
WSU800	7.96	28.03	10.29	61.68
WSL800	6.40	36.07	12.26	51.66

WSU 800 exhibits lower ash content than WSL800 that could be attributed to the volatilization of alkali metals during the pyrolysis.

Table II: Ultimate analysis of the materials, dry basis (wt%)

Material	N	C	H	S	Cl	O
WSU	0.79	43.70	5.08	0.43	0.44	41.96
WSL	0.57	46.26	5.31	0.20	0.10	41.68
WSU800	1.17	46.57	1.13	n.d.	n.d.	23.10
WSL800	1.34	45.48	0.78	n.d.	n.d.	16.33

Table III: Gross calorific value of the materials, dry basis (MJ/kg)

Material	Calorific value
WSU	18.91
WSL	20.03
WSU800	n.d.
WSL800	n.d.

Table IV: Ash chemical analysis of the materials, wt%

	WSU	WSL	WSU800	WSL800
K_2O	20.95	4.01	18.13	4.57
Na_2O	0.90	1.88	1.58	2.03
CaO	14.40	15.30	6.33	18.35
MgO	2.67	2.49	0.80	3.59
SiO_2	39.20	49.89	51.61	49.54
Al_2O_3	1.95	1.93	1.93	1.22
Fe_2O_3	0.38	0.56	0.56	0.45
TiO_2	0.10	0.12	n.d.	n.d.

3.2 Char yields of pyrolysis

The pyrolysis char yields of the pre-treated and untreated wheat straw samples are calculated as dry as dry and ash free basis (Table V).

Table V: Pyrolysis char yields, %

	WSU	WSL
Dry	30.05	27.13
Dry and ash free	21.11	16.64

The WSU has a higher pyrolysis char yield calculated as dry basis (Table V). The lower pyrolysis char yield of WSL calculated as dry and ash free basis refers to the better carbon conversion to the gaseous products compared with WSU.

3.3 SEM images

The SEM images of the particles of the untreated wheat straw sample are shown in Fig. 1.

The circular silicon particles can be observed in Fig. 1 a and b. We were able to detect pure inorganic particles, mainly consisting of silicon (Fig. 1 c). The parent untreated wheat straw particles also exhibit slits and holes in the surface layer and show some surface roughness (Fig. 1 d and f). The images of the char sample indicate that the changes in morphology are quite evident. The softening of particle surfaces can be seen in Fig. 2 b. Also the growth of the mineral matter deposits on the particle surfaces was observed. The circular silicon particles observed on surface of the parent material (Fig. 2 a-b) have lost their initial morphology and the edges were smoothed in the char samples. The breakage and internal porous structure are seen in the char samples presented on Fig. 2 d and e. This could be characterized as polygonal cell in a pattern that resembles to honeycomb. The opening in the range of 450 nm could be seen in the SEM images of the char samples.

The SEM images of the particles of the leached wheat straw biomass and char samples are shown in Fig. 3 and Fig. 4. It could be seen that the carbon morphology is not affected by the leaching process.

In general, the morphological differences between the parent material and the char sample were observed. Both, the untreated and pre-treated wheat straw pyrolysis chars exhibit the surface softening. Furthermore, a quite clear growth of the inorganic deposits on the surface is observed. This type of migration of inorganic constituents to the surface, as a consequence of thermal conversion process, has also taken place with other types of biomass [24].

3.4 Specific surface area

The nitrogen isotherm BET surface area of WSU800 exhibits a relatively low value – 25 m^2/g (Table VI). The investigated char samples have quite similar CO_2 BET surface areas, indicating that pores are similar and similarly accessible for CO_2. It could be presumed that the super-micropores, present on these char samples, are not always accessible to N_2.

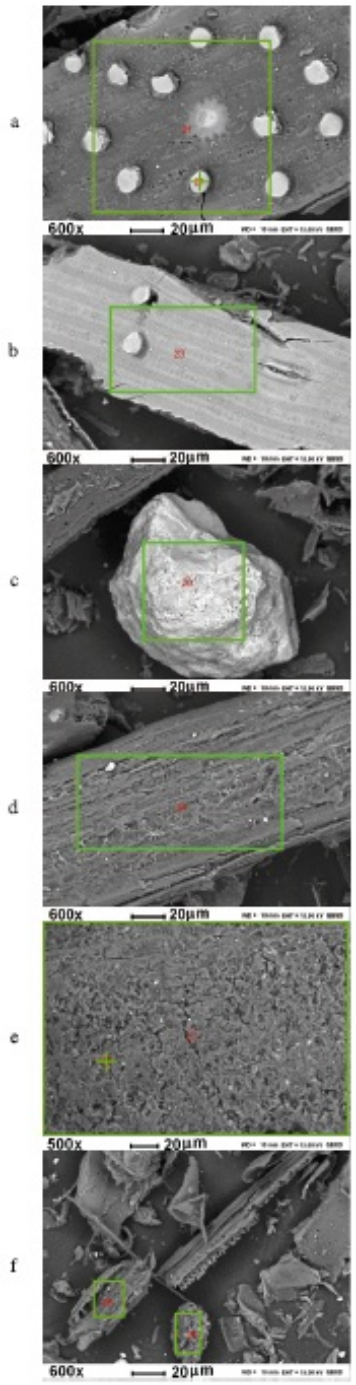

Figure 1: SEM images of WSU

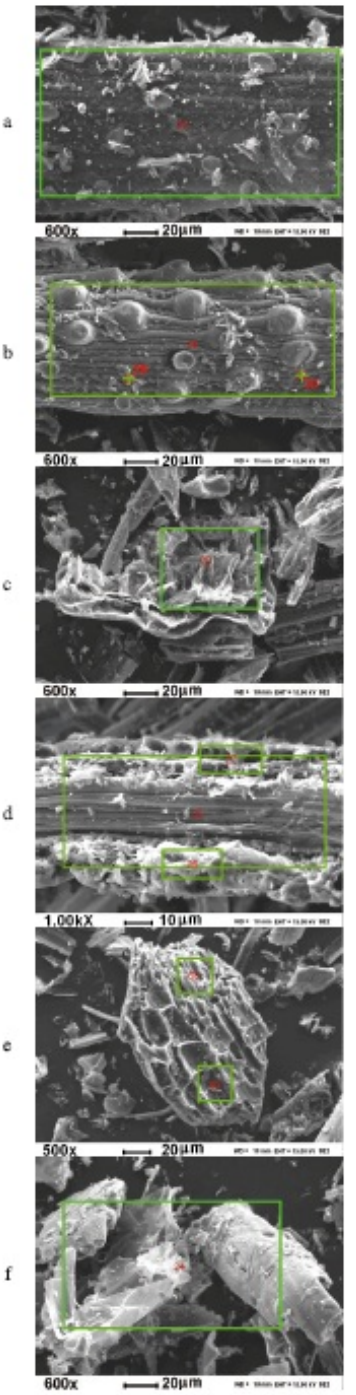

Figure 2: SEM images of WSU800

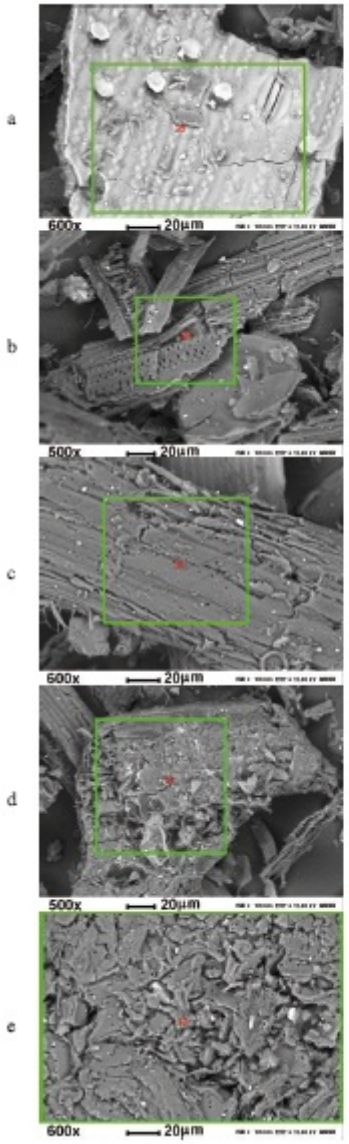

Figure 3: SEM images of WSL

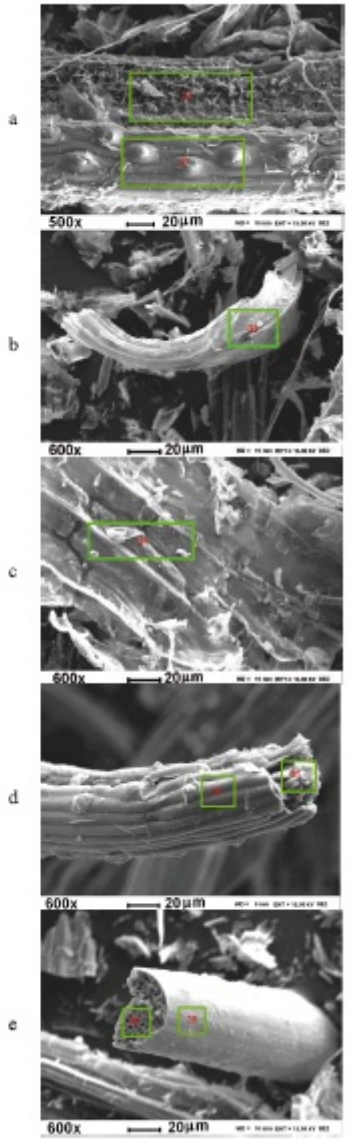

Figure 4: SEM images WSL800

Table VI: BET surface areas, m^2/g

	N_2	CO_2
WSU800	25	348
WSL800	152	354

Table VII: Porosities obtained from N_2 isotherm, ml of N_2/g

	Micro-porosity	Meso-porosity	Macro-porosity	Total Porosity
WSU800	0.009	0.010	0.015	0.034
WSL800	0.051	0.082	0.035	0.168

WSL 800 sample has a network of micropores (Fig. 5), pores with sizes 8Å and 16Å, and wide network of mesopores 25 Å to 55 Å. WSU 800 exhibits little microporosity (pore sizes around 16 Å), and almost zero mesoporosity compared to WSL 800.

Both char samples have a wide range of super-micropores (not seen with N_2 adsorption DFT analysis), pores sizes below 8 Å (Fig. 6). All micropores are similarly accessible for carbon dioxide.

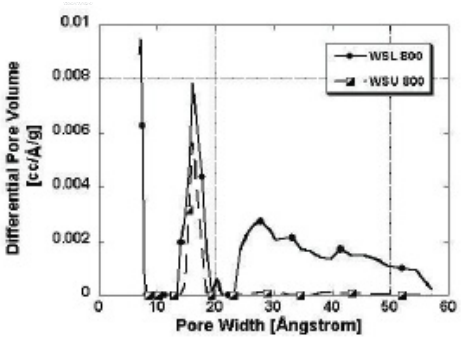

Figure 5: DFT/Monte-Carlo differential pore volume distribution. DFT Kernel used: N_2 at 77 K

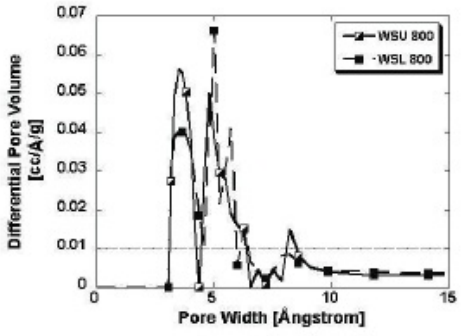

Figure 6: DFT/Monte-Carlo differential pore volume distribution. DFT Kernel used: CO_2 at 273 K

As seen from the results, the leaching affects the porosity and internal surface area of the pyrolysis char sample.

In this study the initial surface areas of the char samples are determined, but it is known that the surface area and porosity of the char changes when oxidized at different char burn-off levels [25, 26], and during the gasification, the surface area increases up to a point at which the rate of formation of the new area is offset by the rate of destruction of the old area. The increase of the char surface area vs the char burn off level usually passes through a maximum.

3.5 Reactivity

The reaction rate versus burn-off of WSU800 and WSL800 are shown in Fig. 7-9. The gasification temperature is 850 °C. The residue yield of the gasification tests and the total residue yield counting from parent material are shown in Table VIII and Table IX.

The residue yield of char gasification as dry basis (Table VIII) is lower in the case of untreated wheat straw, but as dry and ash free basis the gasification residue yield is lower for leached wheat straw pyrolysis char. Similarly to the char gasification residue yield, behaving the values of the total residue yield (Table IX). The lower residue yield dry and ash free basis refers to the circumstance that more carbon is converted to the gaseous substance.

Table VIII: Residue yield of char gasification at 850 °C, %

	WSU800		WSL800	
	Dry basis	Daf basis	Dry basis	Daf basis
100% CO_2	23.72	6.47	38.60	6.11
10% steam	28.56	9.35	33.29	1.96
20% steam	26.25	n.d.	30.76	2.05
100% steam	26.77	10.97	30.65	1.96

Table IX: Total residue yield after pyrolysis and gasification, % (gasification temperature of 850 °C)

	WSU800		WSL800	
	Dry basis	Daf basis	Dry basis	Daf basis
100% CO_2	7.13	1.35	10.47	1.02
10% steam	8.58	1.95	9.03	0.33
20% steam	7.89	n.d.	9.12	0.34
100% steam	8.04	2.29	8.31	0.19

Gasifying the chars with CO_2 (Fig. 7), the reactivity of the char sample increases and exhibits the maximum value at burn-off level of 20-40%. From that point forward the reactivity declines continuously. It is evident that the untreated wheat straw char has higher reactivity than the leached one – the maximum reaction rate differs by a factor of 4.

The reaction rate curves of CO_2 gasification follow the path of the curves of nitrogen BET surface area versus burn-off determined for coal [26]. It seems that the reaction rate along the gasification process using CO_2 as gasification agent is dependent on the porosity, i.e. surface area development during the process.

The reactivity path of steam gasification over burn-off shows different behaviour (Fig. 8-9). The maximum reaction rate is achieved at the beginning and along the process the reactivity values versus burn-off decline. The highest reaction rate of steam gasification is achieved using 100% of steam. In both cases (WSU800 and WSL800) the maximum reaction rate of using 100% and 20% steam diverges by a factor of 2, and using 100% and 10% steam by a factor of 3. The maximum reaction rate

of WSU800 and WSL800 differs by a factor of 1.5, using same proportion of steam as gasification agent.

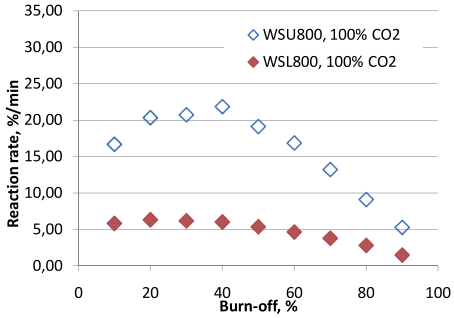

Figure 7: Char gasification reactivity. Gasified at 850 °C in 100% CO_2

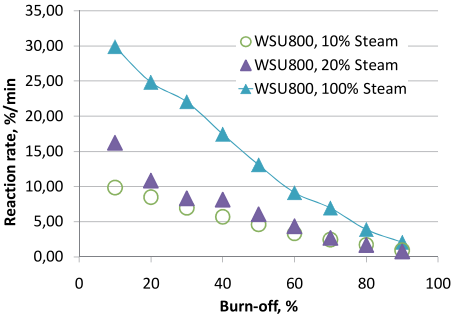

Figure 8: WSU800 gasification reactivity. Gasified at 850 °C in steam

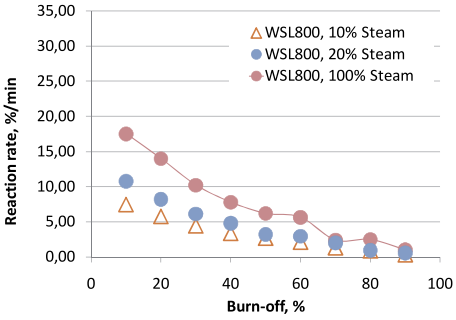

Figure 9: WSL800 gasification reactivity. Gasified at 850 °C in steam

The burn-off vs time of gasification tests is plotted in Fig. 10-12. In Fig. 11, the test with 10% of steam has a shorter duration than the test with 20% of steam. This is caused by the problems with a steam flow occurred during the experiment.

The CO_2 gasification of the leached wheat straw char sample lasts 3.5 times longer than that of untreated one (Fig. 10).

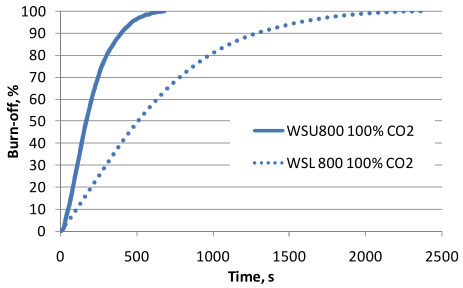

Figure 10: Burn-off vs time, CO_2 gasification

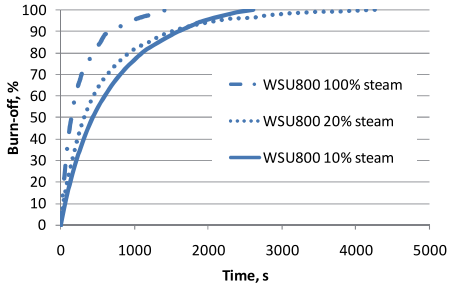

Figure 11: Burn-off vs time, steam gasification of WSU800

In the case of the untreated wheat straw pyrolysis char sample, the gasification test with 100% of steam has a 2 times longer duration than the test with 100% of CO_2 (Fig 10 and 11), and the gasification test with 20% of steam has a 3 times longer duration than the test with 100% of steam.

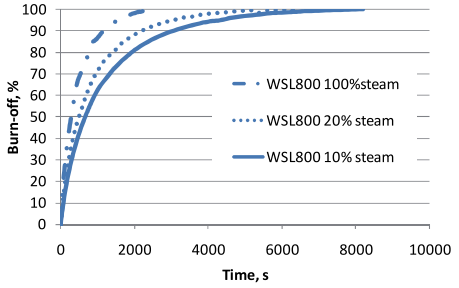

Figure 12: Burn-off vs time, steam gasification of WSU800

The leached wheat straw pyrolysis char gasification tests with 100% of CO_2 and steam exhibit almost the same duration (Fig. 10 and 12). At the beginning of the 100% steam gasification, the reaction rates are significantly higher compared to the case of the 100% CO_2 gasification. The char gasification test of the leached wheat straw pyrolysis char sample with 20% of steam has a 2.4 times longer duration than the test with 100% of steam.

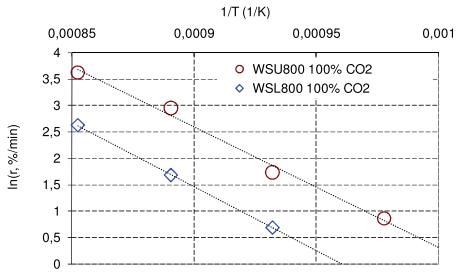

Figure 13: Comparison of gasification reactivities of CO_2 gasification at conversion rate of 50%

In activation energy determination, it is necessary to know when the chemical reaction is the kinetically controlled reaction regime. The Arrhenius plots of the gasification tests are shown in Fig. 13 and 14.

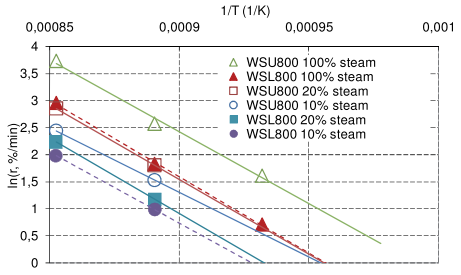

Figure 14: Comparison of gasification reactivities of steam gasification at conversion rate of 50%

Table X: Activation energies at conversion rate of 50%, kJ/mol

	WSU800	WSL800
100% CO_2	190	202
10% steam	199	219
20% steam	230	232
100% steam	221	235

The activation energy values of the pre-treated and untreated pyrolysis chars gasified in steam are in the range of 199-235 kJ/mol. In CO_2 we obtain the activation energies in the range of 190-202 kJ/mol. According to Barrio *et al* [27,28], most values of the activation energy values, gathered from different studies, for steam gasification activation are in the range 180 and 270 kJ/mol, and in CO_2 gasification 196-250 kJ/mol. The activation energies obtained in this work are in good agreement with the literature values. The lower is the activation energy the less heat is needed to promote the reaction. One way to reduce the needed activation energy is by using catalysts such as alkali metals that in the case of biomass might be already present in the material. This circumstance supports the fact that WSL800 has less potassium that acts as catalyst during gasification.

4 CONCLUSIONS

The wheat straw leaching pre-treatment technique is advantageous tool eliminating alkali metal content in the biomass samples. On the other hand, the reactivity measurement shows that the leaching pre-treatment lowers the reactivity of the pyrolysis char of the pre-treated material compared to the untreated one due to the removal of mineral matter such as K, which act like catalysts in the oxidation reaction. The results from the gasification tests with steam indicate that the reaction rate is not affected by the evolution of porosity and internal surface area, but is rather dependent on the alkali content of the biomass materials that acts as a catalyst. The differences in reaction rates between the untreated and leached wheat straw pyrolysis char samples are significantly smaller in the case of steam gasification compared to CO_2 gasification. The tests with 100% CO_2 exhibit higher reactivity than with 100% of steam. Though, it could be considered, in real gasifier running under atmospheric pressure, the CO_2 content in a gas mixture is 10-15% and therefore the reactivity values with CO_2 are also lower. However, the total conversion was seen to be higher in the case of the leached wheat straw material compared to the untreated wheat straw material. The char gasification residue yield differs by 6% and the total yield after pyrolysis and gasification by 24% in the case of the CO_2 gasification, and it is seen to be substantially higher in the case of steam gasification.

5 REFERENCES

[1] S. Arvelakis, P. Vourliotis, E. Kakaras, E.G. Koukis. Effect of leaching on the ash behavior of wheat straw and olive residue during fluidized bed combustion. Biomass and Bioenergy, 20, 2001, 459-470.

[2] C. Di Blasi,. G. Signorelli, C. Di Russo, G. Rea. Product Distribution from Pyrolysis of Wood and Agricultural Residues. Ind. Eng. Chem. Res., 38, 1999, 2216-2224.

[3] A. Cetin, R. Gupta, B. Moghtaderi. Effect of pyrolysis pressure and heating rate on radiata Pine char structure and apparent gasification reactivity. Fuel, 84, 2005, 1328-1334.

[4] R. Zanzi, K. Sjöström, E. Björnbom. Rapid high-temperature pyrolysis of biomass in a free-fall reactor. Fuel, 75, 1996, 545-550.

[5] F. Marques-Montesinos, T. Cordero, J. Rodrígues-Mirasol, J. J. Rodrígues. CO_2 and steam gasification of a grapefruit skin char. Fuel, 81, 2002, 423-429.

[6] S. Arvelakis, E.G. Koukios. Physicochemical upgrading of agroresidues as feedstocks for energy production via thermochemical conversion methods. Biomass Bioenergy, 22, 2002, 331-348.

[7] M.J. Wornat, R.H. Hurt, N.Y.C. Yang, T.J. Headley. Structural and compositional transformations of biomass chars during combustion. Combustion and Flame, 100, 1995, 131-145.

[8] P.A. Della Rocca, E.G. Cerrella, P.R. Bonelli, A.L. Cukierman. Pyrolysis of hardwoods residues: on kinetics and char characterization. Biomass and Bioenergy, 16, 1999, 79-88.

[9] P.R. Bonelli, P.A. Della Rocca, E.G. Cerrella, A.L. Cukierman. Effect of pyrolysis temperature on composition, surface properties and thermal degradation rates of Brazil Nut shells. Biosource Technology, 76, 2001, 15-22.

[10] C. Fushimi, K. Araki, Y. Yamaguchi, A. Tsutsumi. Effect of heating rate on steam gasification of

biomass. 1. Reactivity of char. Ind. Eng. Chem. Res., 42, 2003, 3922-3928.
[11] E.Cetin, B. Moghtaderi, R. Gupta, T.F. Wall. Influence of pyrolysis conditions on the structure and gasification reactivity of biomass chars. Fuel, 83, 2004, 2139-2150.
[12] M. Guerrero, M.P. Ruiz, M.U. Alzueta, R. Bilbao, A. Millera. Pyrolysis of eucalyptus at different heating rates: studies of char characterization and oxidative reactivity. J. Anal. Appl. Pyrolysis, 74, 2005, 307-314.
[13] A.A. Boateng, P.H. Cooke, K.B. Hicks. Microstructure development of chars derived from high-temperature pyrolysis of barley (*Hordeum vulgare* L.) hulls. Fuel, 86, 2007, 735-742.
[14] E. Biagini, P. Narducci, L. Tognotti. Size and structural characterization of lignin-cellulosic fuels after the rapid devolatilization. Fuel, 87, 2008, 177-186.
[15] D. Lozano-Castelló, D. Cazorla-Amorós, A. Linares-Solano. Usefulness of CO_2 adsorption at 273 K for the characterization of porous carbons. Carbon, 42, 2004, 1233-1242.
[16] J. Garrido, A. Linares-Solano, J.M. Martín-Martínez, M. Molina-Sabio, F. Rodríguez-Reinoso, R. Torregrosa. Use of N_2 vs. CO_2 in the characterization of activated carbons. Langmuir, 3, 1987, 76-81.
[17] C.R. Reid, K.M. Thomas. Adsorption of gases on a carbon molecular sieve used for air separation: linear adsorptives as probes for kinetic selectivity. Langmuir ,15, 1999, 3206-3218.
[18] F. Rodríguez-Reinoso, J. de D. Lopez-Gonzalez, C. Berenguer. Activated carbons from almond shells-I. Preparation and characterization by nitrogen adsorption. Carbon, 20, 1982, 513-518.
[19] S. Link, S. Arvelakis, H. Spliethoff, P. De Waard, A. Samoson. Investigation of biomasses and chars obtained from pyrolysis of different biomasses with solid state ^{13}C and ^{23}Na Nuclear Magnetic Resonance. Energy&Fuels, 22, 2008, 3523-3530.
[20] S. Brunauer, P.H. Emmett, E. Teller. Adsorption of gases in multimolecular layers J. Am. Chem. Soc. 60, 1938, 309-319.
[21] S.J. Gregg, K.S.W. Sing. Adsorption, surface area and porosity**.** Academic Press, 1982.
[22] K. Whitty, R. Backman, M. Hupa. Influence of char formation conditions on pressurized black liquor gasification rates. Carbon, 36, 1998, 1683-1692.
[23] K. Raveendran, A. Ganesh, K.C. Khilart. Influence of mineral matter on biomass pyrolysis characteristics. Fuel, 74, 1995, 1812-1822.
[24] P.A. Della Rocca. Study on biomass thermal conversion processes. Facultad de Ciencias Exactas y Naturales. Universidad de Buenos Aires. PhD thesis, 1998.
[25] I. Külaots, I. Aarna, M. Callejo, R.H. Hurt, E.M. Suuberg. Development of porosity during coal char combustion. Proceedings of the Combustion Institute, 29, 2002, 495-501.
[26] I. Aarna, E.M. Suuberg. Changes in reactive surface area and porosity during char oxidation. 27th Symposium (International) on Combustion/The Combustion Institute, 1998, 2933-2939.
[27] M. Barrio, B. Gøbel, H. Risnes, U.Henriksen, J.E. Hustad and L.H. Sørensen. Steam gasification of wood char and the effect of hydrogen inhibition on the chemical kinetics. Progress in thermochemical biomass conversion. IEA Bioenergy, 1, 2001, 32-46.
[28] M. Barrio, J.E. Hustad. CO_2 gasification of birch char and the effect of CO inhibition on the calculation of chemical kinetics. Progress in thermochemical biomass conversion. IEA Bioenergy, 1, 2001, 47-60.

6 ACKNOWLEDGEMENTS

- This research was supported by the Johan Gadolin Scholarship, the Greek Secretariat for Research and Development through the ENTER research grant (AGRO-GONO) 2006-2008, and European Social Fund's Doctoral Studies and Internationalisation Programme DoRa.
- Peter Backman, Linus Silvander, Maaris Nuutre, Raaja Aluvee, Rein Kuusik and Kaia Tõnsuaadu are acknowledged for a comprehensive assistance on carrying out the tests.
- Dr. Matthias Thommes from Quantachrome Inc. is acknowledged for his valuable comments and discussions.

PAPER III

Link, S., Arvelakis, S., Hupa, M., Yrjas, P., Külaots, I., Paist, A. Reactivity of the biomass chars originating from reed, Douglas fir and pine. *Energy Fuels*, 24, 2010, p. 6533-6539.

Energy Fuels **2010**, *24*, 6533–6539 · DOI:10.1021/ef100926v
Published on Web 11/16/2010

energy&fuels
article

Reactivity of the Biomass Chars Originating from Reed, Douglas Fir, and Pine

Siim Link,*[,†] Stelios Arvelakis,[‡] Mikko Hupa,[§] Patrik Yrjas,[§] Indrek Külaots,[∥] and Aadu Paist[†]

[†]*Thermal Engineering Department, Tallinn University of Technology, Kopli 116, 11712 Tallinn, Estonia,* [‡]*Department of Chemical Engineering, National Technical University of Athens, Zografou Campus, GR-15700 Athens, Greece,* [§]*Combustion and Materials Chemistry, Åbo Akademi Process Chemistry Centre, Biskopsgatan 8, FI-20500 Åbo, Finland, and* [∥]*Division of Engineering, Brown University, Box D, Providence, Rhode Island 02912, United States*

Received July 20, 2010. Revised Manuscript Received November 5, 2010

In this study, the oxidation reactivity of the chars derived from the pyrolysis of reed, pine pellets, and Douglas fir wood chips was investigated. The direct reactivity measurements were compared to the results from the indirect reactivity methods used to characterize the physical properties and chemical composition of material, such as proximate and ultimate analyses, ash chemical analysis, and specific surface area measurements. The direct reactivity measurements of the chars showed that the reed chars had lower reactivity compared to the chars derived from woods. The pine pellet char exhibited higher reactivity compared to the reed and Douglas fir wood chip char. The reed char showed the lowest reactivity because of high reaction inhibitor silicon content in the char, and in comparison to the Douglas fir wood chip char, the contents of alkali, alkali earth, and iron together were lower as well. The reed sample exhibited the highest char gasification yield on a dry and ash-free basis and the highest total residue yield after pyrolysis and gasification as well. The results of this study imply that the highly microporous structure together with a higher internal surface area and number of active sites and low Si content of the pine pellet char had a stronger impact on the gasification reactivity than the alkali/alkali earth metal contents of the Douglas fir wood chip and reed chars. The activity of alkali/alkali earth metals on gasification catalysis was inhibited by high Si content in the case of Douglas fir wood chip and reed chars, and the higher Si content and lower alkali, alkali earth, and iron contents together for the reed char are expected to be a main reason for the lower gasification reactivity compared to the Douglas fir wood chip char.

1. Introduction

Reed is a widely spread plant among others in the Estonian and southern Finnish coastal areas both on- and offshore, and the species is well-known all over the world. Reed has gradually encroached upon the coastline, and its expansion has been accelerated by human activities: eutrophication, climate change, and the cessation of coastal meadow management. Being a rotting stationary biomass, reed beds reduce water quality, deplete oxygen supplies in water, and release methane into the atmosphere. The expanse of reed beds also has an adverse effect on the landscape and jeopardizes nature's biodiversity. When dry, reed has quite a low weight, and therefore, without preliminary treatment, its transportation costs are high. Reed has been used to provide energy in various parts of Europe, such as Estonia, Finland, The Netherlands, Hungary, and Romania.[1]

The annual reed energy production potential is modest (for instance, in Estonia, 292 GWh/year[1]), and therefore, it could be used by blending with other types of biomasses, such as woods. Douglas fir has been widely planted for 30 years in Europe, especially in France and Germany, and nowadays, this wood represents an emerging resource for sawing logs, thinning logs, top logs, and sawmill chips. It is estimated that the French annual harvest of Douglas fir will be around 6 million m^3 by the year 2015.[2] In Europe as well as around the world, the wood pellet production extends to the tens of millions of tons per year.[3]

The gasification technology together with combined heat and power production gives an opportunity to use fuels with higher efficiency. The application of the integrated gasification combined cycle (IGCC) is commonly considered to have higher efficiency compared to the Rankine cycle.

The char conversion stage, following the pyrolysis step in the gasification process, is generally much slower than the pyrolysis itself and is therefore the rate-determining step.[4] High char reactivity is needed to obtain higher energy outputs from the reactors.[5]

Gasification rates are influenced by a number of process variables, such as particle size and size distribution, char porosity and pretreatment, mineral content of char, and temperature and partial pressures of the gasifying agents.[6]

Several studies have focused on the influence of the wood type in the CO_2 gasification process. In general, the mineral matter content, composition, and its catalytic properties explain the differences of reactivity among the fuels.[7] The presence of inorganic constituents in chars plays an important

*To whom correspondence should be addressed. Telephone: +372-6203903. Fax: +372-6203901. E-mail: siim.link@ttu.ee.

(1) Ikonen, I.; Hagelberg, E. *Read up on Reed!*; Southwest Finland Regional Environment Centre: Turku, Finland, 2007.
(2) Chantre, G.; Rozenberg, P.; Baonza, V.; Macchioni, N.; Le Turcq, A.; Rueff, M.; Petit-Conil, M.; Heois, B. *Ann. For. Sci.* **2002**, *59*, 583–593.
(3) Bioenergy International. *Bioenergy International* **2009**, *6*, 9.
(4) Cetin, A.; Gupta, R.; Moghtaderi, B. *Fuel* **2005**, *84*, 1328–1334.
(5) Zanzi, R.; Sjöström, K.; Björnbom, E. *Fuel* **1996**, *75*, 545–550.
(6) Liliedahl, T.; Sjöström, K. *Fuel* **1997**, *76*, 29–37.
(7) Barrio, M.; Gøbel, B.; Risnes, H.; Henriksen, U.; Hustad, J. E.; Sørensen, L. H. *Progress in Thermochemical Biomass Conversion*; IEA Bioenergy: Cornwall, U.K., 2001; Vol. 1, pp 32−46.

Table 1. Analysis and Characterization of the Biomass Samples

	proximate analysis, on a dry basis (wt %)				ultimate analysis, on a dry basis (wt %)						
	moisture	ash	volatile matter	fixed carbon	N	C	H	S	Cl	O	gross calorific value (MJ/kg)
R	5.40	3.21	80.26	16.53	0.44	47.36	5.66	0.19	nd	43.14	20.41
DF	7.74	6.73	72.28	20.99	0.63	48.49	4.85	0.05	nd	39.25	19.12
PP	5.89	0.22	83.29	16.49	0.32	50.49	5.85	0.15	nd	42.97	19.13
R800	6.90	16.01	6.73	77.25	1.72	59.19	1.23	nd	nd	21.85	nd
DF800	6.47	20.80	9.54	69.66	1.45	56.71	0.92	nd	nd	20.12	nd
PP800	8.60	4.08	7.11	88.81	1.03	64.13	1.19	nd	nd	29.57	nd

role in oxidation kinetics because of their catalytic effects. Sodium, potassium, and calcium, which are commonly present in biomass, show a significant activity as gasification catalysts.[8−10] It was shown that alkali metals are approximately 10 times more active at catalyzing the char gasification than alkali earth metals.[11] According to Kannan et al.,[12] the catalytic effect of potassium was reduced by the reaction with silica to form silicate during pyrolysis but catalysis of gasification by Ca does not appear to be significantly reduced by silica. The CO_2 gasification rate depends upon the silicon content in the parent fuel and, when the silicon content is low, also the sum of K and Ca contents. The gasification rate dependency upon parent fuel silicon content was also discussed by Moilanen.[13] Experimental and theoretical studies made by Sørensen et al.[14] have shown that the reactivity of char is dependent upon the silicon as well as the potassium contents and the form of the potassium compound. As can be seen in the literature, the catalytic effect of mineral matter content on biomass char reactivity is mainly related to alkali/alkali earth metals versus silicon content.

On top of the conventional proximate, ultimate, and ash chemical analyses, there are several analytical techniques to determine the physical characteristics of a material, such as N_2 and CO_2 adsorption techniques for surface area and porosity determination.

Reed and woods are renewable energy sources and are considered to be CO_2-neutral. In addition, fuel alternatives, such as biofuel use, save otherwise depleting resources of fossil fuels. The usage of residues originating from the reed treatment processes as the roof material and as the energy source, together with the wood residue, serves the goals of the European Union policy for wastes and environment. The present work focuses on the characterization of the chars from reed and two wood chars (Douglas fir and pine).

2. Experimental Section

2.1. Materials. The samples selected for the investigation were the following: pelagian reed, coming from the west coast shorelines of Estonia and the islands of Estonia, and commercial pine pellets and Douglas fir wood chips, both originating from the area of Munich in Germany.

Table 2. Ash Chemical Analysis, Expressed as Oxides, of the Biomass Samples (wt %)

	R	DF	PP	R800	DF800
K_2O	5.87	4.13	7.66	3.28	4.74
Na_2O	8.39	1.48	1.31	2.27	1.36
CaO	2.90	10.90	37.30	4.07	9.64
MgO	1.37	4.90	9.08	1.46	7.73
SiO_2	73.70	55.50	11.20	83.42	51.92
Al_2O_3		11.60	5.00	0.86	13.73
Fe_2O_3	1.09	7.24	4.83	1.44	6.61
Cl	0.56	0.73	0.99	0.19	0.36

The reed, Douglas fir wood chip, and pine pellet samples, as well as their char samples (hereafter referred as R, DF, and PP and char samples R800, DF800, and PP800) were analyzed and characterized regarding their proximate and ultimate composition analyses, gross calorific value, and ash chemical analysis (in all cases, the oxidation for the ash chemical analysis was performed at a temperature of 600 °C) in accordance with American Society for Testing and Materials (ASTM) methods, as shown in Tables 1 and 2. Because of the relatively low char yield of pine pellets in the pyrolysis experiments, the proximate analysis of pine pellet char was performed by a SDT Q600 thermogravimetric analyzer (TGA). In these TGA experiments, first the sample was heated 20 °C min^{-1} from ambient temperature to 105 °C in nitrogen gas flow of 90 mL min^{-1} to determine the moisture content. Then, the temperature was increased with the heating rate of 50 °C min^{-1} to 900 °C, where it was kept for 7 min to determine the sample volatile content. After this, the temperature was lowered to 600 °C in 20 min, which, after the 100 mL min^{-1} of air flow, was initiated to determine the ash content.

After each direct reactivity measurement of the char sample, the gasification residue remained. Because of the limited amount of the gasification residue (some milligrams), the ash content of this residue was determined applying the Setaram TGA apparatus. The heating rate of 10 °C min^{-1} to 600 °C and the air flow rate of 50 mL min^{-1} were used. The ash content was calculated according to the mass loss data. Because of the insufficient amount of gasification residue of the pine pellet sample, the ash content determination was not performed.

2.2. Pyrolysis. An atmospheric fixed-bed reactor was used to prepare the char samples. The R, PP, and DF parent samples were heated with a heating rate of 20 °C min^{-1} to 800 °C and held isothermally for 15 min before cooling to ambient temperature. The methodology together with a detailed description of the system has been reported elsewhere.[15] Nitrogen was used as a carrier gas with a flow rate of 1 L min^{-1} in all pyrolysis experiments.

2.3. Surface Area and Porosity. Nitrogen adsorption isotherms at −196 °C and carbon dioxide isotherms at 0 °C were obtained from all of the char samples by a volumetric technique using a Quantachrome Autosorb-1 instrument. Prior to surface

(8) Figueiredo, J. L.; Moulijn, J. A. *Carbon and Coal Gasification: Science and Technology*; Springer: New York, 1986; p 291.
(9) Jüntgen, H. *Fuel* **1983**, *62*, 234–238.
(10) Wood, B. J.; Sancier, K. M. *Catal. Rev.−Sci. Eng.* **1984**, *26*, 233–279.
(11) Risnes, H.; Sørensen, L. H.; Hustad, J. E. *Progress in Thermochemical Biomass Conversion*; IEA Bioenergy: Cornwall, U.K., 2001; Vol. 1, pp 61−72.
(12) Kannan, M. P.; Richards, G. N. *Fuel* **1990**, *69*, 747–753.
(13) Moilanen, A. Thermogravimetric characterisations of biomass and waste for gasification processes. Ph.D. Thesis, VTT Technical Research Centre of Finland, Espoo, Finland, 2006.
(14) Sørensen, L. H.; Fjellerup, J.; Henriksen, U.; Moilanen, A.; Kurkela, E.; Winther, E. An evaluation of char reactivity and ash properties in biomass gasification. *Fundamental Processes in Biomass Gasification*; ReaTech: Roskilde, Denmark, 2000; p 87.
(15) Link, S.; Arvelakis, S.; Spliethoff, H.; De Waard, P.; Samoson, A. *Energy Fuels* **2008**, *22*, 3523–3530.

area analysis, all of the char samples were outgassed at 280 °C overnight under vacuum to ensure complete removal of surface contaminants. Because of the pressure limitation of the instrument, the maximum relative pressure of 0.03 is obtained when CO_2 isotherms at 0 °C were recorded ($P_{CO_2}^{sat}$ = 3484.8 kPa at 0 °C). The adsorption uptake data at partial pressures of N_2 from 10^{-6} to 1 were requested to obtain full N_2 isotherms. The specific Brunauer−Emmett−Teller (BET) surface areas from the N_2 isotherms of the char samples are determined over the partial pressure (P/P_0) range, where the BET equation has the highest correlation coefficient (at least 0.9999).[16,17] For most nonmicroporous samples, the commonly accepted range of P/P_0 for the BET equation is from 0.05 to 0.3 (N_2 isotherms). However, because of the highly microporous nature of the char samples, the relative pressure range of the isotherms for BET surface area determination requires adjustment. Therefore, the BET surface areas were, in this work, defined at significantly lower relative pressure P/P_0 values, down to 0.01−0.05.

The porosity values presented in this work were calculated using the N_2 adsorption isotherms of the char samples. The microporosity of the char samples was determined using the Dubinin−Radushkevich (DR) model.[17] The mesoporosity of the char samples was determined by subtracting the DR microporosity value from the total porosity at an isotherm relative pressure of P/P_0 = 0.95. The macroporosity of the char sample was calculated by subtracting the total porosity at relative pressure P/P_0 = 0.95 from the porosity value at relative pressure P/P_0 = 0.99.

The pore size distribution (PSD) of the char samples is determined from the N_2 adsorption isotherms at −196 °C and from the CO_2 adsorption isotherms at 0 °C using density functional theory (DFT).[18,19] The PSDs of the char samples are reported according to the classification of the International Union of Pure and Applied Chemistry (IUPAC), which defines micropores as pores less than 20 Å, mesopores as pores in the range of 20−500 Å, and macropores as pores above 500 Å.

2.4. Char Reactivity Measurement. The Deutsche Montan Technologie (DMT) high-pressure thermogravimetric apparatus (HPTGA) operating at atmospheric pressure was applied in the char reactivity tests. At first, the sample was held in the reactor under He gas flow. Then, the desired reaction temperature was selected, and the reactor was heated to the target temperature (reactivity tests were performed at 750, 800, 850, and 900 °C). After the reactor reached the target temperature, the sample holder was lowered to the preheated reactor. A steady sample mass was achieved in 150−300 s (phase I), after which a gasification agent CO_2 with the flow rate of 1 L min^{-1} was introduced to the reactor (phase II). A schematic diagram together with the detailed description of the system is reported elsewhere.[20]

2.5. Reactivity Data Analysis. A typical HPTGA mass loss curve is shown in Figure 1. The M_o represents the initial mass of the char; $M(t)$ is the mass of the char at time t; and M_f is the mass of the residue.

Different definitions are used for determination of reactivity.[7] In this work, the reactivity results are presented in the figures as the char gasification rate as a function of char conversion. The char gasification rate in units of min^{-1} at any particular conversion value is defined as shown in eq 1

$$r = dX/dt \quad (1)$$

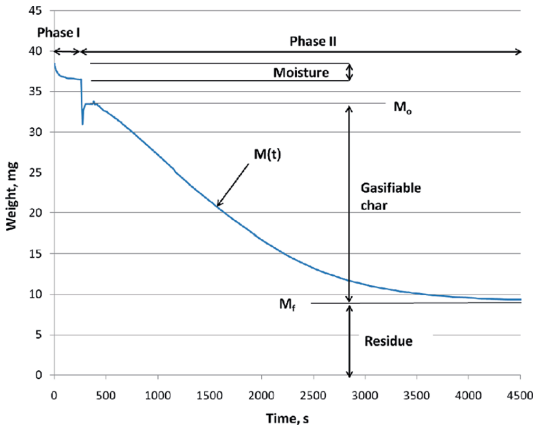

Figure 1. Typical HPTGA weight-loss curve.

Table 3. Char Yield (wt %)

	R800	DF800	PP800
dry	19.73	29.35	17.27
daf	15.75	23.02	15.67

Table 4. Specific BET Surface Areas (m^2 g^{-1})

	N_2	CO_2
R800	357	435
DF800	316	398
PP800	485	536

where r is the reaction rate

$$X = (M_o - M(t))/(M_o - M_f) \quad (2)$$

3. Results and Discussion

3.1. Material Characterization. The PP exhibited relatively low ash content (0.22 wt % on a dry basis), and the ash contained mainly calcium oxide (37.3 wt %), which corresponds to 0.08 wt % in parent fuel (see also Tables 1 and 2). The DF had the highest ash content (6.73 wt % on a dry basis) and the highest potassium oxide content in parent fuel (0.28 wt %). The ash content of the reed was 3.21 wt % (on a dry basis), and the ash consisted mainly of silica (73.7 wt %), which corresponds to 2.37 wt % from the parent material, compared to the 3.74 wt % for the DF sample.

3.2. Char Yields. The char yields of the R, DF, and PP samples shown in Table 3 were calculated on a dry and ash-free (daf) basis. The DF exhibited the highest char yield on both dry (29.35 wt %) and daf bases (23.02 wt %) compared to reed (19.73 wt % on a dry basis and 15.75 wt % on a daf basis) and PP (17.27 wt % on a dry basis and 15.67 wt % on a daf basis) char yields. The results of the char yields during pyrolysis calculated on dry and daf bases refer to a higher volatile content of the R and PP in parent materials compared to the DF sample.

3.3. Specific Surface Area and Porosity. Both N_2- and CO_2-specific BET surface areas of all chars tested shown in Table 4 are quite comparable. The N_2-specific BET surface areas range from 316 to 485 m^2 g^{-1}, and the CO_2-specific BET surface areas range from 398 to 536 m^2 g^{-1}. The specific BET surface area is clearly higher for the PP800 char sample compared to the other

(16) Brunauer, S.; Emmett, P. H.; Teller, E. *J. Am. Chem. Soc.* **1938**, *60*, 309–319.
(17) Gregg, S. J.; Sing, K. S. W. *Adsorption, Surface Area and Porosity*; Academic Press: London, U.K., 1982.
(18) Lastoskie, C.; Gubbins, K. E.; Quirke, N. *J. Phys. Chem.* **1993**, *97*, 4786–4796.
(19) Lozano-Castello, D.; Cazorla-Amoros, D.; Linares-Solano, A. *Carbon* **2004**, *42*, 1233–1242.
(20) Whitty, K.; Backman, R.; Hupa, M. *Carbon* **1998**, *36*, 1683–1692.

Table 5. Porosities Obtained from N_2 and CO_2 Isotherms (mL g^{-1})

	DR CO_2 microporosity	DR N_2 microporosity	N_2 mesoporosity	N_2 macroporosity	N_2 total porosity
R800	0.203	0.137	0.033	0.031	0.200
DF800	0.190	0.121	0.039	0.017	0.176
PP800	0.257	0.184	0.038	0.010	0.231

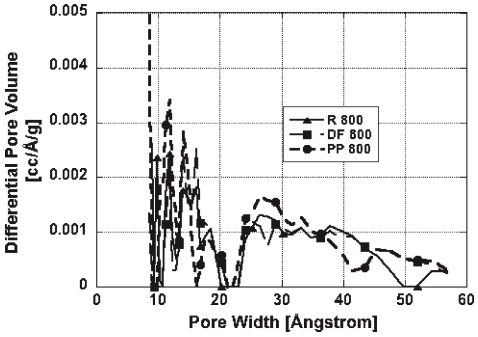

Figure 2. DFT/Monte Carlo differential pore volume distribution. DFT kernel used: N_2 at −196 °C on carbon.

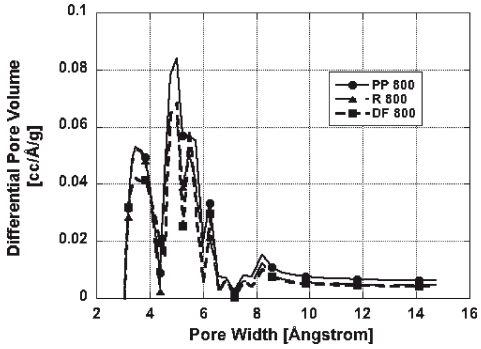

Figure 3. DFT/Monte Carlo differential pore volume distribution. DFT kernel used: CO_2 at 0 °C on carbon.

studied chars. In the literature, Matsumoto et al.[21] report that the cedar char N_2-specific BET surface area is 184 m^2 g^{-1}, and Zhou et al.[22] report that the pine tree char N_2-specific BET surface area is 379 m^2 g^{-1}. Other studies also suggest that the N_2-specific BET surface areas of other types of wood chars are in the same range of area values if compared to our N_2-specific BET surface areas presented in Table 4. However, all of the CO_2-specific BET surface areas are slightly higher compared to N_2-specific BET surface areas.

The porosity values in Table 5 show that the chars tested are mostly microporous. Approximately 80% of the pores in the char account for the micropores (pore sizes below 20 Å), and only about 15% account for the mesopores (pore sizes from 20 to 500 Å). The results in Table 5 also show that the DR CO_2 microporosity is slightly higher than the DR N_2 microporosity.

The results of DFT PSD analysis for R800, DF800, and PP800 chars are shown in Figures 2 and 3. The results clearly indicate that the PSDs of all chars presented are all quite similar and are, therefore, completely independent of the char origin, whether it is reed or wood. The CO_2 DFT PSD analysis also shows that the super-micropores (pores smaller than 8 Å) in these chars are not available in the N_2 DFT analysis plot presented in Figure 2. It seems quite evident that the use of both adsobates, N_2 and CO_2, is needed when adsorption characteristics of carbonaceous samples with significant microporosity are investigated.[19,23]

3.4. Char Reactivity. The series of the char reactivity measurement tests of the studied chars were performed at 750, 800, 850, and 900 °C. The weight signal curve shifts downward (phase I; see also Figure 1), and the increase in sample weight at the beginning of phase II was likely due to the buoyancy effect resulting from the change in the reactor feed gas.

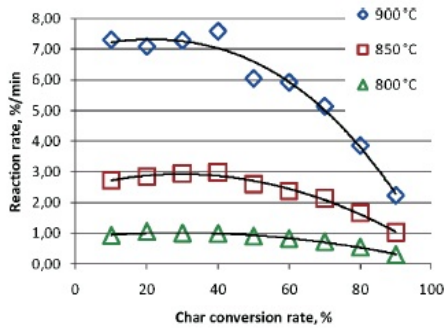

Figure 4. Char gasification reactivity of R800.

The reaction rates versus char conversion of the R800, DF800, and PP800 samples at the different gasification temperatures are shown in Figures 4−6. The reaction rate of R800 was constant until the conversion rate of 40% and then declined. The reaction rate of DF800 at gasification temperatures of 850 and 900 °C decreased until the conversion rate of 40−50%, then remained constant until the conversion rate of 60−70%, and then declined. The reaction rates of PP800 were constant, with the exception at the beginning in the temperature of 900 °C experiment, until the conversion rates of 60−70%, and then the reaction rate decreased.

It could be seen that the wood chars exhibited higher reactivity than the reed char. For instance, the reaction rate of PP800 was approximately 4 times higher between the conversion rates of 20 and 40% compared to that of R800. The reaction rate of DF800 was 3 times higher compared to R800. The clear distinction of the reaction rates between DF800 and PP800 is seen at the gasification temperature of 900 °C.

As expected, the char reaction rates increase with the increase of the temperature. The reaction rate of the R800 sample was enhanced 3 times between the conversion rates of 20 and 40%, while the temperature was increased by 50 °C, and for woods, the rate increased 2 or 3 times depending upon the fuel and gasification temperature.

(21) Matsumoto, K.; Takeno, K.; Ichinose, T.; Ogi, T.; Nakanishi, M. *Fuel* **2009**, *88*, 519–527.
(22) Zhou, Z. L.; Shi, D. J.; Qiu, Y. P.; Sheng, G. D. *Environ. Pollut. (Oxford, U. K.)* **2010**, *158*, 201–206.
(23) Della Rocca, P. A.; Cerrella, E. G.; Bonelli, P. R.; Cukierman, A. L. *Biomass Bioenergy* **1999**, *16*, 79–88.

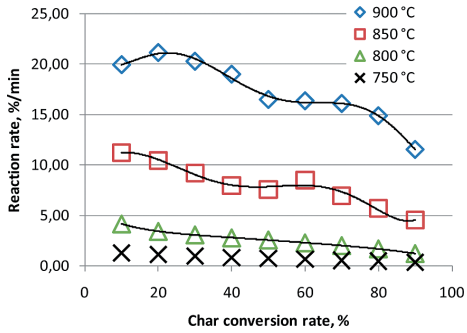

Figure 5. Char gasification reactivity of DF800.

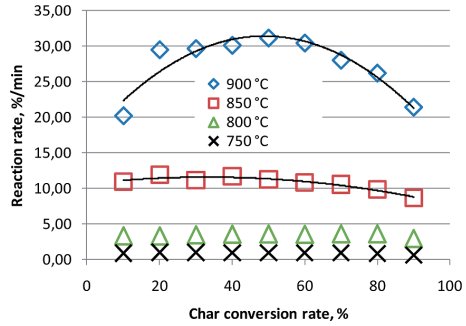

Figure 6. Char gasification reactivity of PP800.

The conversion rate versus time of the gasification tests are shown in Figures 7−9. PP800 exhibited the shortest gasification time in all cases, and R800 exhibited the longest gasification time. When the gasification temperature was increased by 50 °C, the gasification proceeded faster, from the temperature level of 750 to 800 °C, 3.2−3.5 times, from 800 to 850 °C, 3.1−3.6 times, and from 850 to 900 °C, 2.4−2.8 times. The conversion rate versus gasification time supports the order of the reactivity rate values as discussed above.

The R800 and DF800 samples have a higher ash content compared to the PP800 char sample, as well as higher alkali/alkali earth metal, chlorine, and silicon contents.

The interaction between the compounds present in mineral matter could inhibit the catalytic effect of the alkali/alkali earth metals, which could lead to the compound in which, for instance, potassium is totally inactive.[24] The catalytic deactivation reaction only depends upon time and not so much the temperature and pressure. At high conversion, the catalyst seems to lose its contact with carbon and, consequently, its activity.[25] The deactivation process of catalysts takes place already in the pyrolysis step, which is, in our study, so-called slow pyrolysis and continues in the gasification step.

According to Zevenhoven-Onderwater et al.[26] the next processes are expected to take place: (1) The formation of calcium, potassium, magnesium, sodium, and aluminum silicates during thermal treatment is expected. (2) High silica content of reed and Douglas fir chars yielded potassium

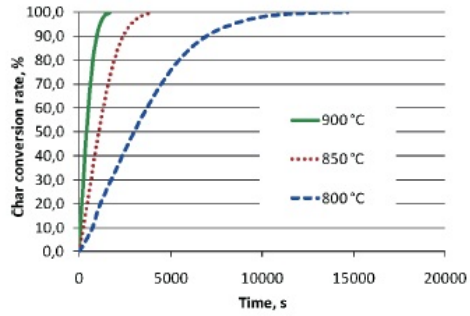

Figure 7. Conversion rate versus time of the gasification tests of R800.

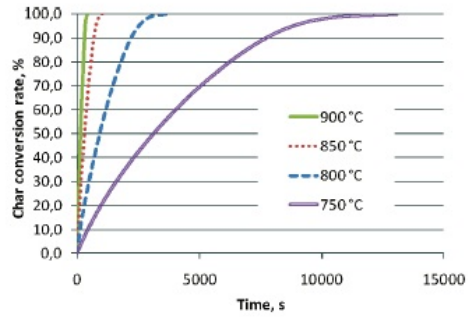

Figure 8. Conversion rate versus time of the gasification tests of DF800.

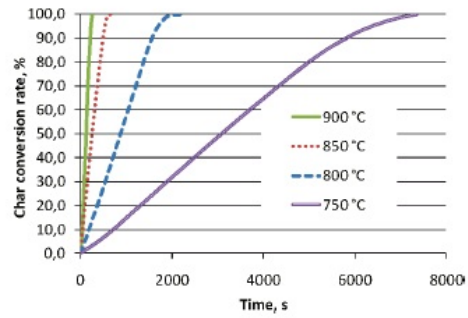

Figure 9. Conversion rate versus time of the gasification tests of PP800.

silicates, whereas high silica and high chlorine contents gave potassium silicate formation combined with the release of HCl and the formation of K_2CO_3 did not occur. (3) In the case of the pine pellet, which is low in silica content, K_2CO_3 was formed during the gasification (known as a better catalyst, for instance, compared to sodium and calcium carbonates[27]). The formation of KCl was expected as well.

The formation of silicates reduces the amount of available alkali and alkaline earth metal taking part in the solid−gas reaction on active sites. According to Radovic et al.,[28] the

(24) van Heek, K. H.; Mühlen, H.-J. *Fuel* **1985**, *64*, 1405–1414.
(25) Moilanen, A.; Mühlen, H.-J. *Fuel* **1996**, *75*, 1279–1285.
(26) Zevenhoven-Onderwater, M.; Backman, R.; Skrifvars, B.-J.; Hupa, M. *Fuel* **2001**, *80*, 1489–1502.
(27) Sutton, D.; Kelleher, B.; Ross, J. R. H. *Fuel Process. Technol.* **2001**, *73*, 155–173.
(28) Radović, L. R.; Walker, P. L., Jr.; Jenkins, R. G. *Fuel* **1983**, *62*, 849–856.

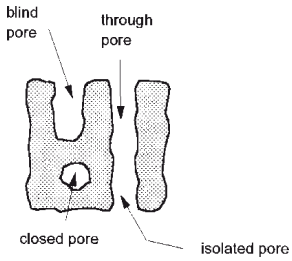

Figure 10. Types of pores.

Table 6. Residue Yield of Char Gasification at 850 °C (%)

	dry basis	daf basis
R800	15.62	0.80
DF800	20.26	0.09
PP800	1.96	nd

Table 7. Total Residue Yield after Pyrolysis and Char Gasification with a Gasification Temperature of 850 °C (%)

	dry basis	daf basis
R800	3.08	0.17
DF800	5.94	0.02
PP800	0.34	nd

reactivity is rather dependent upon carbon active sites than total surface area. van Heek et al.[24] have concluded that the extension of total surface area could not be alone the dominating factor, which is more likely to be the qualities of the surface, such as activity and accessibility, which give the possibility of blockage areas by minerals.

The initial increase in the reaction rate in the case of R800 and DF800 could be associated with the increase of the surface area as well as active sites in the early phase of gasification. The maximum in the reaction rate considering porosity is thought to arise from two opposing effects, namely, the increase in the reaction surface area as the micropores grow and their declines as the pores collapse progressively at their intersection (coalescence).[29] The decrease in the reaction rate is affected by the deactivation of catalysts, and therefore, less active sites are available along the process as well.

The 20% higher Si and 3.0 times lower alkali, alkali earth, and iron contents of R800 compared to the DF800 char sample could enhance the interaction between the mineral matter compound more toward inhibiting the catalysts and active sites available for the solid−gas reaction, and therefore, the reactivity of R800 is lower compared to that of DF800.

Our results indicate that PP800 is more reactive compared to R800 and DF800, despite the fact that the pine pellet contains over 5 and 15 times less elements acting as catalysts (K, Na, Ca, Mg, and Fe) compared to reed and Douglas fir wood chips, respectively. The ash content of pine pellet char is 4%, and according to the parent material ash chemical analysis, it contains mainly Ca and K as well and is not rich in silicon. Therefore, according to the results, the higher porosity of PP800, together with the structure of pores, K and Ca contents of mineral matter are seen to be the reason for

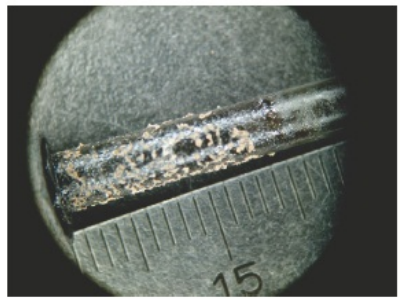

Figure 11. Sample of the gasification residue of PP800.

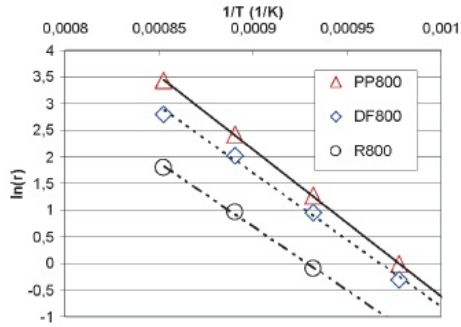

Figure 12. Arrhenius plots when gasifying the chars in CO_2 (rates taken at 50% conversion).

the highest reactivity among the studied chars. K and Ca did not form the silicates but rather compounds bound to the carbon matrix acting as the active site. The steady reaction rate of PP800 along the gasification process can be attributed to the pores opened at both ends (through pore), as shown in Figure 10.[30] The gasification agent reacts with the char material on the pore walls and consumes the material, but the total and active surface areas together did not change along the process significantly. The evolution of the total surface area of studied chars along the gasification process needs further investigations.

The results of the residue yields, i.e., ash and unconverted carbon, in the char gasification tests at the temperature of 850 °C and the total residue yields calculated from the initial parent material mass after the conversion because of pyrolysis and gasification are shown in Tables 6 and 7. PP800 exhibited the lowest residue yield after char gasification on a dry basis (see also Table 6). The residue yield from the gasification of DF800 was higher by 4.6% compared to the R800 yield, but if calculated on a daf basis, then R800 exhibited a 9 times higher residue yield compared to DF800. Accordingly, it can be seen that DF800 reached a higher carbon conversion during gasification compared to R800, indicating that DF800 is more reactive compared to R800.

The total residue yield shown in Table 7 is calculated over the pyrolysis and gasification steps. A lower total residue yield of DF800 on a daf basis indicates better carbon conversion to a gaseous substance along the pyrolysis and gasification steps compared to R800. It could be considered

(29) Struis, R. P. W. J.; von Scala, C.; Stucki, S.; Prins, R. *Chem. Eng. Sci.* **2002**, *57*, 3581–3592.

(30) Leofanti, G.; Padovan, M.; Tozzola, G.; Venturelli, B. *Catal. Today* **1998**, *41*, 207–219.

Table 8. Gasification Activation Energies at 50% Conversion (kJ/mol)

	activation energy
R800	199
DF800	208
PP800	229

that there is almost no carbon left in the gasification residue for PP800 (see also Figure 11), and therefore, the total residue yield on a daf basis is principally almost zero.

For the activation energy determination in the gasification reaction, it is necessary to know when the process is in a kinetically controlled regime (see also Figure 12). The activation energies of the chars tested as shown in Table 8 were in the range of 199−229 kJ/mol. According to Barrio et al.,[31] most values of the activation energy for different biomasses, gathered from different studies, for CO_2 gasification are in the range of 196−250 kJ/mol, which is in good agreement with our results.

4. Conclusions

The gasification time reaching the conversion rate of 100% was the longest for reed char and the shortest for pine pellet char under the same gasification conditions (the chars were produced under the same conditions as well), indicating the highest reactivity of pine pellets among the studied samples. When the gasification temperature was increased by 50 °C, the duration of the process was shortened by a factor of 2−3.

The chars of reed, Douglas fir wood chips, and pine pellets showed different reactivity under CO_2 gasification conditions. In general, the R800 samples exhibited a lower reactivity compared to both DF800 and PP800.

The distinctions in reactivity can be explained by the differences in the mineral matter content, internal surface area, active sites, and nature of the porous structure. The pine pellet char had the highest internal surface area. It could be considered that PP800 has pores opened at both ends, as described above, and the gasification agent reacts with the char material on the pore walls. Because of the reaction, the mass of char material declines but the surface area remains almost constant along the process, until the amount of the material decreased in such an amount that the surface area decreased together with the mass of the char at the end of the process. The results of this study imply that the highly microporous structure together with a higher internal surface area and number of active sites and low Si content of the pine pellet char had a stronger impact on the gasification reactivity than the alkali/alkali earth metal contents of the Douglas fir wood chip and reed chars. The activity of alkali/alkali earth metals on gasification catalysis was inhibited by high Si content in the case of Douglas fir wood chip and reed chars, and the higher Si content and lower alkali, alkali earth, and iron contents together for the reed char are expected to be a main reason for the lower gasification reactivity compared to the Douglas fir wood chip char.

The reed char sample exhibited the lowest carbon conversion during gasification, together with the longest process time, and pine pellets exhibited the highest carbon conversion to the gaseous substances, together with the shortest reaction time as well. For pine pellets, it could be considered that almost all carbon was converted to a gaseous product.

On the basis of our results, pine pellets would be preferred as the fuel source compared to reed and Douglas fir samples. Pine pellets show higher reactivity, which means a smaller size of the reactor requirement at the same output, and lower ash amount removal from the reactor to save on otherwise high ash landfilling costs. On the other hand, a high reed ash fusion temperature allows for the use of reactor temperatures of 1000 °C and above, resulting in higher reactivities than shown in this study and enhanced thermal cracking of tar evolved in the gasification process. The melting behavior of the ash remaining after cogasification of different biomasses, i.e., reed and woods, needs further investigation.

Acknowledgment. This research was supported by the Johan Gadolin Scholarship. Peter Backman, Linus Silvander, Maaris Nuutre, Raaja Aluvee, Rein Kuusik, and Kaia Tõnsuaadu are acknowledged for a comprehensive assistance on carrying out the tests. Dr. Matthias Thommes from Quantachrome, Inc. is acknowledged for his valuable comments and discussions.

(31) Barrio, M.; Hustad, J. E. *Progress in Thermochemical Biomass Conversion*; IEA Bioenergy: Cornwall, U.K., 2001; Vol. 1, pp 47−60.

DISSERTATIONS DEFENDED AT TALLINN UNIVERSITY OF TECHNOLOGY ON *MECHANICAL AND INSTRUMENTAL ENGINEERING*

1. **Jakob Kübarsepp**. Steel-Bonded Hardmetals. 1992.

2. **Jakub Kõo**. Determination of Residual Stresses in Coatings &Coated Parts. 1994.

3. **Mart Tamre**. Tribocharacteristics of Journal Bearings Unlocated Axis. 1995.

4. **Paul Kallas**. Abrasive Erosion of Powder Materials. 1996.

5. **Jüri Pirso**. Titanium and Chromium Carbide Based Cermets. 1996.

6. **Heinrich Reshetnyak**. Hard Metals Serviceability in Sheet Metal Forming Operations. 1996.

7. **Arvi Kruusing**. Magnetic Microdevices and Their Fabrication methods. 1997.

8. **Roberto Carmona Davila**. Some Contributions to the Quality Control in Motor Car Industry. 1999.

9. **Harri Annuka**. Characterization and Application of TiC-Based Iron Alloys Bonded Cermets. 1999.

10. **Irina Hussainova**. Investigation of Particle-Wall Collision and Erosion Prediction. 1999.

11. **Edi Kulderknup**. Reliability and Uncertainty of Quality Measurement. 2000.

12. **Vitali Podgurski**. Laser Ablation and Thermal Evaporation of Thin Films and Structures. 2001.

13. **Igor Penkov**. Strength Investigation of Threaded Joints Under Static and Dynamic Loading. 2001.

14. **Martin Eerme**. Structural Modelling of Engineering Products and Realisation of Computer-Based Environment for Product Development. 2001.

15. **Toivo Tähemaa**. Assurance of Synergy and Competitive Dependability at Non-Safety-Critical Mechatronics Systems design. 2002.

16. **Jüri Resev**. Virtual Differential as Torque Distribution Control Unit in Automotive Propulsion Systems. 2002.

17. **Toomas Pihl**. Powder Coatings for Abrasive Wear. 2002.

18. **Sergei Letunovitš**. Tribology of Fine-Grained Cermets. 2003.

19. **Tatyana Karaulova**. Development of the Modelling Tool for the Analysis of the Production Process and its Entities for the SME. 2004.

20. **Grigori Nekrassov**. Development of an Intelligent Integrated Environment for Computer. 2004.

21. **Sergei Zimakov**. Novel Wear Resistant WC-Based Thermal Sprayed Coatings. 2004.

22. **Irina Preis**. Fatigue Performance and Mechanical Reliability of Cemented Carbides. 2004.

23. **Medhat Hussainov**. Effect of Solid Particles on Turbulence of Gas in Two-Phase Flows. 2005.

24. **Frid Kaljas**. Synergy-Based Approach to Design of the Interdisciplinary Systems. 2005.

25. **Dmitri Neshumayev**. Experimental and Numerical Investigation of Combined Heat Transfer Enhancement Technique in Gas-Heated Channels. 2005.

26. **Renno Veinthal**. Characterization and Modelling of Erosion Wear of Powder Composite Materials and Coatings. 2005.

27. **Sergei Tisler**. Deposition of Solid Particles from Aerosol Flow in Laminar Flat-Plate Boundary Layer. 2006.

28. **Tauno Otto**. Models for Monitoring of Technological Processes and Production Systems. 2006.

29. **Maksim Antonov**. Assessment of Cermets Performance in Aggressive Media. 2006.

30. **Tatjana Barashkova**. Research of the Effect of Correlation at the Measurement of Alternating Voltage. 2006.

31. **Jaan Kers**. Recycling of Composite Plastics. 2006.

32. **Raivo Sell**. Model Based Mechatronic Systems Modeling Methodology in Conceptual Design Stage. 2007.

33. **Hans Rämmal**. Experimental Methods for Sound Propagation Studies in Automotive Duct Systems. 2007.

34. **Meelis Pohlak**. Rapid Prototyping of Sheet Metal Components with Incremental Sheet Forming Technology. 2007.

35. **Priidu Peetsalu**. Microstructural Aspects of Thermal Sprayed WC-Co Coatings and Ni-Cr Coated Steels. 2007.

36. **Lauri Kollo**. Sinter/HIP Technology of TiC-Based Cermets. 2007.

37. **Andrei Dedov**. Assessment of Metal Condition and Remaining Life of In-service Power Plant Components Operating at High Temperature. 2007.

38. **Fjodor Sergejev**. Investigation of the Fatigue Mechanics Aspects of PM Hardmetals and Cermets. 2007.

39. **Eduard Ševtšenko**. Intelligent Decision Support System for the Network of Collaborative SME-s. 2007.

40. **Rünno Lumiste**. Networks and Innovation in Machinery and Electronics Industry and Enterprises (Estonian Case Studies). 2008.

41. **Kristo Karjust**. Integrated Product Development and Production Technology of Large Composite Plastic Products. 2008.

42. **Mart Saarna**. Fatigue Characteristics of PM Steels. 2008.

43. **Eduard Kimmari**. Exothermically Synthesized B_4C-Al Composites for Dry Sliding. 2008.

44. **Indrek Abiline**. Calibration Methods of Coating Thickness Gauges. 2008.

45. **Tiit Hindreus**. Synergy-Based Approach to Quality Assurance. 2009.

46. **Karl Raba**. Uncertainty Focused Product Improvement Models. 2009.

47. **Riho Tarbe**. Abrasive Impact Wear: Tester, Wear and Grindability Studies. 2009.

48. **Kristjan Juhani**. Reactive Sintered Chromium and Titanium Carbide-Based Cermets. 2009.

49. **Nadežda Dementjeva**. Energy Planning Model Analysis and Their Adaptability for Estonian Energy Sector. 2009.

50. **Igor Krupenski**. Numerical Simulation of Two-Phase Turbulent Flows in Ash Circulating Fluidized Bed. 2010.

51. **Aleksandr Hlebnikov**. The Analysis of Efficiency and Optimization of District Heating Networks in Estonia. 2010.

52. **Andres Petritšenko**. Vibration of Ladder Frames. 2010.

53. **Renee Joost**. Novel Methods for Hardmetal Production and Recycling. 2010.

54. **Andre Gregor**. Hard PVD Coatings for Tooling. 2010.

55. **Tõnu Roosaar**. Wear Performance of WC- and TiC-Based Ceramic-Metallic Composites. 2010.

56. **Alina Sivitski**. Sliding Wear of PVD Hard Coatings: Fatigue and Measurement Aspects. 2010.

57. **Sergei Kramanenko**. Fractal Approach for Multiple Project Management in Manufacturing Enterprises. 2010.

58. **Eduard Latõsov**. Model for the Analysis of Combined Heat and Power Production. 2011.

59. **Jürgen Riim**. Calibration Methods of Coating Thickness Standards. 2011.

60. **Andrei Surzhenkov**. Duplex Treatment of Steel Surface. 2011.

61. **Steffen Dahms**. Diffusion Welding of Different Materials. 2011.

62. **Birthe Matsi**. Research of Innovation Capasity Monitoring Methodology for Engineering Industry. 2011.

63. **Peeter Ross**. Data Sharing and Shared Workflow in Medical Imaging. 2011.